Multiplexed Biosensors for Drug Discovery Applications

Jha, Jahnavi

Award date:
2019

Awarding institution:
University of Bath

Multiplexed Biosensors For Drug Discovery Applications

Jahnavi Jha

A thesis presented for the degree of Doctor of Philosophy

University of Bath

Department of Electronic and Electrical Engineering

February 2019

Abstract

The phosphorylation of proteins, catalysed by protein kinases, play an important role in nearly every aspect of cell life. The abnormal phosphorylation of proteins is responsible for the onset of several diseases and disorders including various types of cancers, diabetes, Alzheimer's disease, etc. Therefore, the discovery of protein kinase inhibitors is a major focus of the pharmaceutical companies. Drug discovery today is dominated by number a of processes that require expensive chemicals, fluorescent tags and radio-labelling and can often be time consuming and laborious. Through this research, a new process for the screening of protein kinase inhibitors has been explored. In order to improve the cost effectiveness and efficiency of the process, biosensors have been developed using printed circuit board (PCB) technology and made compatible with commercially available complementary metal oxide semiconductors (CMOS). Designing a REFET structure for biosensing where the reference electrode can be eliminated was the final aim.

In this thesis, the techniques which are already in use are reviewed in order to understand their drawbacks and to help improve our design. A sensor array that can fit under the industrially used 96 well microtitre plate has been designed such that the existing techniques of liquid handling for drug discovery can be used.

In the first technique an electrolyte-insulator-semiconductor structure is interfaced with a PCB for sensing pH changes associated with phosphorylation, through capacitance versus voltage measurements. Next, organic thin film transistors with gold extended gates have been used to detect charge changes during a phosphorylation reaction. Thin films of evaporated tin oxide and tantalum oxide on a PCB have also been tested as pH sensitive membranes for this

reaction. The thin films have been used as extended gates for commercial CMOS circuits and the shift in their drain current versus gate voltage characteristics have been measured.

The REFET structure has been finally designed with tin oxide as the sensing layer. The reference layer has been designed using a thin film made of SU-8 photoresist as a pH insensitive layer. The two thin films have been used as extended gates to a commercially available matched pair CMOS integrated circuit and a differential measurement in their drain current for a fixed gate voltage is conducted for the phosphorylation reaction. Finally, array of REFET structures are multiplexed for the possibility of high throughput screening. The final device provides an excellent starting point for fabricating sensor arrays compatible with the widely accepted well plate structure and associated liquid handling systems.

Keywords: biosensor, REFET, high throughput screening, PCB based biosensor

Abbreviations

FRET	Fluorescence Resonance Energy Transfer
ELISA	Enzyme Linked Immunosorbent Assay
ALPHA	Amplified Luminescence Proximity Homogeneous Assay
DNA	Deoxyribonucleic Acid
RNA	Ribonucleic Acid
PCB	Printed Circuit Board
MOS	Metal Oxide Semiconductor
AFP	Autofluorescent Proteins
SPA	Scintillation Proximity Assay
FP	Fluorescence Polarization
ATP	Adenosine Triphosphate
ADP	Adenosine Diphosphate
HTS	High Throughput Screening
SDS-PAGE	Sodium Dodecyl Sulfate Polyacrylamide Gel Electrophoresis
EIS	Electrolyte-Insulator Semiconductor
FET	Field Effect Transistor
IC	Integration Circuit
MOSFET	Metal Oxide Semiconductor Field Effect Transistor
ISFET	Ion Sensitive Field Effect Transistor
EGFET	Extended Gate Field Effect Transistor
REFET	Reference Field Effect Transistors
APTES	(3-Aminopropyl)triethoxysilane
GOPTS	(3-Glycidyloxypropyl)trimethoxysilane
PDMS	Polydimethylsiloxane

PBS	Phosphate Buffered Saline
OTFT	Organic Thin Film Transistor
MBP	Myelin Basic Protein
HPLC	High Performance Liquid Chromatography
SLA	Stereolithography
EG	Extended Gate
EDC	1-ethyl-3-(-3-dimethylaminopropyl) carbodiimide hydrochloride
NHS	N-hydroxysuccinimide
MUA	11-mercaptoundecanoic acid
MCH	6-mercapto-1-hexanol
OTFT	Organic Thin Film Transistor
PECVD	Plasma Enhanced Chemical Vapour Deposition
CMOS	Complementary Metal Oxide Semiconductor
SAM	Self Assembled Monolayer
SEM	Scanning Electron Microscope
AFM	Atomic Force Microscope
C-V	Capacitance-Voltage

List of Figures

List of Tables

Contents

Chapter 1

Introduction

1.1 Motivation

Over the years, advances in chemistry and chemical engineering have made it possible to rapidly and efficiently synthesise a large number of novel compounds which have the potential to be therapeutic drugs. This has led to the development of several high throughput screening (HTS) techniques to economically and quickly eliminate compounds and identify hits[1]. The advances in high throughput screening technologies over the last decade have led to the incorporation of automatic sample delivery systems and specialised software. As a consequence, it is now possible to screen over 10,000 compounds daily. Today, high throughput screening has been adopted by the pharmaceutical industry as well as academia as the standard technique for drug discovery [1].

The high cost associated with bringing a new drug to market is resulting in a number of productivity challenges for the pharmaceutical companies. New drugs undergo several stages of assessment such as clinical trials and pre-clinical trials. The use of high throughput screening techniques has successfully shown to reduce the cost of drug development [2]. The effectiveness of high throughput screening comes from the fact that drugs are screened with a focus on a single mechanism. The use of an array of microreaction wells in the form of a microtitre plate (96

[1]The compound that displays the desired characteristics of the drug is known as a hit

wells or more) has gained popularity in the field of HTS drug discovery. Figure 1.1 shows a typical 96 well plate used for drug discovery. A library of molecules is usually tested for binding or biological activity against one or more targets using these microtitre plates [1].

Figure 1.1: High Throughput Screening Using Microtitre Plates [Image Source: http://www.ddw-online.com]

Protein phosphorylation is a reversible process catalysed by enzymes called protein kinases where a phosphate group is transferred from a phosphoryl donor like adenosine triphosphate (ATP) to certain amino acid residues. The extensive study of protein phosphorylation, since it was first discovered in 1954, has led to the understanding of its cardinal role in almost all aspects of cell life. So, abnormal phosphorylation of proteins is responsible for a number of diseases and disorders ranging from neurodegenerative diseases, inflammatory diseases, various types of cancers, cardiovascular disorders, diabetes, infectious diseases, etc [3] [4] [5]. Therefore, it is not surprising that protein kinases which regulate the phosphorylation process are major drug targets of the twenty first century [6].

Protein kinase inhibitors take up a major share of research and development in pharmaceutical companies. Almost 50-70% of cancer drug discovery initiatives

are centred around protein kinase inhibitors [4].

There are numerous assays commercially available for the drug discovery of kinase inhibitors. The traditional methods such as western blot are laborious, time consuming and not suitable for HTS. The existing HTS technologies also suffer from major drawbacks such as the need for labelling biomolecules with radio isotopes (radio-labelling) and the presence of specific antibodies. The processes are labour intensive and contain repeated washing steps. The radioactive materials pose a safety risk and hence their disposal requires special techniques and precautions. The reagents used in the studies are expensive and add to the overall cost of drug development.

This research project attempts to improve the process of high throughput screening of kinase inhibitors by developing a cost effective, label free alternative to existing techniques using field effect devices. An interface is made between the sensors and commercial complementary metal oxide semiconductor (CMOS) integrated circuits (ICs) to make this screening technique more cost effective than designing a monolithic integrated circuit.

1.2 Background

Biosensors are analytical devices that can convert a biological response into a measurable electrical signal [7]. The basic concept of a biosensor was first reported by pioneers Clark and Lyons in 1962 with the 'enzyme electrode' [8]. Since then, the field of biosensors has developed rapidly with applications in food, pharmaceuticals, healthcare, defence and environmental monitoring to name a few [9]. The commercial biosensors that dominate the market are in the healthcare sector and medical diagnostics with an estimated market value of over 13 billion US dollars [10].

Rapid progress in solid state technologies has led to the emergence of field effect transistor (FET) based biosensors. Biomolecules often carry electrostatic charges and biochemical activities result in changes in electrical potential which can be utilised in field effect based sensors. The complementary metal oxide semiconductor (CMOS) manufacturing process is widely accepted and has facilitated the development of miniaturised sensor arrays which can be integrated with electronic circuits and instrumentation [11].

FET based biosensors are similar to Metal Oxide Semiconductor Field Effect Transistors (MOSFETs) where the metal gate has been replaced by an electrolyte. The change in potential at the gate terminal induces band bending of the semiconductor channel due to the electric field and the carrier concentration changes. The potential at the gate can be is influenced by the solution potentials such as pH and presence of charged biomolecules. The current voltage characteristics are shifted positively or negatively as a result [11].

Since the discovery of the ion sensitive field effect transistor (ISFET) in 1970 by P. Bergveld [12], FET based biosensors have made significant progress. ISFETs fabricated through the unmodified CMOS process have proved to be very successful in designing pH sensitive sensor arrays [13, 14]. The advantages of this process are the scalability, low power operation and the ability to use the passivation layer as the pH sensitive layer. There are some drawbacks to this process. Use of the passivation layer causes a variation in threshold voltage between individual sensors due to the presence of trapped charges [15].

Another widely used field effect based biosensor is the extended gate FET. The sensing structure connected to the gate extends off the chip and allows the separation of wet and dry environments. The biochemical modifications and exposure to the analyte in solution can be performed on the extended gate independent of the transducer [16]. This structure has been used for a number of studies like pH sensing [17], DNA sensing [18] and enzyme sensing for cholesterol

detection to name a few [19].

Electrolyte-insulator-semiconductor (EIS) structures are another type of field effect device. They are often preferred for being easier to fabricate than ISFETs or EGFETs [20]. Several pH sensors [21] [22] and biosensors, such as glucose sensors, based on EIS structures [23] have been reported in literature.

Other structures like dual-gate FET sensors and floating gate sensors have been reported in literature. Floating gate structures have two gates where one gate serves as the control gate and the other as a sensing gate. They are both capacitively coupled to the floating gate. The principle of detection is usually dependant on the charged molecule under study inducing a change in the threshold voltage which allows for the elimination of the reference electrode [24]. Biosensors like DNA sensors using this structure have been reported [25]. Some studies have reported significant instabilities due to the gate being at a floating potential [26]. Dual-gate FETs are similar except that they employ an addition back gate for an increased slope in the sensor response [26]. This has been used for DNA and pH detection, among other studies [27] [28].

1.3 Aim

Field effect biosensors are very promising candidates for biosensing applications. They are easy to fabricate and interface with low cost commercially available electronic components. In this thesis, different field effect structures will be assessed as potential biosensors for screening protein kinase inhibitors. The overall aim is to design a sensor array consisting of field effect devices that can be multiplexed for measurement. The sensor array will be designed such that its dimensions and spacing are according to the layout of the 96 well microtitre plate. Although having a sensor compatible with a 96 well plate is not strictly essential, a system compatible with a widely accepted component of HTS will make

assessment of the device by end-users easier. In future applications, it would be desirable to move towards a miniaturised system.

For ease of fabrication and reduction of cost, an FR4 substrate is chosen for most of the studies in this thesis. The final aim is to eliminate the reference electrode and instead use a differential measurement between a 'sensitive' and an 'insensitive' biosensor. The research problems that will be explored in study are as follows:

1. Suitable pH sensitive material for detection of pH changes due to phosphorylation
2. Suitable field effect device for forming an array of sensors on a printed circuit board (PCB)
3. A device configuration that permits the elimination of the reference electrode
4. A sensor array compatible with commercially available integrated circuits for measurement

1.4 Overview of the Thesis

This thesis details the process of development of a field effect based biosensor for screening protein kinase inhibitors. The biosensor ideally will be compatible with a 96 well microtitre plate so that existing processes of solution handling can be used in the future.

Chapter 2: This chapter explores the existing techniques for the screening of protein kinase inhibitors. The drawbacks of these techniques are highlighted to establish the need for a new and improved system. The drawbacks are addressed in our device design in the later chapters. The importance of the phosphorylation

reaction and its role in major diseases is also described. Finally, the background of the field effect devices used in this research is presented.

Chapter 3: Initial attempts to select a suitable field effect based device for this research is described in this chapter. Electrolyte-Insulator-Semiconductor (EIS) structures made from Si_3N_4 coated silicon wafers mounted on printed circuit board (PCB) is tested for its pH sensitivity and used to detect protein phosphorylation. In the second part of this chapter, organic thin film transistors with extended gates are assessed for their suitability for this application.

Chapter 4: Tin oxide as a pH sensitive sensing layer for protein phosphorylation is explored in the first part of this chapter. The layer is deposited directly on to the PCB. pH sensitivity and phosphorylation studies are performed in this study. Tantalum oxide is briefly studied in view to replace tin oxide. In the second part of this chapter, attempts to fabricate a pH insensitive device that can act as a 'reference' measurement is described. The thin films in this study are tested for their lack of sensitivity to pH and the phosphorylation reaction.

Chapter 5: In this chapter the attempts to interface the biosensors in chapter 4 with commercial CMOS integrated circuits is described. A device consisting of the sensing layer and the reference layer are used for differential measurements to detect protein phosphorylation. The sensors are multiplexed using commercial low cost integrated circuits and the data is collected through an Arduino.

Chapter 6: Overall conclusions and future outlook is addressed in this chapter.

Chapter 2

Literature Review

2.1 Importance of Protein Phosphorylation

The phosphorylation of proteins plays a significant role in regulating cellular events. Protein phosphorylation is a reversible process catalysed by enzymes called kinases whereby phosphate groups from a phosphate donor like Adenosine Triphosphate (ATP) are attached to specific amino acid residues post translation[1]. The reverse process or dephosphorylation is catalysed by a class of enzymes known as phosphatases. In eukaryotic cells, phosphorylation mainly occurs on serine, threonine and tyrosine residues [29]. Phosphorylation is of cardinal importance in regulating processes like cell growth, apoptosis, proliferation and differentiation [30]. The abnormal phosphorylation of proteins is the cause of several human diseases. The mutation of protein kinases and phosphatases results in diseases like Parkinson's disease, muscular dystrophy, viral infections, cardiovascular diseases and various types of cancers [31] [3]. Figure 2.1 illustrates the reversible protein phosphorylation process.

The activity of protein kinase was first discovered in 1954 by Gene Kennedy who observed the phosphorylation of casein by a liver enzyme [32]. Fischer and Krebs [33] [34] along with Wosilait and Sutherland [35] described the mechanism

[1]The process by which proteins are created by the ribosomes present in the cells is known as translation

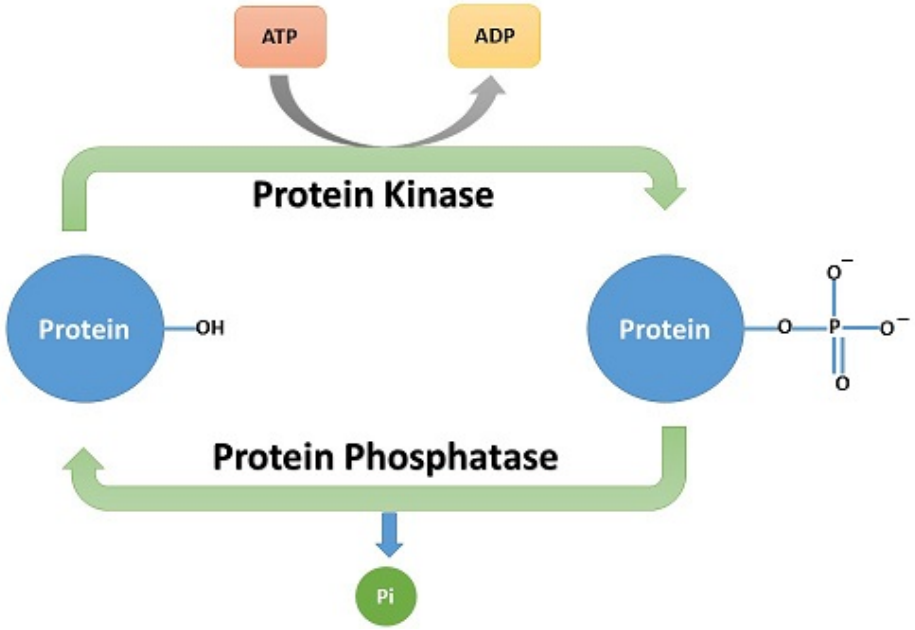

Figure 2.1: Reversible Protein Phosphorylation (Pi symbolises a hydrolysed phosphate group)

of phosphorylation and dephosphorylation that occurs during the interconversion of phosphorylase b to phosphorylase a in the presence of Mg-ATP and an enzyme. This is when the termed phosphorylase kinase was coined. The work done by Fischer and Krebs earned the Nobel prize in 1992. A number of diseases that result from abnormal protein phosphorylation are listed in Table 2.1.

Table 2.1: Some Diseases Caused by Abnormal Protein Phosphorylation [3]

Disease	**Kinase/Phosphatase**
Myotonic muscular dystrophy	Myotonin protein kinase
X-Linked agammaglobulinaemia	Bruton tyrosine kinase
Hirschsprungís disease	Ret2 kinase
Autosomal recessive SCID	Zap70 kinase

Disease	**Kinase/Phosphatase**
X-Linked SCID	Jak3 kinase
Chraniosynostosis	FGF receptor kinase
Papillary renal cancer	Met receptor kinase
Chronic myelomonocytic leukaemia	Tel-PDGF receptor kinase
Chronic myelogenous leukaemia	Abelson tyrosine kinase
Non-Hodgkins lymphoma	Alk kinase
Peutz–Jeghers syndrome	Lkb1 kinase
Coffin–Lowry syndrome	MAPKAP-K1b (RSK-2)
Ataxia-telangiectasia	Atm kinase
Li–Fraumeni syndrome	Chk2 kinase
Williams syndrome	Lim kinase-1
Leprechaunism, diabetes	Insulin receptor kinase
Wolff–Parkinson–White syndrome	AMP activated kinase
Wolcott–Rallison syndrome	eIF2A-kinase 3
X-Linked myotubular myopathy	MTM1 Tyr phosphatase

2.2 Protein Kinase Inhibitors

It took several years, since their discovery in 1955, before the importance of protein kinases was appreciated. Today mutations in protein kinases are known to result in abnormal phosphorylation and lead to a number of diseases. Protein kinase inhibitors emerged as an important class of drugs that targeted the ATP binding pockets of the enzyme. Figure 2.2 shows the Web of Science citation reports for the keywords "kinase inhibitor" and "discovery". It is evident that research on the discovery of kinase inhibitors has increased significantly over the years. Based on

their binding modes, kinase inhibitors may be classified as reversible and irreversible. In reversible inhibition, the inhibitor covalently binds to the ATP binding pocket to prevent the binding of ATP while in the case of reversible inhibition the molecule interacts with kinase in order to prevent access to the ATP binding site [36] [37]. Table 2.2 lists some of the kinase inhibitors from major pharmaceutical companies which are in advanced clinical trial or have been approved for clinical use.

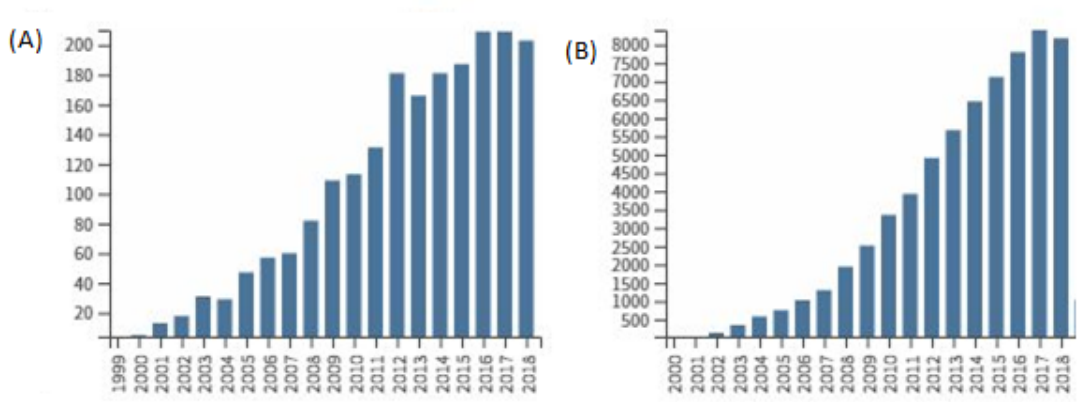

Figure 2.2: Web of Science citation reports for "kinase inhibitor" and "discovery" search terms. (A) Publications per year (B) Citations per year (Data collected in February 2019)

Table 2.2: Protein Kinase Inhibitors from Major Pharma Companies which are in Advance Clinical Trial or Approved for Clinical Use: From the Blue Ridge Institute for Medical Research in Horse Shoe, North Carolina USA [4]

Name	**Company**	**Approval**
Eril-Fasudil	Eisai	1995 cerebral vasospasm
Rapamune-Sirolimus	Wyeth Pfizer	1999 kidney transplantation

Name	**Company**	**Approval**
Imatinib	Novartis	2001 chronic myelogenous leukemia
Gefitinib	Astra Zeneca	2003 lung cancer
Erlotinib	Genetech Roche	2005 lung, pancreatic and others cancers
Sorafenib	Onyx Bayer	2005 renal cancer
Nilotinib	Novartis	2007 chronic myelogenous leukemia
Temsirolimus	Wyeth Pfizer	2007 advanced renal cell carcinoma
Everolimus	Novartis	2009 several cancers
Pazopanib	GlaxoSmith Kline	2009 renal cancer
Ruxolitinib	Incyte	2011 myelofibrosis
Crizotinib	Pfizer	2011 NSCLC with Alk mutation
Vemurafenib	Roche	2011 melanoma
Vandetanib	Astra Zeneca	2011 thyroid cancer
Axitinib	Pfizer	2012 renal cell carcinoma
Bosutinib	Pfizer	2012 chronic myelogenous leukemia
Tofacitinib	Pfizer	2012 rheumatoid arthritis
Regorafenib	Stivarga Bayer	2012 colorectal cancer, GIST
Cabozantinib	Cometriq Exelixis Inc	2012 medullary thyroid cancer
Lenvatinib	Eisai	2013 thyroid cancer
Dabrafenib	GlaxoSmith Kline	2013 skin cancer
Trametinib	GlaxoSmith Kline	2013 skin cancer
Ceritinib	Novartis	2014 NSCLC
Nintedanib	Boehringer Ingelheim	2014 idiopathic pulmonary fibrosis

Name	Company	Approval
Alectinib	Roche, Chugai	2014 Alk-rearranged NSCLC
Palbociclib	Pfizer	2015 advanced (metastatic) BC
Cobimetinib	Roche, Exelixis	2015 melanoma
Osimertinib	Astra Zeneca	2015 NSCLC with EGFR mutation
Abemaciclib	Lilly	2017 Breast Cancer
Midostaurin	Novartis	2017 Acute myeloid leukemia, mastocytosis, mast cell leukemia
Acalabrutinib	Acerta Pharma	2018 Mantle cell lymphoma
Baricitinib	Lilly	2018 Reumatoid arthritis
Binimetinib	Array	2018 Melanoma
Dacomitinib	Pfizer	2018 EGFR-mutant NSCLC
Encorafenib	Array	2018 Melanoma

2.3 Screening Process for Protein Kinase Inhibitors: Traditional Methods

2.3.1 Western Blot

The most commonly used assay for detecting the phosphorylation state of a protein is western blot. The proteins are first separated using SDS- PAGE[2] and then transferred to a polyvinylidene difluoride or nitrocellulose membrane. A phospho-specific antibody is employed to identify the protein. Many of the antibodies are quite sensitive and can easily detect the phosphorylated protein. Commonly used

[2]Separation of proteins by electrophoresis utilizes a discontinuous polyacrylamide gel as a support medium and sodium dodecyl sulfate (SDS) to denature the proteins. This method is called sodium dodecyl sulfate polyacrylamide gel electrophoresis (SDS-PAGE).

detection methods use the princliples of chemiluminescence or colorimetry. [38] [39].

Major Drawbacks:

1. This is a time consuming and labour intensive process
2. It requires optimisation of experimental conditions like separation process, buffers, etc
3. Antibodies are required for this technique, which are expensive and non-sustainable
4. Not suitable for high throughput screening

2.3.2 Mass Spectrometry

Mass spectrometry is a two-step process. The protein under study is first proteolytically digested[3] with the protease trypsin. The peptide chains are then investigated for phophorylation. The phosphorylated peptides are further studied using tandem mass spectrometry (MS/MS) to locate the phosphorylation sites. The phosphorylated peptides can be identified by comparing their masses to the list of expected peptide masses for mass increases of 80 Da, which is the mass of the phosphate group [40] [41] [42].

Major Drawbacks:

1. The signals from less abundant phosphorylated peptides may be lost amongst the more abundant non-phosphorylated peptides.
2. Peptide fragmentation and improper sample preparation may lead to decomposition of phosphate groups on the protein.

[3]The breakdown of proteins into smaller peptide chains and amino acids, catalysed by proteases is known as proteolytic digestion

2.3.3 Filtration Binding Assay

In this assay, the protein phosphorylation reaction is conducted by utilising radio-labelled [γ-^{33}P]ATP or [γ-^{32}P]ATP. The phosphorylation reaction is followed by binding of the radio labeled products to filters. The unreacted phosphate is washed away. This method is universal and can be used for any kinase and substrate without limitations. Labelling or modification of the substrate is not required and detection is independent of interference from the unreacted radioisotope [43].

Major Drawbacks:

1. This process requires radioisotopes. The handling of these need special care and precaution. The disposal of samples also needs to be done with special considerations.

2. Complex washing steps are labour intensive and time consuming.

2.3.4 Enzyme Linked Immunosorbent Assay (ELISA)

Before being taken over by more advanced techniques, ELISA systems were very widely used for drug discovery. This assay uses antibodies specific for the protein used in the test. Microtitre plates coated with antibodies are used to bind the protein. A separate antibody specific to the detection site to be analysed is then introduced. Before detection, the chemical compounds are washed away. The analysis of the phosphorylated proteins is usually by fluorometric or colorimetric techniques as the antibodies are usually labelled with highly fluorescent dyes. The intensity of the signal depends on the concentration of phosphorylated protein. The use of multiwell plates allows higher throughput as compared to other processes like Western Blot [44] [45] [46].

One of the commercially available ELISA kits is DiscoveryDot^{TM}.

Major Drawbacks:

1. The need to develop specific antibodies
2. The need for multiple washing steps limits the throughput of the assay

2.4 Screening Process for Protein Kinase Inhibitors: High Throughput Screening

Though there are different approaches to modulate the activity of protein kinases, inhibition of the catalytic site of the enzyme with ATP-competitive inhibitors remains the most promising technique. The process of drug discovery is initiated by high throughput screening of a large number of molecules [47]. Traditional methods like gel based assays, ELISAs and filter binding assays are not useful in screening a large number of molecules because they are time consuming and require postreaction steps.

In order to screen kinases, the pharmaceutical industry makes a choice between cellular based assays and biochemical assays. Cell based assays suffer from a major disadvantage where a number of 'off-target hits' or false hits are produced due to inhibition of activities other than the one being studied as number of targets are unintentionally being screened. This complicates the process by introducing the need for further analysis after the screening. Therefore, biochemical assays are preferred as a mode of screening inhibitors. Not only is it possible to fix the targets during the assay but a higher concentration of the chemical under test can be used [48]. Fluorescence based assays have been adopted for high throughput screening where the optical readout signal is generated by scintillation, chemiluminescence and electrochemiluminescence [49]. Some of the fluorescence based assays used industrially are Scintillation Proximity Assay,

Fluorescence Resonance Energy Transfer, Fluorescence Polarization and Amplified Luminescence Proximity Homogeneous Assay.

2.4.1 Scintillation Proximity Assay (SPA)

The transfer of the ^{32}P from [γ-^{32}P]ATP to a synthetic peptide or protein causes the peptide or protein to be labelled with ^{32}P. These can be captured on a filter and washed in order to separate them from ATP. The phosphorylated proteins or peptides now emits beta particles due to radioactive decay and can be measured by a scintillation counter [50]. The use of ^{33}P instead of ^{32}P allows the elimination of the washing step as separation can be done using scintillation crystals functionalized with streptavidin to which biotinylated peptides bind. The decay of the radioactive ^{33}P in close proximity to the scintillation crystal is what generates the signal for measurement [51].

GE's LeadSeeker™ is one of the commercially avialable SPAs. PerkinElmer's Flashplate® and Scintiplates® also provide this assay using microtitre plates coated with scintillation material [43].

Major Drawbacks:

1. The safety considerations while handling radioactive materials
2. The cost of disposing of the radioactive waste materials
3. False signals due to radioactive decay of [γ-^{32}P]ATP [52]

2.4.2 Fluorescence Resonance Energy Transfer (FRET)

FRET based screening techniques make use of an autofluorescent protein (AFP) couple or antibodies labelled with fluorophores, separated by a substrate

sequence and a linker. The AFP couple is capable of energy transfer between the donor and acceptor fluorophore [53]. When the substrate sequence is phosphorylated, the linker causes a conformational change of the sensor as a result of which the AFP pairs are brought together. The fluorescence resonance energy transfer between the pair of AFPs causes the donor AFP to lose fluorescence intensity and lifetime while the acceptor AFP gains in fluorescent intensity and lifetime [31] [54].

A commercially available FRET based assay is Z-Lyte^{TM} developed by Invitrogen [43].

Major Drawbacks: The need for specific antibodies is a major drawback of this approach.

2.4.3 Fluorescence Polarization (FP):

Fluorescence polarization assay is based on the principle that a heavier molecule, when excited with polarized light, will rotate more slowly compared to a lighter molecule. Polarization can be measured when a fluorescent molecule is excited with polarized light. The assay uses anti-phosphopetide antibodies and fluorescence tagged peptides. The phosphorylation of the peptides during the assay results in an increase in binding to the antibodies. The fluorophore on the antibody can now rotate more slowly, which causes the polarization of the light to change [55] [56].

There are a number of commercially available assay kits using fluorescence polarization. BellBrook's Transcreener^{TM} FP assay, DiscoveRx's HitHunter^{TM} FP assay and Millipore's KinEASE^{TM} are a few of them [43].

Major Drawbacks:

1. Antibodies required for this assay

2. Generation of false signals due to the interference from fluorescent tagging molecules and other coloured or fluorescent compounds [57] [58].

2.4.4 Amplified Luminescence Proximity Homogeneous Assay (ALPHA)

This assay utilizes two reagent coated polystyrene microbeads, a donor and an acceptor, of 250 nm diameter. The microbeads coated with anti-phosphotyrosine and anti-peptide antibodies come into proximity by a biomolecular interaction. Next, assay mixture, with the donor bead containing a photosensitizer, is irradiated with a high intensity laser at 680 nm which causes the ambient oxygen to convert to an excited singlet state. The singlet oxygen can react with the thioxene derivative present in the acceptor bead if it is in the proximity and can generating chemiluminescence. The chemiluminescenese can stimulate the fluorophores present on the acceptor bead. The detection wavelength is shorter than the excitation wavelength which reduces the chances of interference [59] [60].

A commercially available assay is PerkinElmer's $ALPHAScreen^{TM}$ [43].

Major Drawbacks:

1. Antibodies required for this assay

2. Generation of false signals due to the interference from fluorophors [49].

2.5 Electrolyte-Insulator-Semiconductor (EIS) Structures as Biosensors

Capacitive EIS structures are attractive candidates when it comes to fabrication of multiplexed electronic sensors. The main reason for their widespread use is the fact that they provide the possibility of on-chip integration to yield sensor arrays. The speed of response coupled with the ease of fabrication allows them to be applied as sensors in a number of different fields [61]. Figure 2.3 shows the schematic of a typical EIS structure.

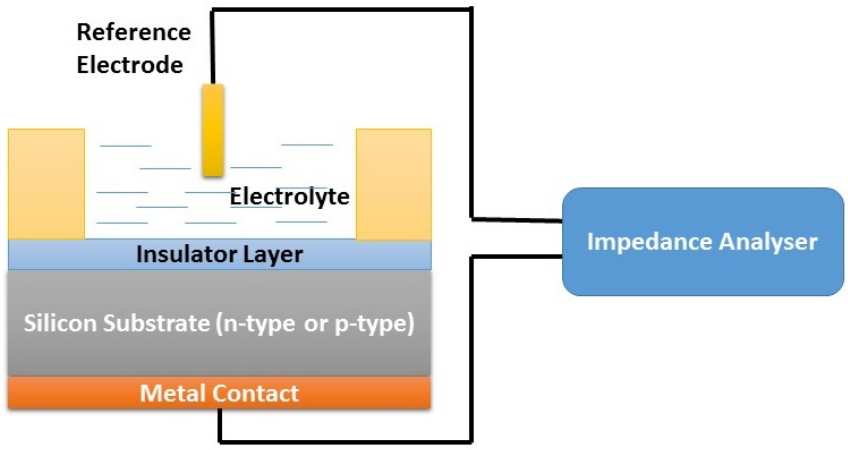

Figure 2.3: Schematic of EIS Structures

The sensor design consists of a silicon substrate (p-type or n-type) which is separated from the electrolyte by an insulator layer. A 'binding' or sensing layer is present on top of the silicon substrate. The mechanism of charge detection is that the presence of the biomolecule exerts an electric field on the substrate and modifies its space charge or depletion region. The presence of immobilized ions acts as an added dielectric along with the insulator. The overall capacitance of the structure is the sum of series capacitance of silicon dioxide and the depletion layer capacitance. The oxide layer capacitance being constant, the total capacitance depends on the depletion layer [62].

The charges from solution accumulate on top of the insulator layer. The ions that accumulate between the electrolyte and charges on the active surface form an electrical double layer close to the surface [63].

When silicon nitride layer is used as an insulator, the exchange of H^+ ions between the solution and the binding sites on the Si_3N_4 surface determines the surface potential. The silanol (SiOH) and the primary amine $SiNH_2$ groups are the two binding sites on silicon nitride which undergo the following reactions to generate a surface potential [64] [65]:

$$SiOH \longleftrightarrow SiO^- + H^+$$

$$SiOH + H^+ \longrightarrow SiOH^{2+}$$

$$SiNH_2 + H^+ \longrightarrow SiNH_3{}^+$$

Change in the surface charge occurs due to change in the pH of the electrolyte. The typical capacitance versus voltage characteristics of an EIS structure with p-type silicon substrate (using a varying dc voltage superimposed on a small ac signal) is shown in Figure 2.4. When a negative voltage is applied, the holes from the bulk silicon are attracted to the semiconductor-insulator interface where they accumulate. In the accumulation region, the EIS capacitor behaves like a conventional parallel plate capacitor and the total capacitance is the measure of the capacitance of the insulator layer (C_i). This is also the maximum capacitance of the system (C_{max}).

When a small positive voltage is applied, the holes are repelled from the same interface resulting in a region depleted of majority charge carriers. The total capacitance is now represented as the series combination of C_i and the varying capacitance of the depletion region. At higher values of positive voltages, the electron concentration at the interface exceeds the hole concentration and the device begins to behave like an n-type semiconductor. If the frequency of the signal

is high (1000 Hz or more), the generation of the charge carriers is not fast enough to attain equilibrium. Hence, the change is not reflected in the C-V curve [66]. The device contains some electrically active defects located at the interface between the insulator and the semiconductor which is capable of trapping and de-trapping charge carriers. These are known as interface traps. At high frequencies (100Hz or more), the effect of these traps is dampened. The time required to generate a trapped charge response is longer than an untrapped charge carrier. At low frequencies, the interface traps are able to follow the oscillations and contribute to the excess capacitance seen at the output. This is the reason why high frequencies are preferred during the capacitance-voltage measurements [62] [67].

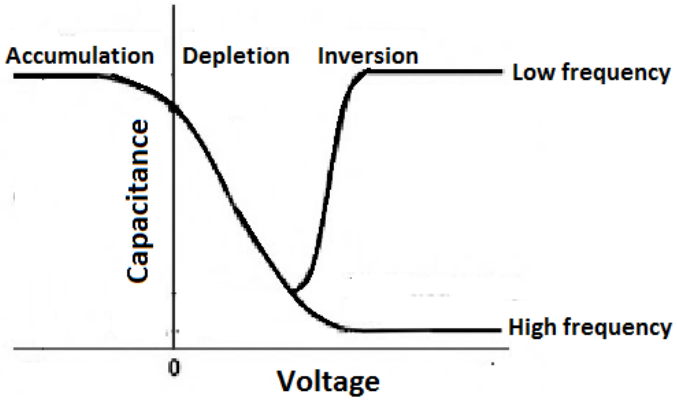

Figure 2.4: Capacitance versus voltage curves for EIS structures with p-type semiconductor

EIS sensors have been used extensively for the detection of biomolecules like DNA [68] [69], enzyme reactions [70] [71] and other charged macromolecules [72]. Miniaturised pH sensors integrated within flow cells have also been reported in literature [73]. In 2014, Bhalla and co-workers reported the detection of protein phosphorylation by detecting the changes in pH due to release of protons during the process, using EIS structures. For the phosphorylation of Myelin Basic Protein (MBP), a change in surface of +3.3 C was observed which results in a local pH change from 7.2 to 8.8. As a consequence of this, the threshold potential of the EIS structures (n-type silicon substrate) changed by 37 mV as compared to the control.

A pH sensitivity of 51.7 mV/pH was achieved in this study. [74].

2.6 Ion Sensitive Field Effect Transistors (ISFET) as Biosensors

An ISFET can be simply described as a MOSFET where the gate metal is replaced by an electrolyte which is in direct contact with the gate insulator. The expression for drain current is the same as the one for MOSFET when it is not in the saturation mode, as shown below:

$$I_{DS} = C_{ox}\mu\frac{W}{L}(V_{GS} - V_t) - \frac{1}{2}V_{DS}^2$$

where C_{ox} is the oxide capacity, μ is the electron mobility in the channel, W/L is the ratio of width and length of the channel, V_t is the threshold voltage.

When the geometric sensitivity parameter $\beta = C_{ox}\mu\frac{W}{L}$, threshold voltage and the applied drain to source voltage are constant, the drain current I_{DS} is a function of the gate to source voltage V_{GS} [75]. The schematic of a typical ISFET is shown in Figure 2.5.

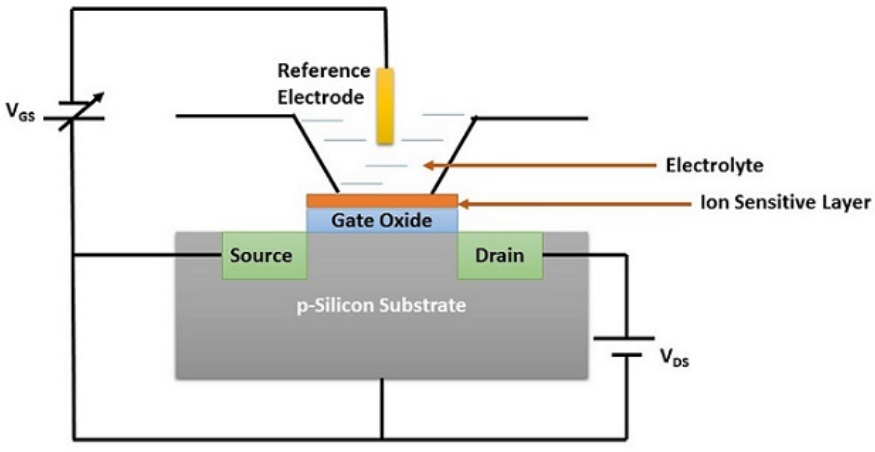

Figure 2.5: Schematic of an ISFET (V_{GS} and V_{DS} are the gate to source and drain to source voltages respectively)

Modifying the gate terminal of the ISFET with ion sensitive materials like silicon nitride makes it sensitive to pH variations. The binding of charged biomolecules at the gate terminal is analogous to changing the gate voltage. The charged molecules result in a change in electric field at the gate, which is responsible for change in channel conductance of the ISFET. This affects the value of external gate voltage required to switch the device to its on or off state [76] [77]. Figure 2.6 shows the pH dependent drain current versus gate voltage characteristics of an n-type ISFET containing silicon nitride at the gate.

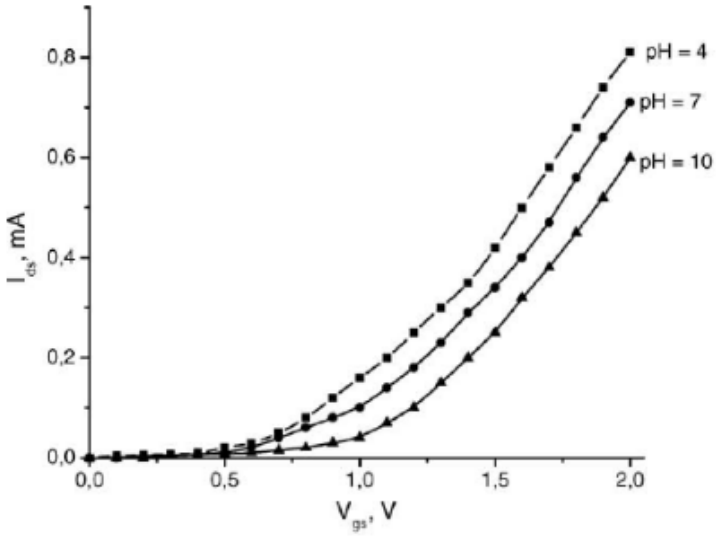

Figure 2.6: Change in drain current versus gate voltage for a fixed drain to source voltage measured at different pHs for an n-type ISFET with silicon nitride at the gate [78]

ISFETs have been commercialised as pH sensors by several companies. One example of a commercial ISFET pH sensor is Durafet® by Honeywell. Over the years, the surface charge sensitivity of ISFETs have been exploited for a number of sensors for charged molecules like DNA, RNA, peptides, proteins, enzymes and cells [77] [79]. In 2007, Freeman and co-workers studied the phosphorylation and dephosphorylation of a peptide using ISFETs in the presence of a protein kinase [80].

2.7 Organic Thin Film Transistors (OTFTs) as Biosensors

The increasing popularity of OTFTs compared to silicon based field effect transistors can be attributed to a number of reasons. Conventional silicon technology requires high temperature high vacuum processes for deposition and sophisticated photolithography techniques for patterning. OTFTs can be fabricated using low temperature deposition and solution methods which facilitates the use of high-throughput manufacturing like spin coating [81] or printing [82]. Organic materials also possess mechanical flexibility which makes them compatible with flexible substrates such as plastic. This makes them excellent candidates for low cost, lightweight, foldable products [83].

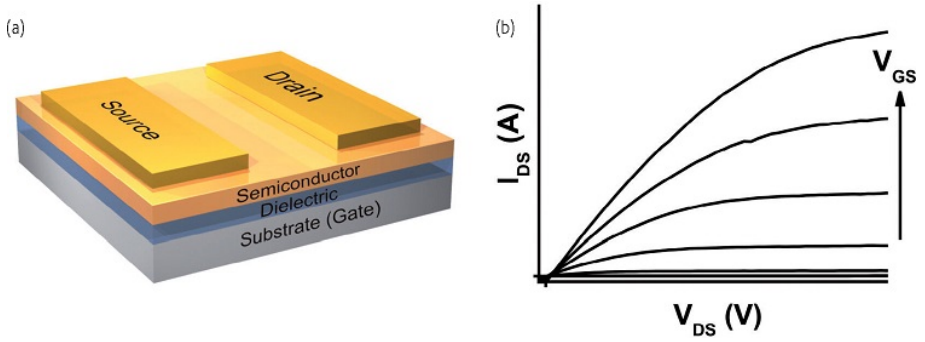

Figure 2.7: (a) Schematic of a typical organic thin-film transistor and (b) Typical output curves for an OTFT highlighting the relationship between I_{DS}, V_{DS} and V_{GS}. [84]

Similar to inorganic FETs, OTFTs consist of three device terminals. There are three metal electrodes, a dielectric layer and a thin film of organic semiconductor. The dielectric or insulator layer separates the semiconductor from the metal gate electrode. [84]. The semiconductor layer may consist of small molecules like pentacene [85], anacene [86], oligomeres [87] or polymers like

polythiophenes [88] [89] or carbon nanotubes [90].

The operation of the OTFTs is analogous to inorganic FETs. The current flow between source and drain can be controlled by the bias applied to the gate terminal. Unlike inorganic materials, current is carried by majority charge carriers in organics [83]. Capacitive coupling between the gate electrode and semiconductor layer induces charges on the semiconductor layer on application of the gate bias [91]. The channel current of an OTFT is given by: [92]

$$I_{DS} = C_i \mu \frac{W}{L}(V_g - V_t - \frac{V_{DS}}{2})V_{DS} \qquad V_{DS} << V_g - V_t$$

$$I_{DS} = C_i \mu \frac{W}{2L}(V_g - V_t)^2 \qquad V_{DS} > V_g - V_t$$

where I_{DS} is the channel current between source and drain, W and L are the width and length of the channel, respectively, μ is the mobility of the carrier, C_i is the capacitance of the gate insulator, V_g is the gate voltage, V_{DS} is the applied source-drain voltage, and V_t is the threshold voltage of the device. The channel current can be modulated by change in device parameters namely, μ and V_t due to interaction with the target analyte [93].

Several biosensors such as glucose sensors [94], dopamine sensors [95] and DNA hybridisation sensors [96] employ OTFT devices for measurement. They can also be integrated within cells due to their inherent biocompatibility [97].

2.8 Reference Field Effect Transistors (REFET) for Biosensing

The REFET configuration (shown in Figure 2.7) involves the design of two transistors on the same chip. One of them is an ISFET sensitive to ions while the other is a reference FET desensitized to ions. A metallic pad or strip acts as a pseudo or quasi reference electrode to ground the measuring solution [98]. The two FETs should ideally have identical electrical and chemical properties. The metal-electrolyte interface may generate an unstable potential which when measured by a differential configuration of the ISFET and REFET does not result in an output voltage as it is suppressed as a common mode signal. When a change in pH of the solution occurs, a differential signal will be generated at the output because the ISFET is sensitive to the change while the REFET is not [99].

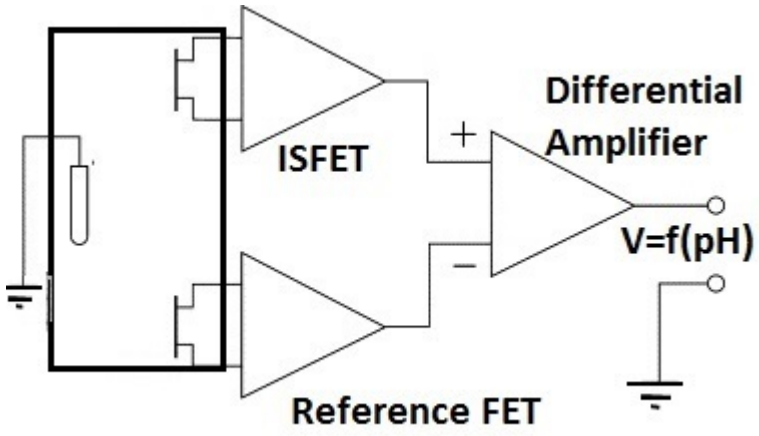

Figure 2.8: Block diagram of ISFET/REFET measuring system where the output voltage is a function of pH changes in the solution

Since the ISFET and REFET are used in a differential configuration effects due to changes in light, ambient temperature and other sources of noise are eliminated as common mode signals [75]. Modifying the gate of a MOSFET such

that it is completely insensitive to pH or any changes in concentration has proved to be a challenge. The first reported REFET was constructed by coating the silicon nitride gate of a MOSFET with parylene and showed a pH sensitivity of 10 to 30 mV/pH [100] [101]. Since then a number of applications of REFETs with varying pH sensitivities have been developed. This configuration is compatible with the commercial CMOS process which allows the ease of fabrication, miniaturization, low cost and simple packaging [102] [103] [104].

Several different materials have been used to form the inert layer of the reference FET. Oxidizing the Si_3N_4/SiO_2 dielectric to $SiO_xN_y/Si_3N_4/SiO_2$ showed a pH sensitivity of 18-20 mv/pH [105]. Others have used polymers such as polypyrrole on tin oxide/indium tin oxide surface [106] and teflon [107]. Low pH sensitivities have been reported with the use of a thick layer of polyvinyle chloride (PVC) (pH sensitivity 1.8 mV/pH) [108] and acrylate layers (pH sensitivity less than 1 mV/pH) [99]

REFETs have been used as sensors for a number of applications other than simple pH sensors. The detection of urea [109], glycated haemoglobin [110] and nucleic acid amplification [111] to name a few.

2.9 Field Effect Devices for Detecting Protein Phosphorylation

A number of studies have utilised field effect devices for the detection of protein or peptide phosphorylation. The change in charge of the substrate protein and the release of proton on phosphorylation can be used to detect this reaction. Freeman *et al.* in 2007 reported an ISFET based detection system for the activity of casein kinase II enzyme. The aluminium oxide gate of an ISFET was modified with a self assembled monolayer of peptide. The shift in transfer characteristics were

measured on introduction of the enzyme and ATP. A shift of 40 mV was achieved over 20 minutes. This sensor was made reusable by dephosphorylating the peptide on introducing an alkaline phosphatase [80].

In a study conducted by Bhalla *et al.* in 2014, protein phosphorylation was detected based on proton release phenomena. Electrolyte-insulator-semiconductor structures made by silicon nitride coated silicon wafers were modified with myelin basic protein. The shift in capacitance versus voltage characteristics was 37 mV after 13 minutes of incubation with ATP, PKC lipid activator and PKC-α kinase. The control signal showed a negligible shift of 1.9 mV [74]. In another study by the same author, aluminium oxide extended gates modified with protein was used for phosphorylation detection through ISFETs. A 44 mV shift in the transfer characteristics was reported after 10 minutes of incubation with ATP, PKC lipid activator and enzyme [112].

Measurement of phosphorylation kinetics on a large array of ISFETs was patented in 2012 by Lindsay and Labaer. Nucleic Acid Programmable Protein Arrays (NAPPA) were proposed in combination with ISFET arrays to to enable very large kinase enzyme activity assays [113].

2.10 Summary of the Literature Review

Protein kinases are major drug targets and the drug discovery of protein kinase inhibitors is of paramount importance for both industry and academia. The drug discovery process of protein kinase inhibitors has moved towards high throughput screening with the ability of screen large libraries of molecules per day as opposed to the traditional labour intensive and time consuming processes. From the literature, it can be concluded that the present high throughput assays for protein kinase inhibitors still rely heavily on the use of radio tags, fluorophores and/or antibodies and the readouts are predominantly fluorometric. The problems

associated with assays can be summarized as follows:

1. Traditional methods cannot be used for HTS assays as they are labour intensive, time consuming and cost inefficient
2. Radio tagging requires safety considerations and proper reagent disposal infrastructure
3. Use of fluorescent tags, fluorophores and antibodies come with an added cost
4. The readout systems are susceptible to false signals and interference from other compounds

Field effect devices like EIS structures, ISFETs and OTFTs are excellent for biosensing technologies that require low cost of production, ease of fabrication and can be constructed into sensor arrays.

2.11 Objectives of the Project

In this project, the development of a high throughput multiplexed sensor array for the screening of protein kinase inhibitors is investigated which can address the drawbacks of the present systems. It is our aim to move towards a low cost, high throughput, portable sensor for drug discovery.

1. To design a label free, antibody free biosensor array for high throughput screening of kinase inhibitors. The sensor array should be compatible with the 96 well microtitre plate such that it is compatible with exiting methods of sample delivery.
2. To identify a suitable pH sensitive field effect device to act as an ISFET. The device should be easy to interface with a printed circuit board (PCB). The

activity of the device will be tested using a single protein kinase inhibitor to prevent phosphorylation, as a proof of concept.

3. To develop a suitable pH insensitive layer to act as a reference FET. The device should ideally have no response to the protein phosphorylation reaction or the presence of the inhibitor.

4. To construct a REFET structure along with the necessary instrumentation for the biosensor. The 'active' and the 'inactive' device should combined to provide a system for differential measurement such that the reference electrode can be eliminated.

Chapter 3

EIS Structures and Organic Thin Film Transistors for Screening Protein Kinase Inhibitors

3.1 Design and testing of PCB based EIS biosensor for Screening Protein Kinase Inhibitors

3.1.1 Introduction

This section explores the possibility of using an array of EIS capacitive structures mounted on a PCB as a detection tool for protein phosphorylation. The suitability of silicon wafers coated with silicon nitride (Si_3N_4) as EIS biosensors for the detection of protein phosphorylation was investigated by Nikhil Bhalla *et al.* in 2015 [112]. EIS structures are field effect devices similar to a metal oxide semiconductor (MOS) capacitor where the metal layer has been replaced by a reference electrode immersed in an electrolyte. For this study, the Si_3N_4 coated silicon wafers were attached to the copper pads of a PCB to form an electrode array as an extension of Nikhil's research.

Stuart Lindsay in 2012 introduced the concept of associating pH changes with phosphorylation [114]. The change in pH due to release of H^+ ions is responsible for the change in surface charge of the EIS sensor. By observing the capacitance versus voltage (C-V) characteristics of the sensor, the change in its surface potential can be determined.

3.1.2 Materials and Methods

PCB design and processing

A printed circuit board was designed using DesignSpark PCB (version 7.2). The copper contact pads were distributed such that they fitted under the wells of a standard 96 well microtitre plate (Figure 3.1). For testing purposes, a small portion of the PCB (shown in Figure 3.2) containing four contact pads was manufactured on double sided copper clad FR4 material using an LPKF S63 PCB milling machine.

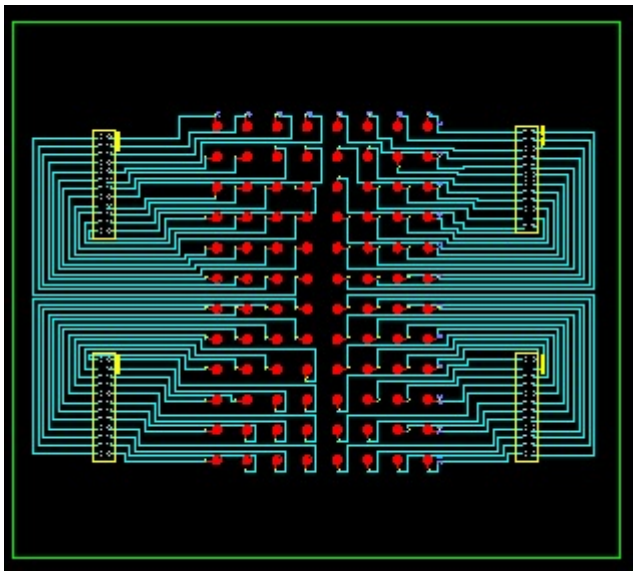

Figure 3.1: PCB design for the 96 well plate compatible sensor array (160 mm x 180 mm

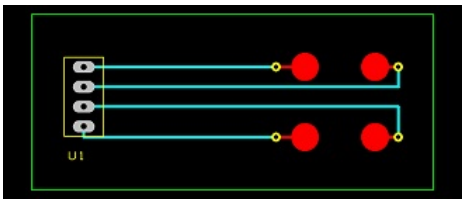

Figure 3.2: Test PCB (52 mm x 25 mm)

P-type silicon wafers (obtained from the University of Applied Sciences Kaiserslautern), coated with 50 nm of silicon dioxide and 100 nm of silicon nitride with 100 nm of aluminium deposited as a back contact, were used for this study.

To clean the wafers RCA cleaning was attempted at first. The wafers were cut into approximately 7mm squares using a diamond scribe. Then they were immersed in a solution of NH_4OH:H_2O_2:H_2O (1:1:5) for 5 minutes at (90°C). This step was performed to remove organic contaminants from the surface. After a thorough rinse in DI water, the wafers were immersed in HCl:H_2O_2:H_2O (1:1:6) for 5 minutes to remove inorganic contaminants. The wafers were rinsed in DI water and dried in nitrogen gas [112]. Unfortunately, this process resulted in the removal of the aluminium back contact on the wafers. Some deposits of aluminium could be observed on the silicon nitride surface. The use of other rigorous chemical cleaning techniques like piranha cleaning was avoided as the acids used in these techniques could similarly damage the wafers. Instead, they were rinsed thoroughly with acetone and isopropanol and dried with nitrogen gas followed by UV-Ozone cleaning.

Biofunctionalisation of the Silicon Nitride Surface

All chemicals were of analytical grade and were used as received, unless otherwise specified. All aqueous solutions were made with double de-ionised water, 18.2 MΩ cm, with a Pyrogard filter (Millipore, USA). Adenosine tri-phosphate (ATP), (3-glycidyloxypropyl)trimethoxysilane (GOPTS) and Dulbecco's

Phosphate Buffered Saline were purchased from Sigma-Aldrich. The peptide under test was synthesised in the Department of Pharmacy and Pharmacology, University of Bath. Protein Kinase C-alpha (PKC-α) human recombinant kinase produced in Sf9, was procured from SignalChem, UK. PKC lipid activator cocktail was obtained from Millipore. Kinase inhibitor used in this study, GF 109203X (90%), was purchased from Sigma Aldrich.

In the study conducted by Nikhil Bhalla, Myelin Basic Protein (MBP) was used along with two peptides for phosphorylation studies. Peptides are molecules smaller than proteins which have 50 or fewer amino acids [115]. The peptides, both containing a single phosphorylation site, were synthesised in the University of Bath, Department of Pharmacy and Pharmacology. Compared to Myelin Basic Protein, choosing a peptide is a more cost effective alternative and is sufficient for proof of concept experiments. In this project one of the two peptides was used, CRRRKGSFRRKK-OH. It was assessed to be 95% pure by High Performance Liquid Chromatography (HPLC). The composition was confirmed using mass spectroscopy. Figure 3.3 shows the structure, sequence, formula and molecular weight of the peptide.

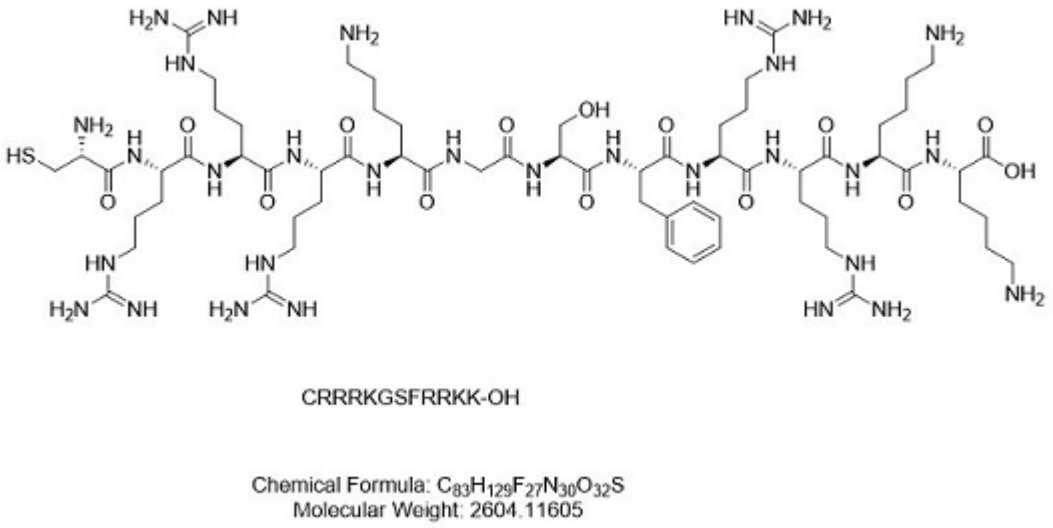

Figure 3.3: Structure, sequence, formula and molecular weight of the peptide used in the study

The silicon nitride coated wafers were attached to copper contacts pads of the PCB using silver conductive paste (RS PRO Silver Conductive Paint procured from RS Components Ltd). This conductive paste has a low volume resistivity of 0.001Ωcm when fully hardened. After applying the paste on to the copper pads, the wafers were attached and the boards were baked at 130°C for 5 minutes to harden and improve electrical characteristics as suggested in the product datasheet. This method proved to be the most successful and reproducible for mounting the wafers on the PCB. Soldering the wafers directly on to the PCB pads was attempted but preventing the solder from flowing to the Si_3N_4 thin film proved to be challenging. The use of reflow soldering using electrically conductive silver epoxy showed similar challenges where the top and bottom of the wafer often became electrically shorted. The sensors were clamped down to the PCB using Teflon tape (3M UHMW tape procured from RS Components) with a 3 mm diameter circular hole punched to expose the silicon nitride surface. The tape had the additional benefit of preventing the edges of the wafer from being exposed and liquids seeping under them. Plastic wells where attached using silicone sealant leaving a circular interrogation area of

approximately 7.07 mm^2 (shown in Figure 3.4).

To silanise the wafers, both liquid and vapour phases were attempted. During UV-Ozone cleaning, the silicon nitride surface is oxidised to generate functional silanol (Si-OH). GOPTS binds covalently to the silanol and leaves a free epoxy end chain on the surface. The amine group of the peptide can bind to the epoxy group of the silane. This process is useful in reducing non-specific peptide absorption on the surface [116]. In the liquid phase, the clean wafers were incubated in 98% GOPTS for 45 minutes after which they were rinsed in de-ionized water (DI) to remove the excess silane. In the vapour phase, GOPTS was heated to its boiling point (120°C) and the clean wafers were exposed to the silane vapours for five seconds. They were rinsed with DI water and dried. The silianised surface contains epoxide groups capable of covalently bonding to the amine groups of the peptide [117]. The binding usually happens preferentially through the primary amine [118]. The immobilisation and phosphorylation protocol was optimised by Nikhil Bhalla [112]. We have attempted to follow the protocols closely by maintaining the same concentration of reagents and incubation times. 2 μl of 156 μM peptide solution was dispensed onto the wafers through plastic wells and left to bind for 40 minutes. Figure 3.5 shows the steps for immobilising the peptide on the silicon nitride surface. Unreacted sites of GOPTS were blocked by washing the wafers with 20% ethanol. The epoxide groups convert to ether on reacting with ethanol [119] . The modified wafers were allowed to incubate in PBS 7.2 for 30 minutes to stabilise the surface before conducting further measurements.

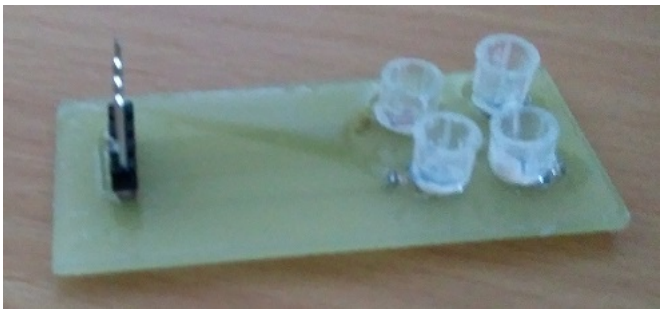

Figure 3.4: PCB used for testing

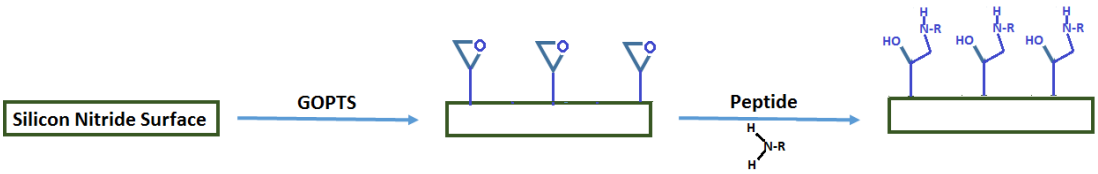

Figure 3.5: Peptide immobilisation steps

Phosphorylation Studies

The phosphorylation reaction was carried out in phosphate buffered saline (PBS) at pH 7.2. The reaction volumes were fixed to 50 μl for all replicates and controls. 1 μM ATP, 2 units of PKC-alpha kinase and 2.5 μl PKC lipid activator (containing containing 0.5 mg/ml phosphatidylserine and 0.05 mg/ml diacyglycerol in 20 mM MOPS (pH 7.2), 25 mM β-glycerol phosphate, 1 mM sodium orthovanadate, 1 mM dithiothretiol and 1 mM calcium chloride) were added to phosphorylate the immobilised peptide on the surface of the sensor. The reaction was allowed to take place for 13 minutes before taking the capacitance vs voltage (C-V) measurements. 13 minutes was the time taken for the phosphorylation reaction to stabilise as reported by Nikhil in his study [112].

The control reaction was carried out in the presence of ATP and PKC activator in the absence of the enzyme to prevent the protein phosphorylation reaction from taking place.

Device Setup

A silver wire coated in silver/silver chloride ink (ALS Co. Ltd) was used as a reference electrode. A two electrode setup, with the copper contact pad acting as the working electrode, was used to measure the capacitance-voltage characteristics of the sensor. Figure 3.6 shows a schematic of the sensor setup.

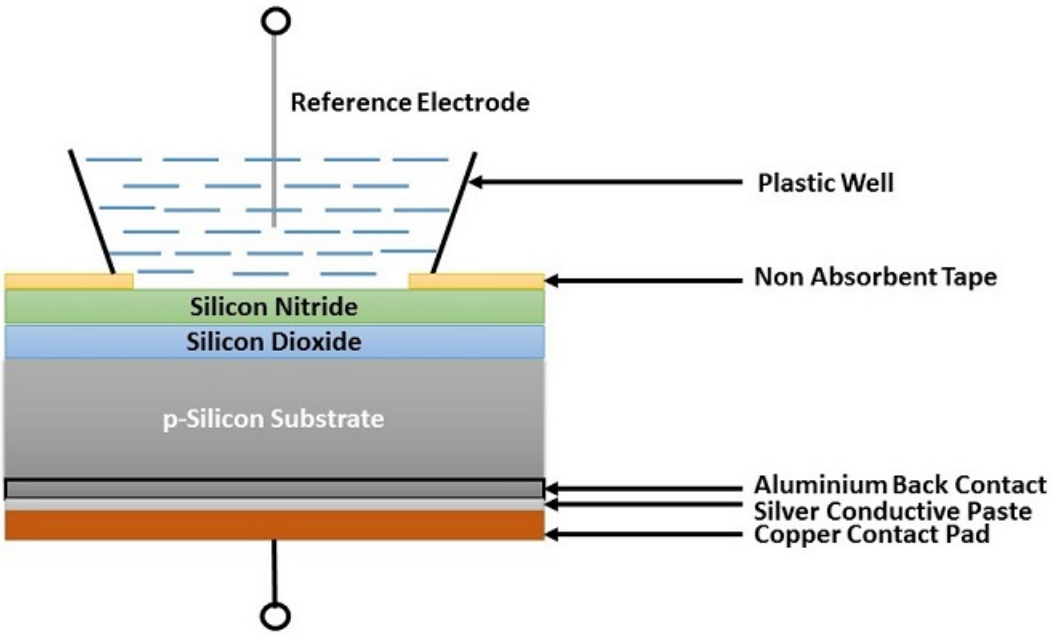

Figure 3.6: Schematic of the sensor setup

Capacitance vs voltage (C-V) measurements were conducted using a CompactStat digital potentiostat (Ivium Technologies, The Netherlands). The dc voltage between the reference electrode and the copper pad was varied between -2 V and 2 V with a superimposed ac signal of 10 mV at 1 kHz. Initial tests to investigate pH variations on the silicon nitride surface showed that 1 kHz produced the most stable and reproducible C-V curves. Measurements at lower frequencies were not reproducible. The experiments were conducted from within a Faraday cage to keep noise levels to a minimum. All measurement were performed on three different test boards containing 4 pads each and the average of the 12 readings

were considered. The voltage shifts were observed as the shift in threshold voltage. The errors was determined by the standard deviation of the data. The measurement setup is shown in Figure 3.7.

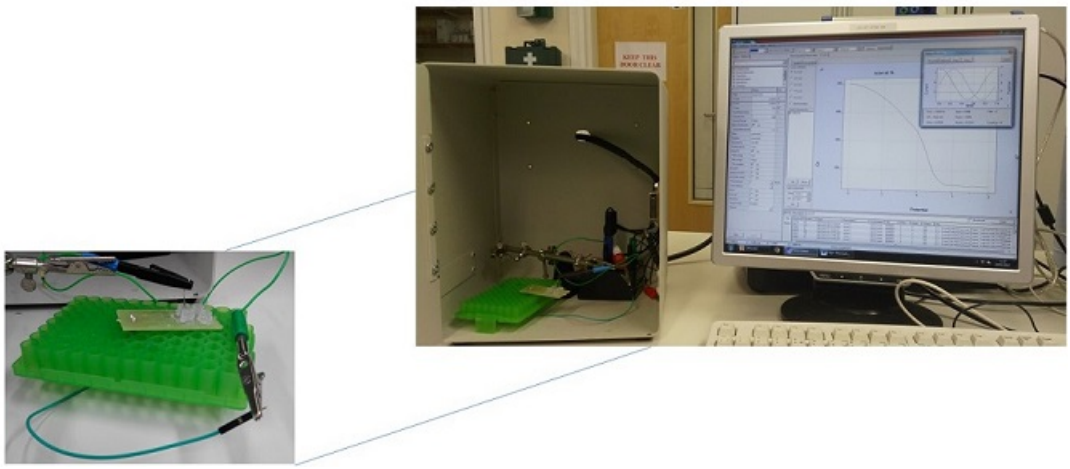

Figure 3.7: The experimental setup

3.1.3 Results and Discussion

pH Sensitivity

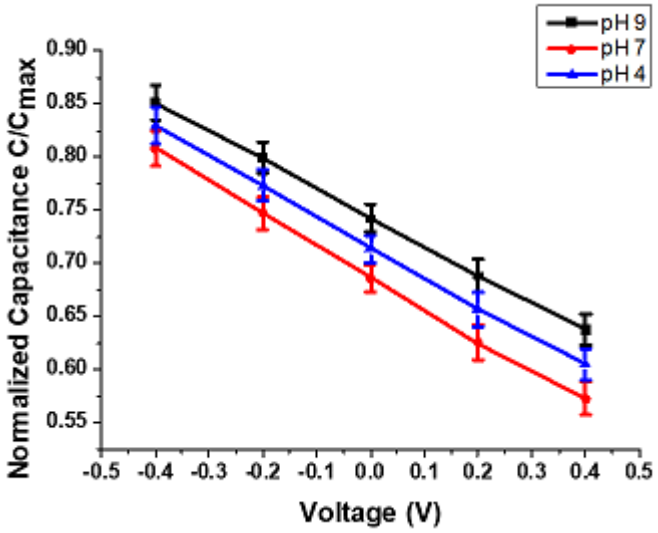

Figure 3.8: C-V curves for pH sensing

Figure 3.8 shows the capacitance vs voltage curves for different pH values on the silicon nitride surface as measured by the Ivium Potentiostat. The wafers were not silanised for this study. 10 mM PBS with pH 4, 7 and 9 was used for the measurement. The buffers were prepared by mixing monobasic and dibasic phosphate solutions at specific ratios. The studies were conducted at 1000Hz in accordance with the studies conducted by Nikhil Bhalla [112] where the results at 1000Hz was found to be the most reproducible. A pH sensitivity of 49.2±4.1 mV/pH was achieved. Figure 3.8 shows a small voltage range between -0.5V to 0.5V. As the voltage changes from negative to positive, the EIS structures move from the accumulation to the depletion region. The change in surface charge due to change in pH of the electrolyte causes this change to happen at different voltages for different pH values. The pH sensitivity is measured around the reported voltage range as this is close to the 'threshold' voltage at which inversion takes place.

Stability

After allowing the wafers with peptide immobilised to stabilise for 30 minutes in PBS 7.2, the C-V curves were measured repeatedly for twenty minutes (Figure 3.9). Any stability measurements carried out prior to the thirty minutes of stabilisation showed a lack of reproducibility. The wafers silanised with GOPTS in the liquid phase and vapour phase did not show any differences in the stability measurements. A maximum of 3 mV shift is observed in the twenty minute interval. This shows that the surface is stable for carrying out the phosphorylation studies which require a 13 minute incubation time.

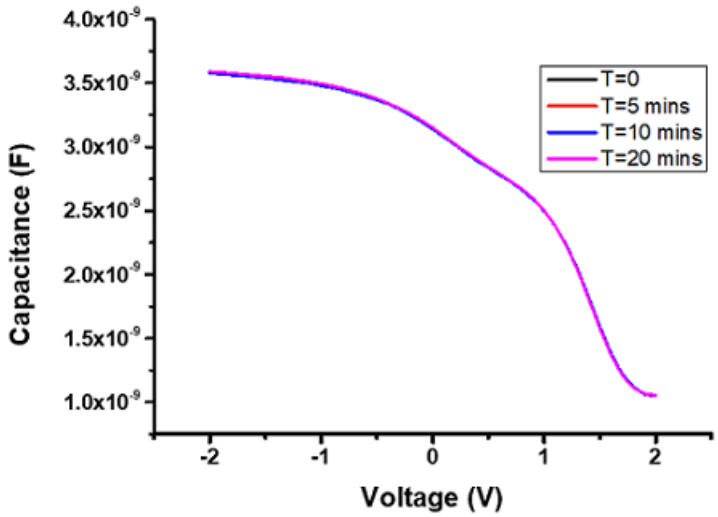

Figure 3.9: Capacitance vs voltage curves depicting the stability of peptide on silicon nitride surface

Phosphorylation

The surface silanised with GOPTS in the liquid phase produced a noisy and unstable C-V curve as shown in Figure 3.10. The reason for this is the possible interaction between the adhesive of the teflon tape and GOPTS which led to the contamination of the sensor surface. On visual inspection of the sensors, a thin

translucent film was observed on the surface. The method of silanisation was then changed to the vapour phase which yielded a smooth C-V curve as shown in Figure 3.11.

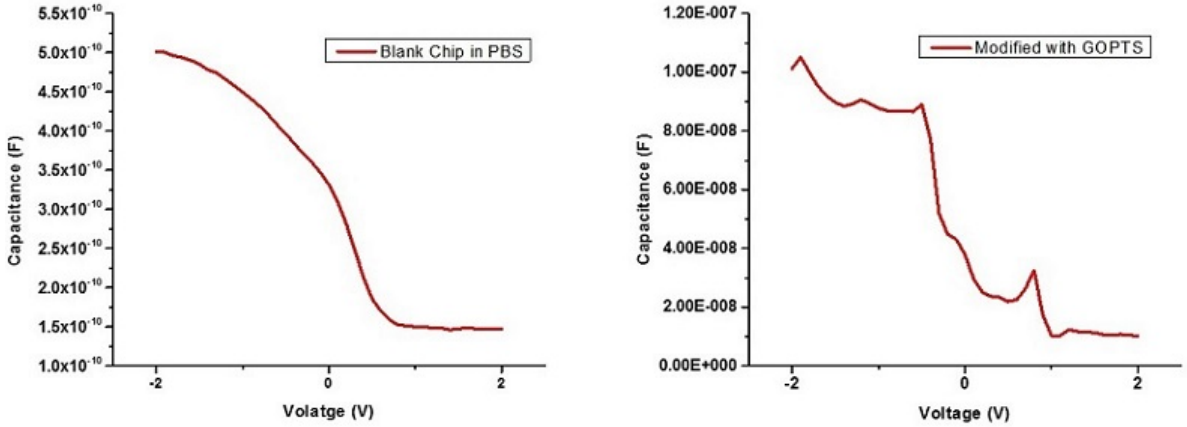

Figure 3.10: Left: C-V curve for a blank chip in PBS, Right: C-V curve after silanization in liquid GOPTS

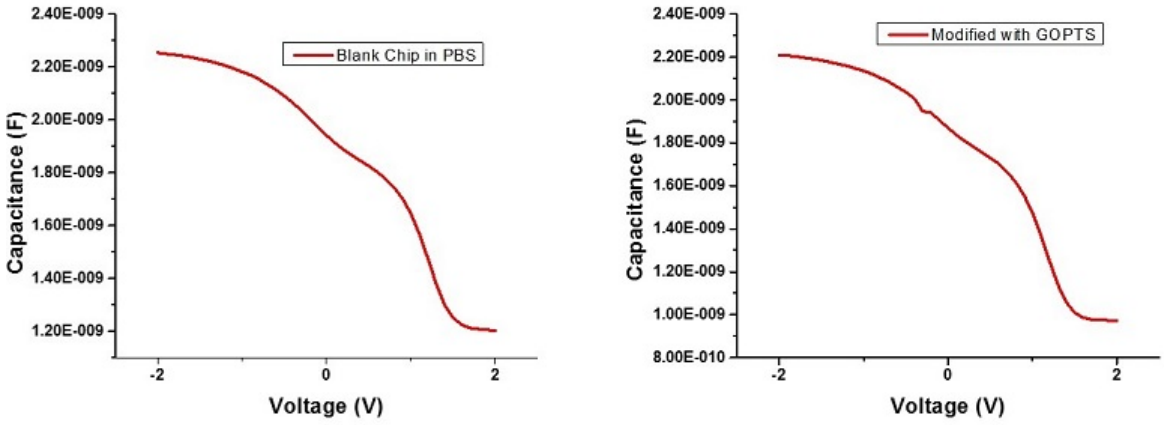

Figure 3.11: Left: C-V curve for a blank chip in PBS, Right: C-V curve after silanization in GOPTS vapours

In the study conducted by Nikhil Bhalla the immobilisation of the protein and peptide is confirmed using the TMB assay. The immobilisation of myelin basic protein (TMB) on the silicon nitride surface was confirmed by adding an anti-MBP

antibody followed by a secondary antibody linked with horseradish peroxide (HRP). TMB, T-4444(3,3,5,5-Tetramethylbenzidine), was then dispensed on the surface and the absorbance was measured by a spectrophotometer. The expected peak at 450nm was 10 times higher for the surface with protein immobilised compared to the blank surface. The results of the phosphoylation studies are shown in Figure 3.12 and 3.13. The sensors modified with peptide were first measured in PBS 7.2. This was followed by the control reaction in the absence of enzyme. This only produced a small shift of 3 mV. The phosphorylation reaction produced a much larger shift of 48 mV which was stable after 13 minutes.

Similarly, the inhibition reaction in the presence of kinase inhibitor was carried out after measurement in PBS and the control reaction. The inhibition reaction produced a shift of 3 mV similar to the control reaction. The inhibition and phosphorylation reactions were not performed on the same sensor surface due to ensure that there are no contamination issues.

When a negative voltage is applied through the solution, the positively charged holes in the bulk silicon are attracted to the semiconductor-insulator surface. The maximum capacitance C_{max} is the measure of capacitance of the insulator layer as the behaviour of this device similar to a parallel plate capacitor. When a small positive voltage is applied, the holes are repelled from the semiconductor-insulator interface resulting in the depletion of majority charge carriers. Due to phosphorylation of the peptide, protons are released which are adsorbed on to the sensor surface resulting in the inversion occurring at a lower voltage.

The capacitance in the accumulation mode is the capacitance of the dielectric, the silicon dioxide and the silicon nitride in series C_{max}.

$$C_{max} = \epsilon_i / t_i$$

where ϵ_i is the permittivity of the insulator and and t_i is the thickness of the insulator layer.

$$\epsilon_i = \epsilon_0 \epsilon_r$$

where ϵ_0 is the permittivity of free space $8.854X10^{-14}F/cm^{-1}$, ϵ_r is the relative permittivity of the insulator (3.9 for silicon dioxide and 7 for silicon nitride). Taking the thickness of the oxide and nitride layer in consideration, the calculated capacitance come out be 2.31 nF which is very close to our observed value of 2.25 nF in Figure 3.11. The variability in the maximum capacitance value between experiments was due to the inability to control the interrogation area on using silicon sealant as an adhesive.

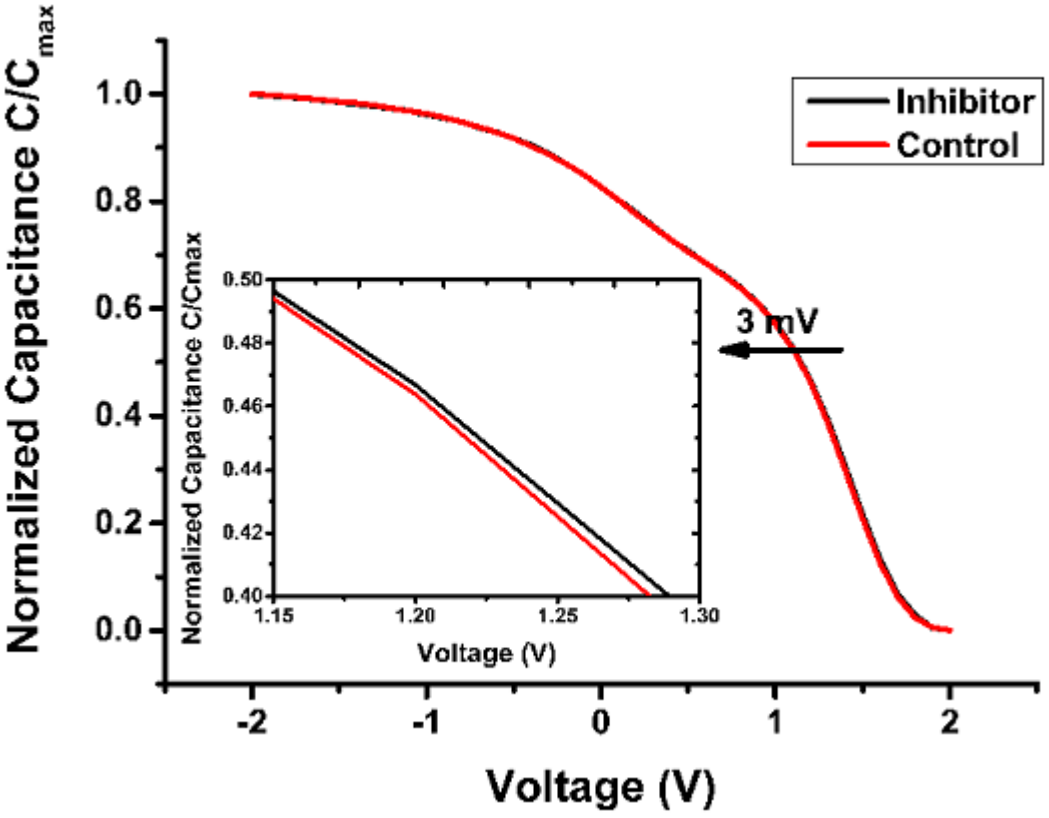

Figure 3.12: C-V curves for control and inhibitor reactions

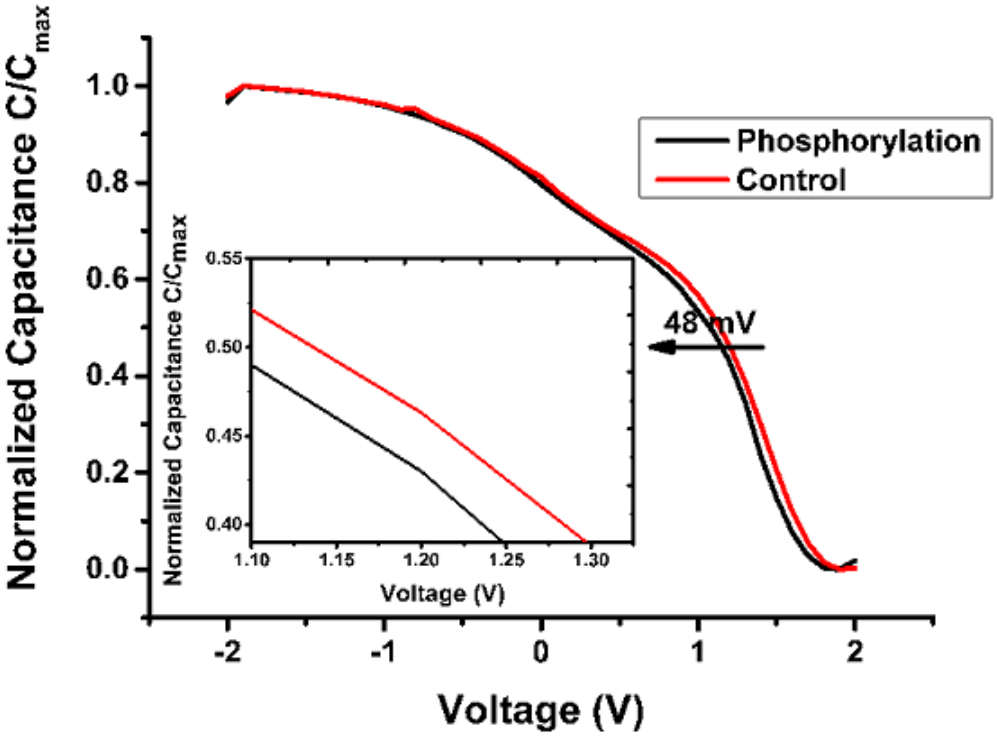

Figure 3.13: C-V curves for control and phosphorylation reactions

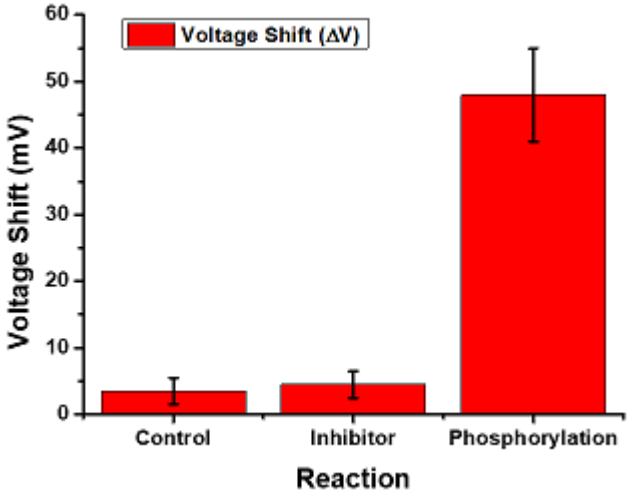

Figure 3.14: Voltage shifts from the baseline for control, inhibitor and phosphorylation reactions

3.1.4 Conclusion

This study was the first step towards developing a printed circuit board based biosensor for the screening of kinase inhibitors. Using silicon nitride wafers attached to a PCB with conductive paste, protein phosphorylation was detected.

However, this approach has some limitations. The process of attaching silicon wafers to the PCB can be quite laborious when the number of sensors on the board are increased from 4 to 96. The presence of silver conductive paste made the process of washing the chips quite challenging as the exposure to liquids results in the paste dissolving and loss of electrical contact between the PCB and the wafers. The adhesion provided by the silver paste is only temporary which limits the portability of the device. On drying completely, the wafers were removed from the surface of the PCB. The use of silicone sealant to secure the wells makes it challenging to maintain the same interrogation area in every experiment. While the results were promising, with a 45mV difference in the phosphorylation and control rections, the preparation of the sensor was time consuming and unreliable.

In conclusion, this approach works in principle but may not be be very practical for scaling up to an array of sensors. Therefore, in the following sections, other techniques were explored to come closer to our aim of developing a portable sensor array for screening protein kinase inhibitors.

3.2 Organic Thin Film Transistors as for Screening Protein Kinase Inhibitors

3.2.1 Introduction

This section evaluates the suitability of gold extended gate organic field effect transitors (OTFTs) for the detection of protein phosphorylation. OTFTs are excellent candidates for producing low cost, disposable arrays of sensors. Organic materials can be coated or printed on a variety of substrates after dissolving them in solvents. The π-conjugated backbone and side chains present in polymer semiconductors is responsible for their excellent solubility [120]. Low temperature and high throughput processes of fabrication like thermal evaporation, screen printing, inkjet printing and spin coating has made OTFTs a very popular component in sensors fabricated on flexible plastic, glass, metal foils and paper [93] [121]. The use of these devices opens up the possibility of an array of extended gate OTFTs for our final design. The presence of miniaturized TFTs on the same substrate can eliminate the need to interface the sensor array with an external MOSFET and aid in further reduction in size of the system.

The sensing principle of OTFTs is based on the interaction between the analyte and the sensing layer which changes the charge distribution at the interface between the semiconductor and the sensing layer. The change in the surface potential affects the flow of current in the device. A comparison between the electrical characteristics before and after exposure to the analyte can be used to determine the device response [122].

3.2.2 Materials and Methods

The extended gate OTFTs were produced and supplied by NeuDrive Limited. Figure 3.15 shows the layout of the sensor. The chip contains two device structures, one with width by length ratio (W/L) 9800/10 (extended gate structures) and the other with W/L 980/10 (test structures). Other than the W/L ratios, the two structures were alike. More intricate details of the devices was not provided by the company to maintain confidentiality.

The fabrication was done on an 8-inch square glass wafer coated in an acrylate polymer. The gold source-drain electrodes (50 nm) were deposited by sputtering followed by patterning using photolythography and wet etching. The organic semiconductor material, 3-flouro-4-methoxythiophenol in solution, was deposited on the substrate followed by a number of post-processing steps. The gold gate electrode (50 nm) was thermally evaporated and patterned using photolithography and wet etching. Three layers of passivation were added with SU-8 and PVA [123]. The details steps for fabrication was not disclosed by the company.

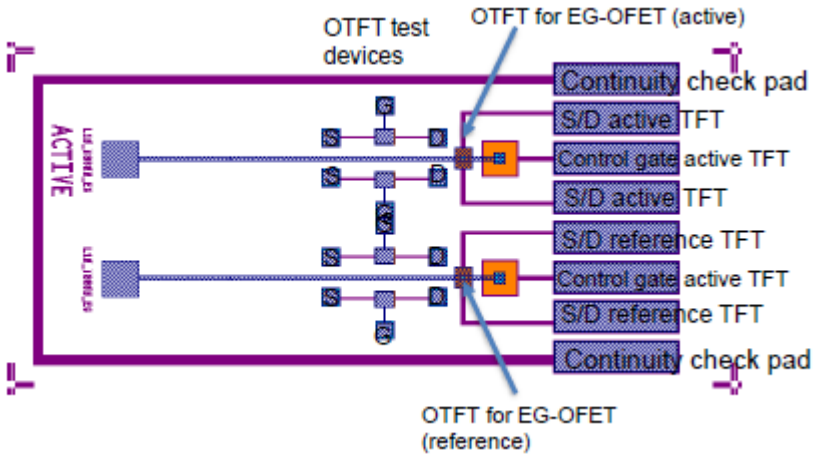

Figure 3.15: EG-OTFT layout (S/D symbolises the interchangeable source and drain connection) [Image source: NeuDrive extended gate transistor sensors datasheet]

1-ethyl-3-(-3-dimethylaminopropyl) carbodiimide hydrochloride (EDC), N-hydroxysuccinimide (NHS), 11-mercaptoundecanoic acid (MUA), 6-mercapto-1-hexanol (MCH) and ethanolamine were procured from Sigma Aldrich. The remaining materials used in this study are similar to section 3.1.2. The enzyme PKC-*alpha* was purchased from ProSpec-Tany TechnoGene Ltd.

Biofuctionalisation of Gold Surface

The gold extended gate areas were cleaned by rinsing in ethanol followed by UV-Ozone cleaning (covered in aluminium foil with only the EGs exposed). Initial attempts to clean by sonication in ethanol resulted in the removal of the gold from the glass wafers. A thick PDMS block with holes punched through to expose the EG areas was used to contain the liquids used in the study. This method proved difficult to produce a leak proof container because of the weak bonding between PDMS and the passivated glass substrate. It was not possible to activate the glass surface using techniques like oxygen plasma cleaning as the devices would be damaged in the process. Instead, teflon tape with hole punched in it to expose the extended gates was used as wells. A self assembled monolayer (SAM) made of 1 mM MUA and 1 mM MCH in ethanol in the ratio of 1:9 was prepared on the gold surfaces by incubation for 18 hours after which the extended gate areas were rinsed in DI water. To cover any pin holes on the surface a 1 hour backfilling step with 1 mM MCH was performed. After rinsing the wafers, an aqueous mixture of 40 mM EDC and 10 mM NHS was used to activate the SAM. The wafers were rinsed and dried with nitrogen gas. 2 μl of 156 μM peptide solution was dispensed on to the surface for 1 hour and then washed with DI water. The unreacted MUA sites were blocked incubating in 10 mM ethanolamine pH 8.5 [124] [125] for 5 minutes. The extended gate areas were rinsed thoroughly to remove any traces of ethanolamine from the surface. The prepared surfaces were incubated in PBS 7.2 for 30 minutes to stabilise before performing any measurements. Figure 3.16 shows the immobilization steps.

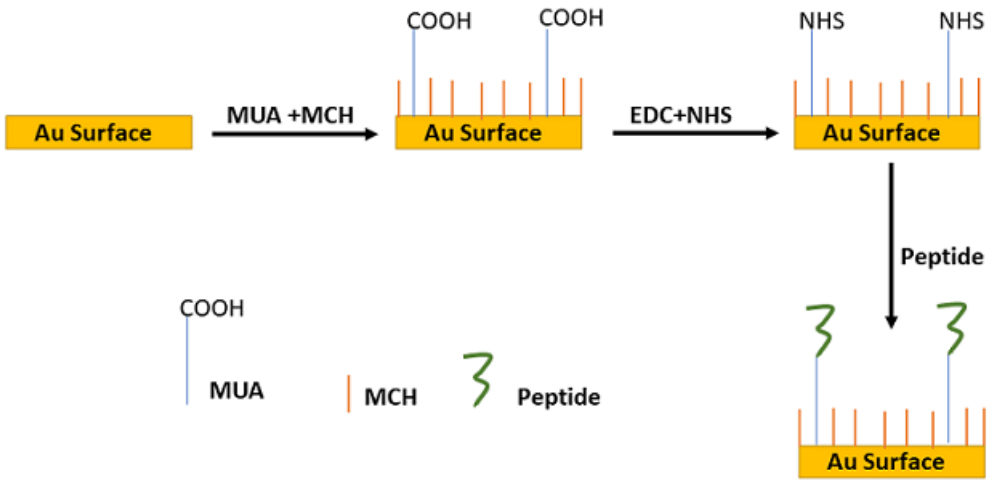

Figure 3.16: Immobilization of peptide on the gold extended gates

Measurement Setup

Contacts were made on gold contact pads using needle electrodes. The drain current versus gate voltage measurements were conducted using Agilent B1500A semiconductor device analyser. A fixed drain to source voltage of -2 V was maintained throughout the experiment. The gate voltage was varied from -20 V to 20 V. This was applied through an Ag wire coated in AgCl paste as a reference electrode or the control capacitor present on the chip. The measurements were performed in a closed Faraday cage to minimise exposure to light because the drain drifts with time due to photo-generated charges with change in illumination levels. The phosphorylation reaction was carried out in the same manner as described in the section 3.1.2. For all replicates, the reaction volume was fixed to 50 μl. All measurements were performed in three individual wafers with two extended gates each and the average values were considered. The errors were calculated using the standard deviation of the data. The shifts in threshold voltage were observed.

3.2.3 Results and Discussion

Characterisation of the OTFTs

The test structures on the TFTs (W/L=980/10) chips were first used to understand the characteristics of the sensor. The test structures do not have extended gates and hence the gate voltage was applied directly to them. The Figure 3.17 and 3.18 shows the characteristics of the extended gate structures and test structures respectively.

It is evident from the graphs that the devices have different threshold voltages even though they are meant to be identical. The two test structures have a difference of 7 V between their threshold voltages. The difference between the extended gate structures is less pronounced and a 1.2 V difference in threshold voltage was observed. It is evident that baseline will vary significantly between experiments as there are some inherent differences between the structures on the chip.

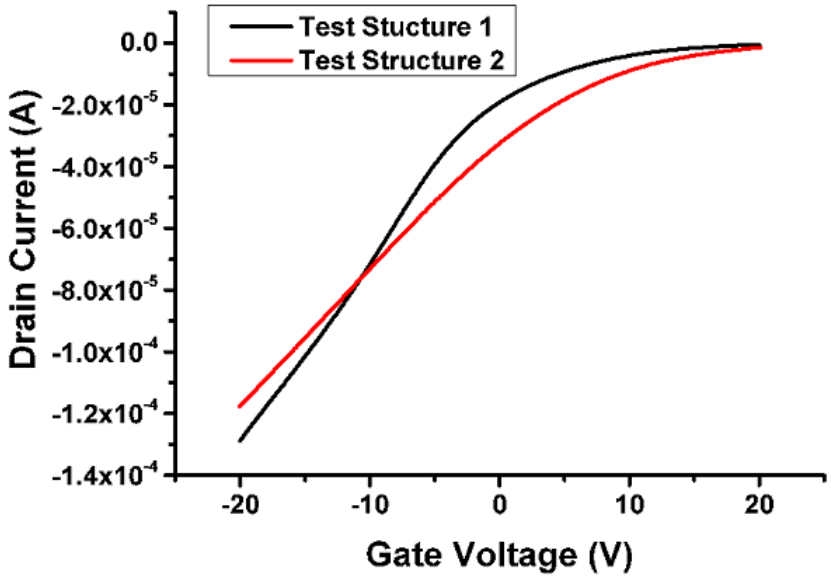

Figure 3.17: Drain current versus gate voltage for the extended gate structures (drain to source voltage=-2V)

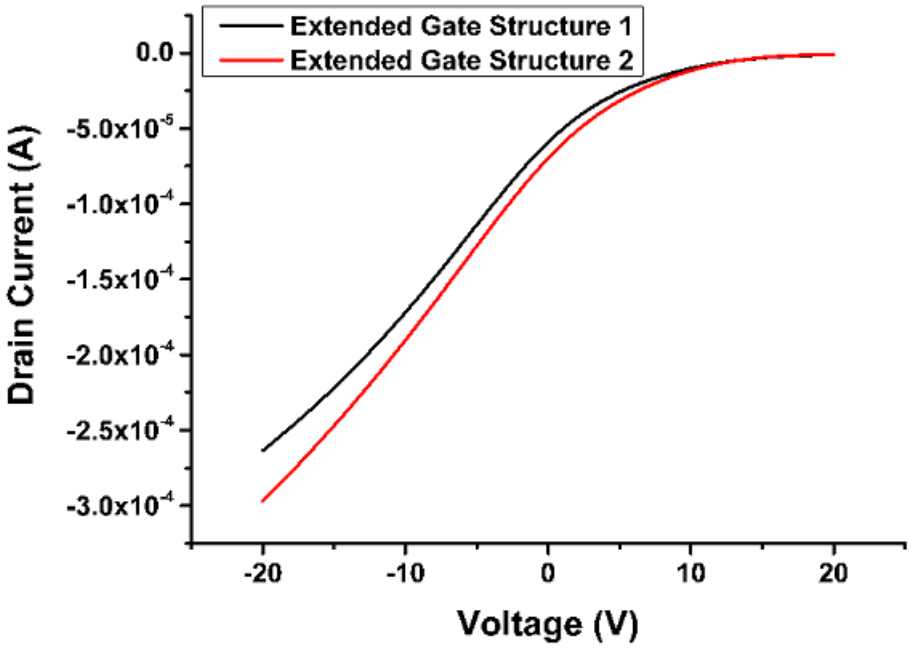

Figure 3.18: Drain current versus gate voltage for the test structures (drain to source voltage=-2V)

Stability

The stability of the extended gate structures was measured after immobilizing the peptide on the gold surface and incubating in PBS buffer pH 7.2 for 30 minutes. The current vs voltage characteristics (shown in Figure 3.19 and Figure 3.20) confirmed that the stability of the surface was poor. The shift in gate voltage over 10 minutes was upto 1 V. The stability measured through the control capacitor on the chip was less reliable than the reference electrode. The devices showed a significant drift in drain current when exposed to light (Figure 3.21). The photogenerated charge carriers resulted in a noisy signal. The signal to noise ratio changed from 13.9 dB in the absence of light to 129.3 dB in the presence of light. The lack of stability of the surface and the drift in drain current with time made it difficult to achieve reliable and reproducible results from the devices. Stable OTFTs in literature have shown only a 0.2 V long periods of time, exceeding 9,000 minutes [126].

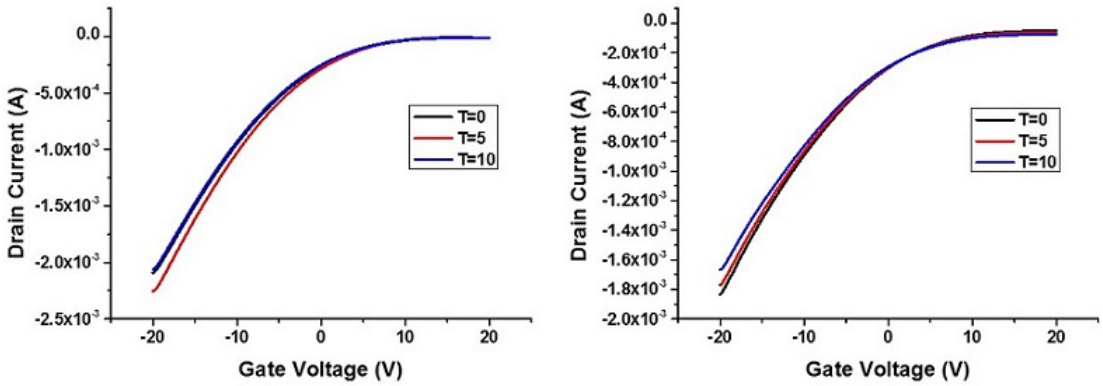

Figure 3.19: Drain current versus gate voltage for the extended gate structures measured using a reference electrode depicting the stability of the peptide on the gold surface (drain to source voltage=-2V) Left: OTFT 1 Right: OTFT 2

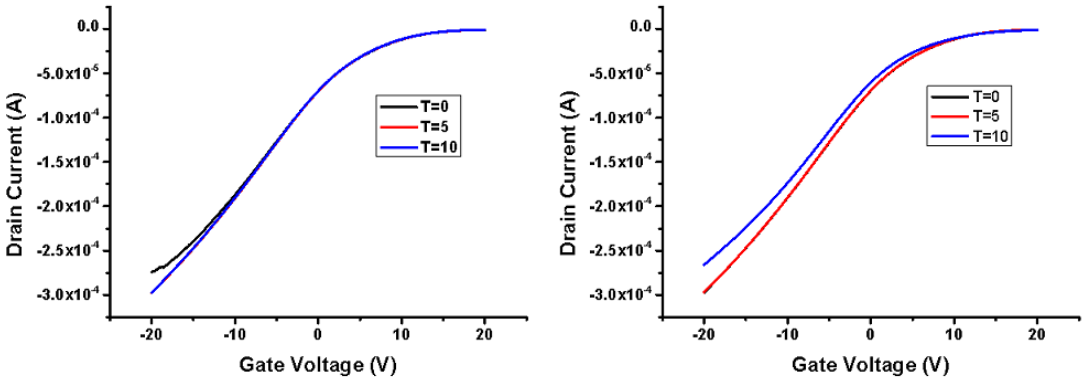

Figure 3.20: Drain current versus gate voltage for the extended gate structures measured using the control capacitor depicting the stability of the peptide on the gold surface (drain to source voltage=-2V) Left: OTFT 1 Right: OTFT 2

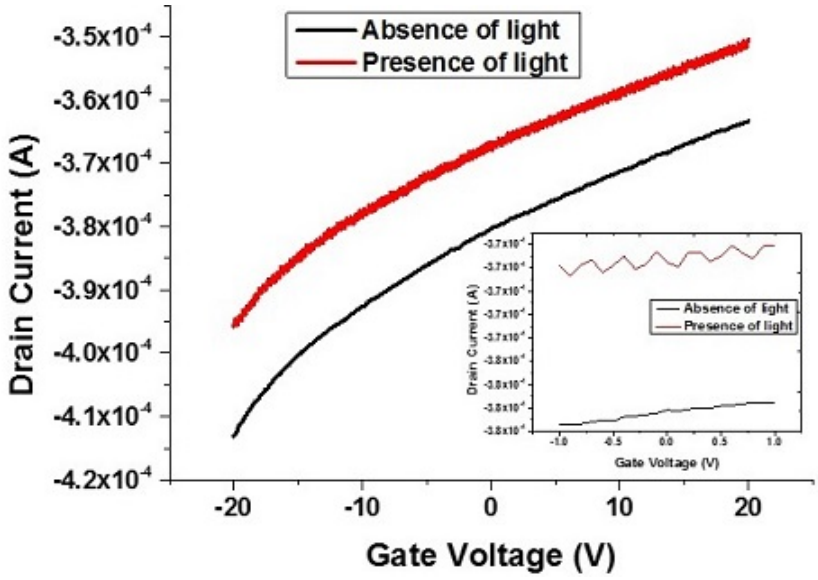

Figure 3.21: Drain current versus gate voltage in the presence and absence of light

Phosphorylation Reaction

Results of the protein phosphorylation reaction are shown in Figures 3.22 and 3.23. The I-V curve for the extended gates structures were first measured in PBS 7.2 for fixing a baseline. The following measurements were taken after incubation

in the measuring solution for 13 minutes. The control reaction containing 1 μM ATP along with 2.5 μl PKC lipid activator showed an average shift of 502 mV from the baseline. On addition of the kinase inhibitor along with the PKC-α enzyme, the signal shifted to an average of 726 mV from the baseline. In the absence of the inhibitor, the protein phosphorylation reaction showed a shift of 2612 mV shift.

These large shifts cannot be attributed to the reaction alone and are heavily influenced by the instability of the surface and the drift in drain current over time with change in illumination levels. Considering that the drain current drift in 10 minutes was already quite high, it is highly likely that the baseline of the measurements have shifted considerably in 13 minutes incubation. The error margins for each of the readings are 50 percent or higher which clearly indicate the lack of reproducible data. Even after 20 minutes of incubation in with the measuring solution, a stable and reproducible result could not be achieved.

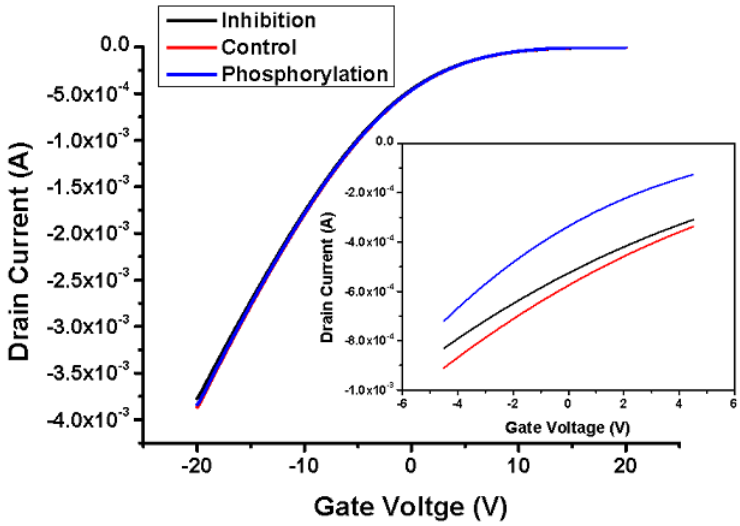

Figure 3.22: Drain current versus gate voltage for the extended gate structures for the control, inhibition and phosphorylation reactions (drain to source voltage=-2 V)

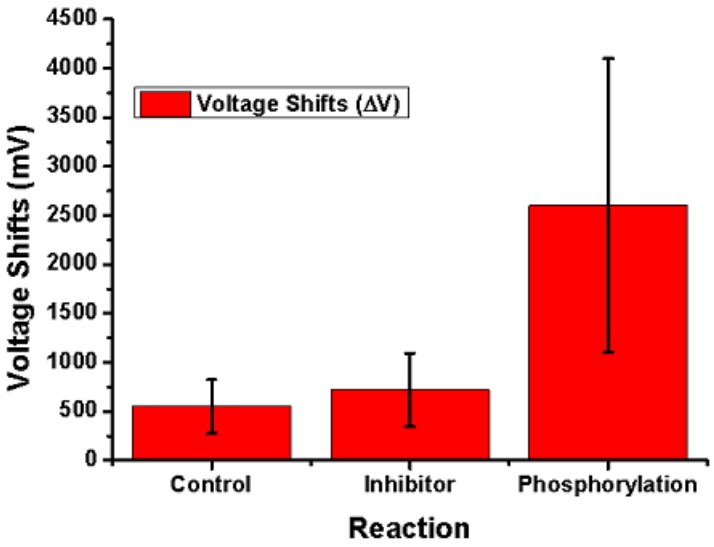

Figure 3.23: Voltage shifts from baseline for control, inhibition and phosphorylation reactions

3.2.4 Conclusion

The study of this batch of extended gate OTFTs show that they are unsuitable for use as a high throughput detection method for protein phosphorylation. The primary reason being the inability to achieve a stable reading when the peptide is immobilized on the gold extended gates. The drift in drain current with time and illumination levels makes it difficult to fix the baseline for the measurements. While some large shifts can be seen after protein phosphorylation as compared with the control and inhibition reactions, they cannot be attributed to the reaction alone due to the above mentioned reasoned. Reliability, reproducibility and stability are essential features of a good biosensor and therefore the OTFTs were not further investigated as a part of this research project.

It is also to be noted that the devices were prone to damage when using needle electrode for measurement. The gold contact pads were easily scratched

resulting in loss of connectivity and the need to repeatedly adjust the point of contact. The use of a glass wafer as a substrate is more expensive than FR4. Due to these drawbacks, in the next chapter we have returned to the FR4 substrate.

Chapter 4

Developing a Sensitive and an Insensitive Sensor for Screening Protein Kinase Inhibitors

4.1 MOSFET with Tin Oxide Extended Gate for Screening Protein Kinase Inhibitors

4.1.1 Introduction

This chapter describes the development of an extended gate field effect transistor (EGFET) based biosensor for screening protein kinase inhibitors. The configuration of the EGFET results in the isolation between the chemical/biological environment and the field effect transistor. The membrane used for biosensing is connected to the gate terminal of a FET through an conductive layer extending from the MOSFET chip. There are several advantages of the EGFET structure. This structure allows the sensing membrane to be processed and modified independent of the transducer. Low cost disposable biosensors can be fabricated easily by replacing the extended gate while keeping the measuring circuitry constant. EGFETs have been reported in literature to have very low sensitivity to changes in illumination [127] [128] [24]. In a study conducted by Chi *et al.* extended gates made of tin oxide

showed only a small shift of 3mV when exposed to 2000lx illumination [129]. .

Moving on from the studies described in section 3.1, the sensing film was thermally deposited directly on the PCB instead of pasting with conductive silver paste. Silicon nitride could not be used in this study because it needs temperatures higher than 300°C for in-situ deposition by chemical vapour deposition. Typically, silane (SiH_4) and ammonia (NH_3) gas react at high temperatures to produce silicon nitride which is deposited on the substrate. The FR4 substrate have an operating temperature between -50 to 110°C and a glass transition temperature[1] of 135°C [Source: Materials for Printed Circuit Boards http://www.nanotech-elektronik.pl]. The chemical vapour deposition of Si_3N_4 on PCB is therefore not possible.

The material chosen for the sensing layer is tin oxide. Several metal oxides were considered for this purpose. The reason for selecting this material is its excellent pH sensitivity and low cost. pH sensitivity of metal oxides was analysed by Yates *et al.* in 1974 using the site binding model . An equilibrium between the AOH sites on the surface (A is the metal) and H^+ ions in the solution is responsible for the charging of an oxide [131].

$$AOH \xleftrightarrow{K_a} AO^- + Hs^+$$

$$AOH_2{}^+ \xleftrightarrow{K_b} AOH + Hs^+$$

Hs^+ are the H^+ ions located near the surface of the metal oxide and K_a and K_b are equilibium constants of the above equations. For the pH sensitive material, the surface potential is determined by the H^+ ions exchanged between the solution and the binding sites on the surface of the sensor [132].

Silicon dioxide is cost effective and easy to deposit using thermal evaporation but has been shown in literature to have low pH sensitivity of about 20-40 mV/pH with a non-linear response [133] [134]. Al_2O_3 shows a good pH

[1] Glass transition temperature is the temperature at which the polymeric substrate changes from a rigid glassy material to a soft material [130]

response of about 53-57 mV/pH [133] [134] and can be deposited by both thermal and electron beam evaporation. Unfortunately, the evaporator (Auto 306 Vacuum Coater, BOC Edwards) failed to reach the temperature required for this deposition. The other option considered was to deposit aluminium and anodise it to produce aluminium oxide. This was not attempted because the process of anodisation requires the electrode to be dipped in sulphuric acid which may react with the copper from the PCB substrate. Furthermore, anodised aluminium has been shown to produce a nanoporous alumina thin films with low pH sensitivity of 23 mV/pH [112]. Tantalum oxide thin films have shown excellent pH sensitivity between 55-59 mV/pH with a linear response [134]. This can be deposited easily using electron beam evaporation. Tin oxide has a similar range of pH sensitivity and the thin films can be fabricated by thermal evaporation. Both materials are equally inexpensive. The initial experiments were conducted using tin oxide with the intention of evaluating tantalum oxide at a later stage.

MOSFETs are one of the most widely used electronic devices. They are cost effective and easily available. MOSFET based sensors have been used extensively for gas sensing, biosensing ans chemical sensing to name a few. The main advantage of these devices is the high input impedance and excellent sensitivity. The change is surface charge at the gate terminal can results in the change in electrical field and can easily be measured from a change in drain current [135]. The device consists of three terminals; namely drain, gate and source. The substrate forms the fourth terminal. Figure 4.1 shows the structure of a typical n-channel MOSFET. The source and drain are isolated by the substrate, preventing the flow of charges between the two n^+ terminals. When a positive voltage is applied at the gate terminal, minority charge carriers (electrons) from the p-type substrate are attracted to the semiconductor-insulator interface. Simultaneously, the holes at the interface are repelled. The voltage at which this conductive channel begins to appear is called the threshold voltage [136].

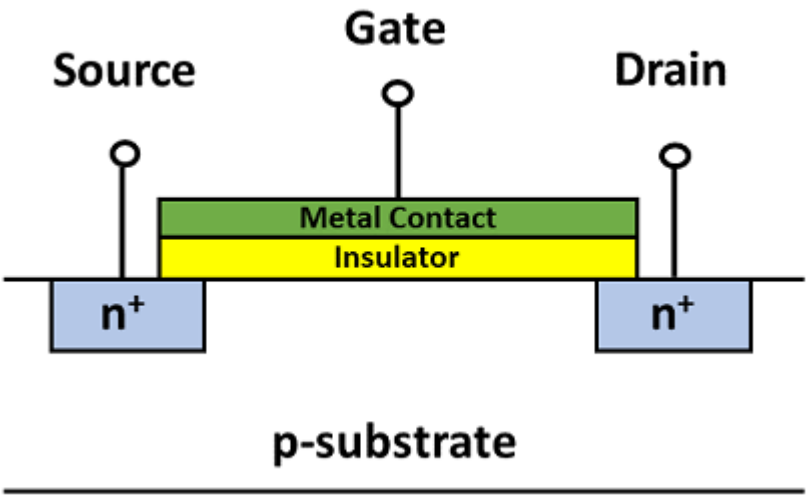

Figure 4.1: Structure of an n-channel MOSFET

Now, if a potential difference is applied between the source and drain terminals, a current can flow. When a potential difference between source and drain exist but the gate voltage is lower than the threshold voltage, no current can flow because no channel exists. The MOSFET is said to be 'off'. On the other hand, when the gate voltage exceeds the threshold voltage, a current flow takes place as the device is 'on'. Ideally, the gate terminal does not draw any current due to the presence of the insulator [136].

The equation for the drain current of a MOSFET is shown below:

$$I_{DS} = C_{ox}\mu\frac{W}{L}(V_{GS} - V_t) - \frac{1}{2}V_{DS}^2$$

where C_{ox} is the oxide capacity, μ is the electron mobility in the channel, W/L is the ratio of width and length of the channel, V_t is the threshold voltage.

When the geometric sensitivity parameter $\beta = C_{ox}\mu\frac{W}{L}$, threshold voltage and the applied drain to source voltage are constant, the drain current I_{DS} is a function of the gate to source voltage V_{GS}.

4.1.2 Materials and Methods

Fabrication of Extended Gates

A printed circuit board (PCB) containing four contact pads was made using the LPKF S63 PCB milling machine on double sided copper clad FR4 material. The dimensions and distances between the pads were decided keeping in mind the 96 well microtitre plate. The PCB was cleaned by sonication in acetone and isopranol for 5 minutes each and dried.

10 nm of aluminium was thermally evaporated on to the copper pads from a tungsten boat to act as an adhesion layer between copper and tin oxide. SnO_2 as sensing layer was then evaporated from an alumina coated tungsten wire basket. The contacts were masked with kapton tape. The thickness of each layer was confirmed using a profilometer (DekTak 6M profiler). Through a series of pH sensitivity experiments, 150 nm of tin oxide was found to be the optimum thickness for the biosensor. The PCBs were used for sensing without further cleaning. Figure 4.2 shows the PCB coated in tin oxide.

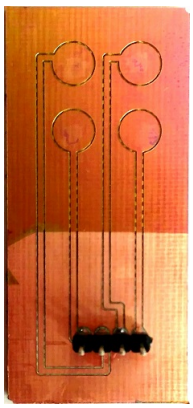

Figure 4.2: PCB coated in tin oxide and aluminium

Silanisation of SnO_2 thin films

It was necessary to determine whether the film could be silanised because it is an important step for immobilisation of the peptide under study. Silanisation of tin oxide has been reported in literature [137]. 3-Aminopropyl)triethoxysilane (APTES) was used for this part of the study instead of GOPTS. APTES contains positively charged -NH_2 groups. If the silanisation of the surface is successful, a shift in I-V characteristics will be observed when the thin films are used as extended gates to a CMOS chip. GOPTS does not contain any detectable charge and hence it will not be possible to determine whether the surface has been silanisaed by this method. A 1% (3-Aminopropyl)triethoxysilane (APTES) (purchased from Sigma Aldrich) solution was prepared in acetone and dispensed on the thin films. The petridish containing the PCBs was sealed with parafilm and incubated at room temperature for two hours. The films were rinsed thoroughly in DI water and dried before curing in a temperature controlled oven for five minutes at 90°C [138]. An aqueous solution of 15% glutaraldehyde (Sigma Aldrich) was dispensed on the films for three hours which were then rinsed thoroughly with DI water and dried.

Immobilisation of peptide

GOPTS was heated to its boiling point (120°C) and the clean films were exposed to the silane vapours for five seconds. They were rinsed with DI water and dried. The silianised surface contained epoxide groups capable of covalently bonding to the amine groups of the peptide [117]. 2 μl of 156 μM peptide solution was dispensed onto the films and left to bind for 40 minutes. Unreacted sites of GOPTS was blocked by washing the wafers with 20% ethanol. The epoxide groups convert to ether on reacting with ethanol [119]. 50 μl of PBS buffer pH 7.2 was dispensed on to the modified thin films and the sensing surface was allowed to stabilise for 30 minutes.

I-V measurements

The modified PCBs were connected to the gate terminal of an n-type MOSFET for measurement. The drain current vs gate voltage for the MOSFET with gate voltage applied directly to the gate terminal is shown in Figure 4.4. This device was fabricated by Austria Microsystems with the 0.35 μm CMOS process. The W/L ratios for the NMOS and PMOS are 104/24 and 2104/24 respectively. A variable gate to source (V_{GS}) voltage of 0-3 V was applied through a reference electrode (silver wire coated with silver chloride paste) dipped in PBS buffer pH 7.2. Agilent B1500A HR CMU Semiconductor Device Analyser was used to record drain current vs gate voltage measurements for a fixed drain to source voltage (V_{DS}) of 50 mV. The typical threshold voltage for for the MOSFET at V_{DS} of 50 mV is 0.4 V. The measurements were performed in a closed Faraday cage in order to minimise noise. For all replicates, reaction volumes were fixed to 50 μl. Measurements were performed on three PCBs containing 4 sensors each and the average values were considered. The errors were calculated from the standard deviation of the data. Shifts in the threshold voltage were observed. Figure 4.3 shows the schematic of the sensor setup.

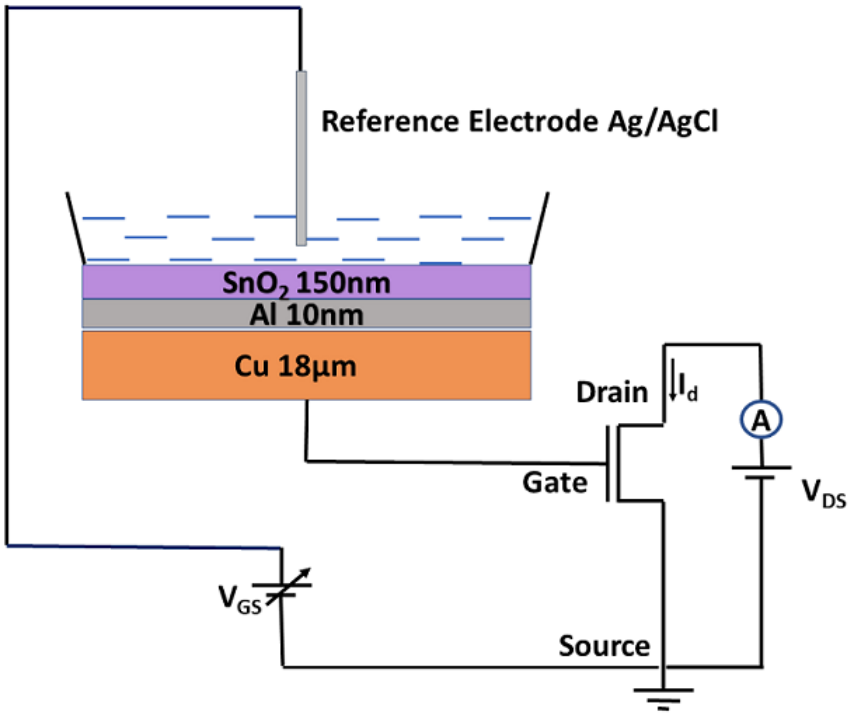

Figure 4.3: Schematic of the sensor setup

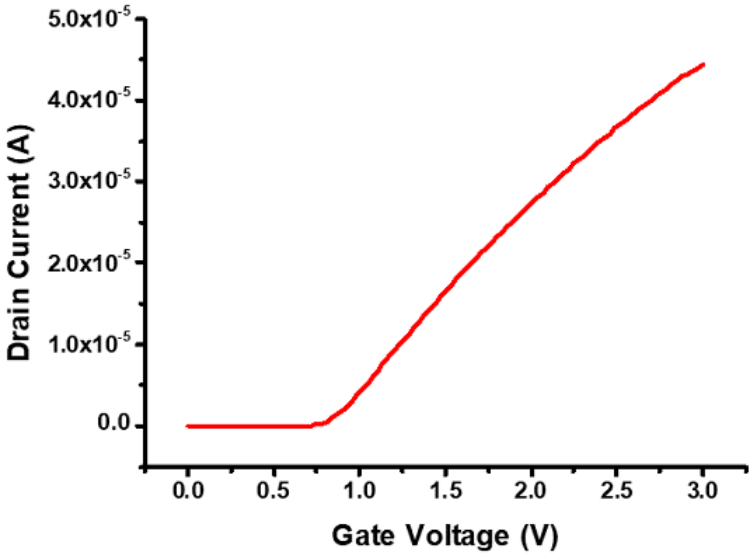

Figure 4.4: Drain current versus gate voltage of MOSFET

4.1.3 Results and Discussion

pH sensitivity

Different thicknesses of tin oxide from 50-300 nm was deposited on the PCB and tested for their pH sensitivity. The films were hydrated for 30 minutes with de-ionized water before the tests. 10 mM PBS with different pH was used for the measurement. 150 nm of tin oxide showed the highest pH sensitivity of 51.3±1.2 mV/pH while the 50 nm film showed the lowest pH sensitivity of 32.7±2.0 mV/pH. The pH sensitivities for different thicknesses of tin oxide are shown in Figure 4.5 and Table 4.1. The changes in pH sensitivity between 100nm and 300nm of tin oxide are not significant but this experiment was conducted solely for the purpose of selecting a thickness of the sensor layer. Since the best pH sensitivity was shown by 150nm, this was the thickness chosen for the rest of the experiments. The drain current versus gate voltage for 150nm of tin oxide for different pH is shown in Figure 4.6. Thermally evaporated tin oxide films of 150nm thickness have been shown to possess a pH sensitivity of 58 mV/pH in literature [139].

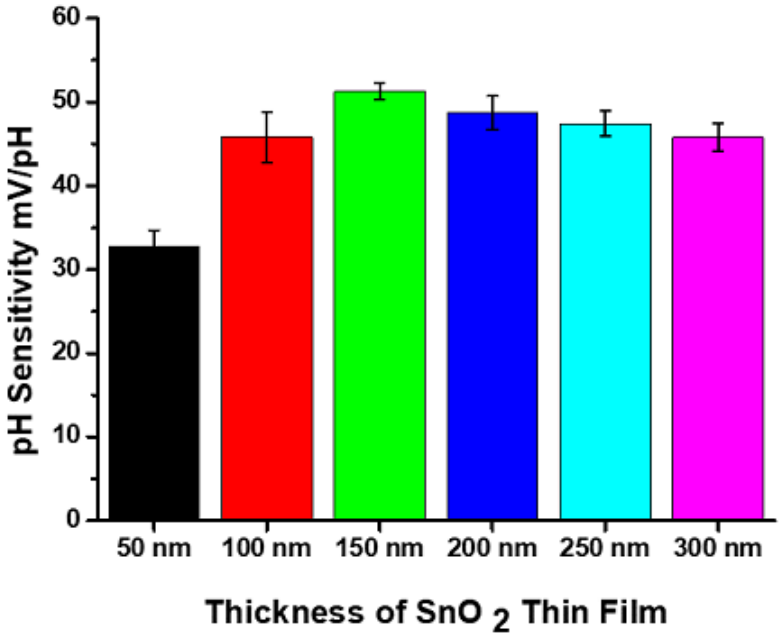

Figure 4.5: pH sensitivity of different thicknesses of thermally evaporated tin oxide thin films

Thickness of SnO_2 film (nm)	pH sensitivity (mV/pH)
50	32.7 ± 2.0
100	45.8 ± 3.2
150	51.3 ± 1.2
200	48.7 ± 2.1
250	47.4 ± 1.5
300	45.8 ± 1.7

Table 4.1: pH sensitivity of thermally evaporated SnO_2 thin films ranging from 50-300 nm

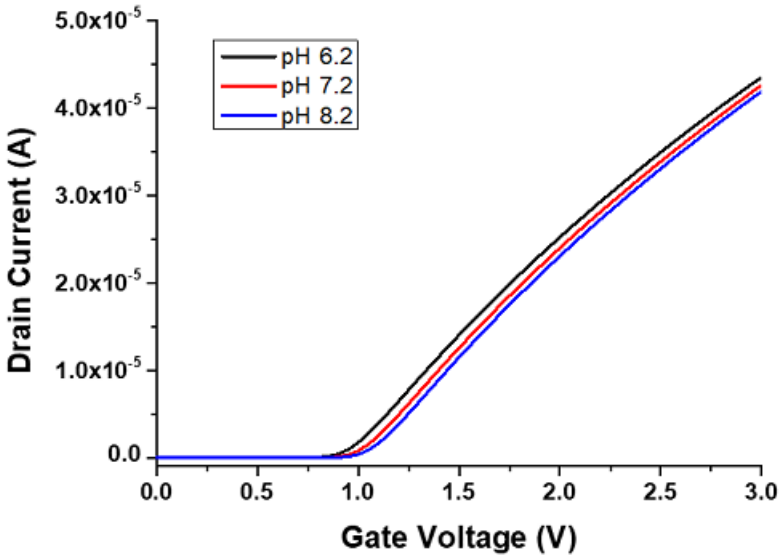

Figure 4.6: pH response of SnO_2 150nm thin film

Temperature sensitivity

Temperature sensitivity was measured with PBS 7.2 between 0-50°C in 5°C increments. PBS buffer at 0°C was heated slowly in a temperature controlled water bath. The temperature of the PBS was monitored closely with a thermometer immersed in buffer. For every 5°C increment, the PBS was dispensed on to the extended gates and the measurements were conducted immediately. The films were hydrated in PBS pH 7.2 at room temperature for thirty minutes prior to the measurements. There was a significant difference between the temperature sensitivity observed between 0-20°C and between 20-50°C (Figure 4.8 and Figure 4.7. Between 0-20°C the temperature sensitivity was found to be 1.0 mv/°C. Between 20-50°C a temperature sensitivity of 0.2 mV/°C observed. The reasons for this difference could not be determined. It was expected that the temperature sensitivity would be roughly uniform for the entire experiment.

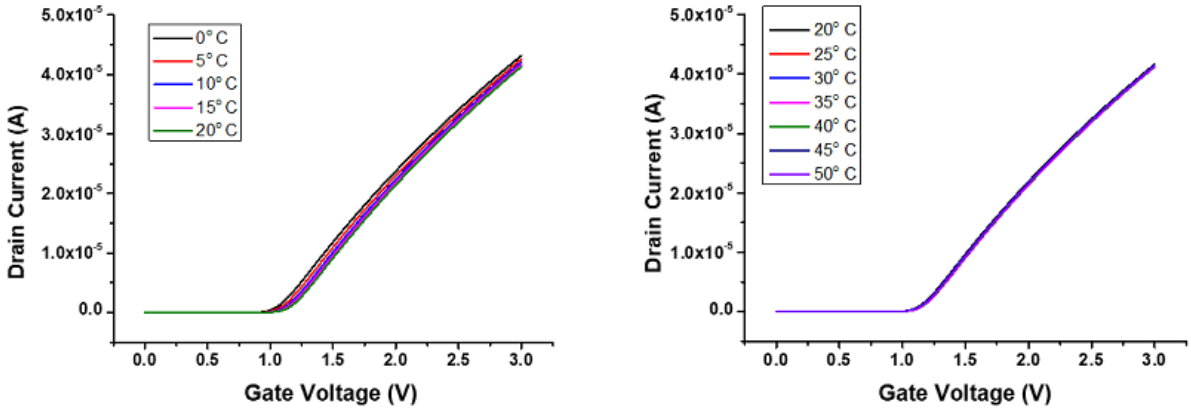

Figure 4.7: Drain current vs gate voltage for different temperatures on SnO_2) thin film. Left: 0-20°C Right: 20-50°C

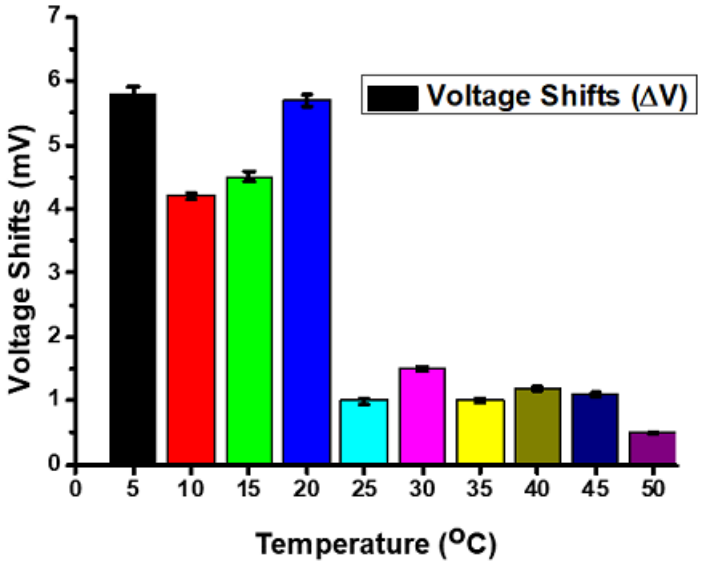

Figure 4.8: Voltage shifts for different temperatures on tin oxide thin film

Silanisation with APTES

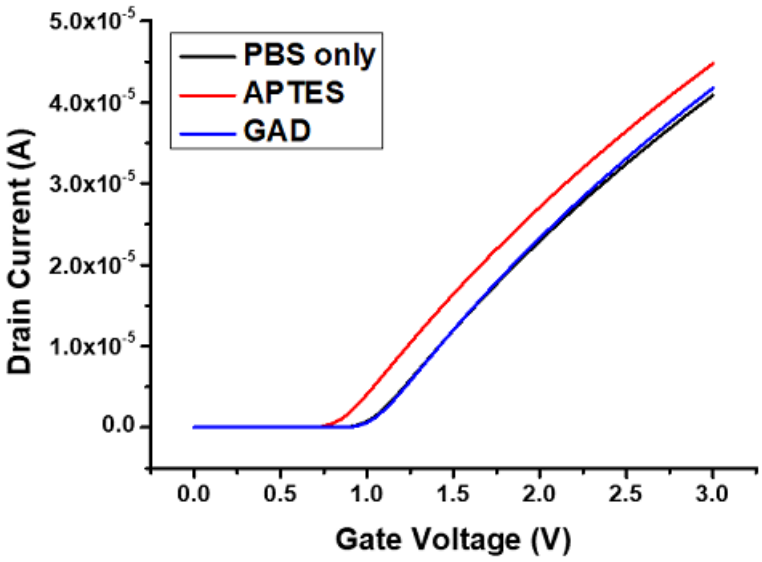

Figure 4.9: Drain current vs gate voltage for silanisation of tin oxide with APTES followed by treatment with glutaraldehyde (GAD)

APTES is used to test whether the tin oxide surface can be silanised. Organosilanes form a self assembled monolayer on metal oxide surfaces. The reason for choosing APTES over GOPTS for this test is the because of the presence of positively charged amino [140] groups on APTES which can be detected as a shift in the drain current vs gate voltage characteristics of the MOSFET. On silanisation, a large shift of 180 mV was observed. Glutaraldehyde was used to neutralise the positive charge by adding aldehyde groups to the surface [141]. After the addition of glutaraldehyde the I-V characteristics return to 5 mV of the baseline (Figure 4.9). While this experiment proved the possibility of the tin oxide thin films being silanised, the shifts were unexpectedly high.

Stability

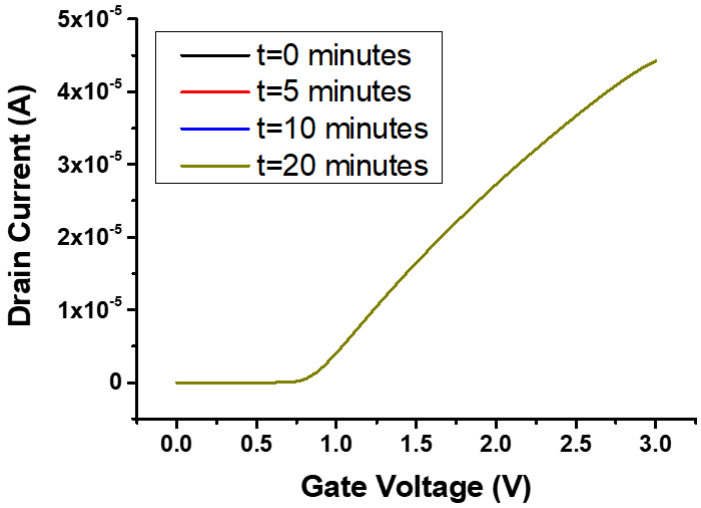

Figure 4.10: Stability of the tin oxide thin films with peptide immobilised

The stability of the SnO_2 thin films were measured after silanisation in vapour phase with GOPTS and immobilisation of peptide. Following the immobilisation, the films were left to stabilise in PBS 7.2 for 30 minutes before the test. The results are shown in Figure 4.10. The voltage shifts over ten minutes was a maximum of 2 mV. The surface proved to be stable for performing the phosphorylation studies.

Phosphorylation Reaction

The results of the phosphorylation reaction are shown in Figure 4.11. The I-V curves were first determined in PBS buffer pH 7.2 to ascertain the baseline. Each of the measurements were conducted after 13 minutes of incubation in the measuring solution. The control reaction was conducted with 1 μM ATP and 2.5 μl PKC lipid activator. An average shift of 30 mV from the baseline was observed. On addition of the kinase inhibitor along with PKC-α enzyme, the signal shifted by an

average of 33 mV from the baseline. The phosphorylation reaction was conducted in the presence of ATP, activator and enzyme. A large shift of 83 mV was observed.

The signals from the control and inhibition reaction were comparable but the size of the shift was very large and unaccounted for because without the phosphorylation reaction taking place, charged species were not produced. The effective shift for the phosphorylation signal (phosphorylation signal-control signal) is 53 mV. The size of the shift from the baseline however, is too large to be attributed to the reaction alone. In the following subsection, attempts to troubleshoot this problem has been discussed. It is unlikely that the pH insensitive reference sensor for the final REFET will have the similar large responses for the control or inhibition reactions and therefore it is necessary to explore methods of reducing these signals.

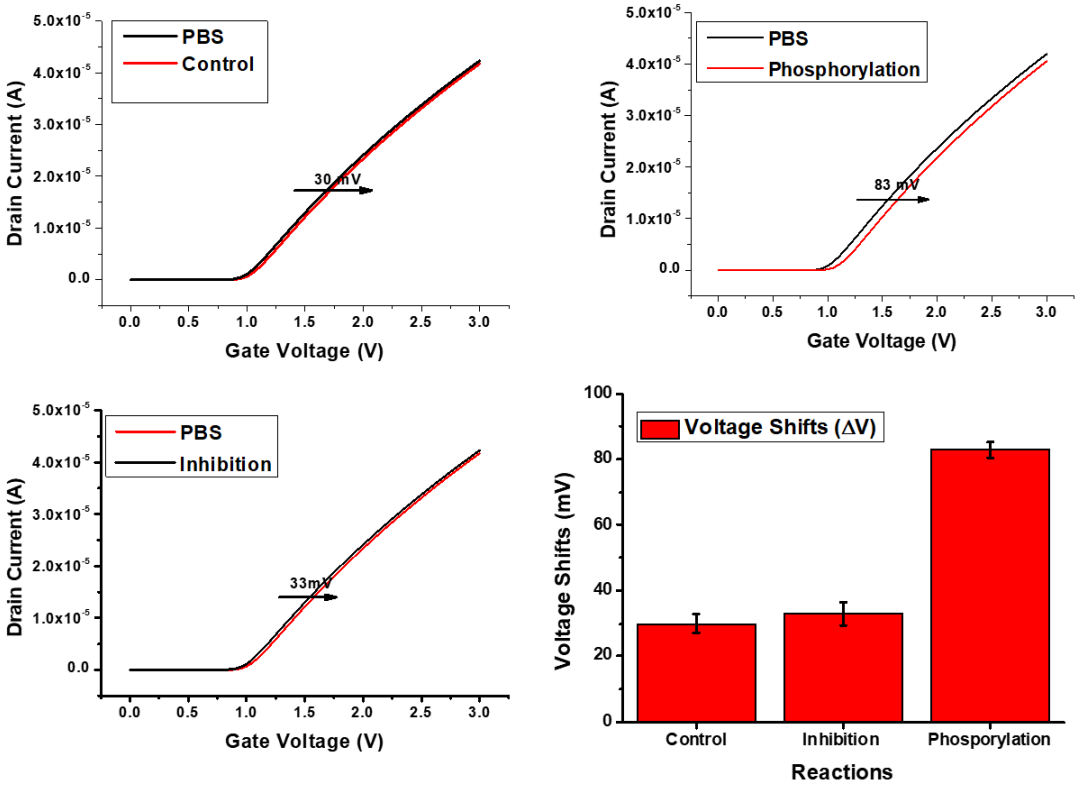

Figure 4.11: Top Left: Drain current vs gate voltage for the control reaction for tin oxide thin films on a PCB. Top Right: Drain current vs gate voltage for the phosphorylation reaction for tin oxide thin films on a PCB. Bottom Left: Drain current vs gate voltage for the inhibition reaction for tin oxide thin films on a PCB Bottom Right: Voltage shifts for phosphorylation studies for tin oxide thin films on a PCB

4.1.4 Troubleshooting the Biosensor

Interaction of individual solution components with the thin films

In the first attempt, it was hypothesised that one or more of the solution components were reacting with the surface of the thin film. To test this theory, the thin films were incubated individually in PBS buffer pH 7.2 containing the

enzyme, PKC lipid activator, ATP and inhibitor separately. The concentration of the individual components in solution was kept the same as that in the phosphorylation studies. The enzyme, ATP and activator individually did not show any significant voltage shifts. The inhibitor, however, showed a significant of 12 mV shift (Figure 4.12).

The thin films with immobilised peptide was allowed to incubate in PBS pH 7.2 for 30 minutes followed by inhibitor for 13 minutes before phosphorylation studies were conducted. The average shifts did not show a significant change after employing this method (Figure 4.12). There was a small decrease of 2 mV for the phosphorylation signal from the previous 83 mV to 81 mV. The inhibition reaction showed a reduction in signal by 7 mV and the control reaction by 3 mV only. This approach did not prove to successful to be reduce the large signals.

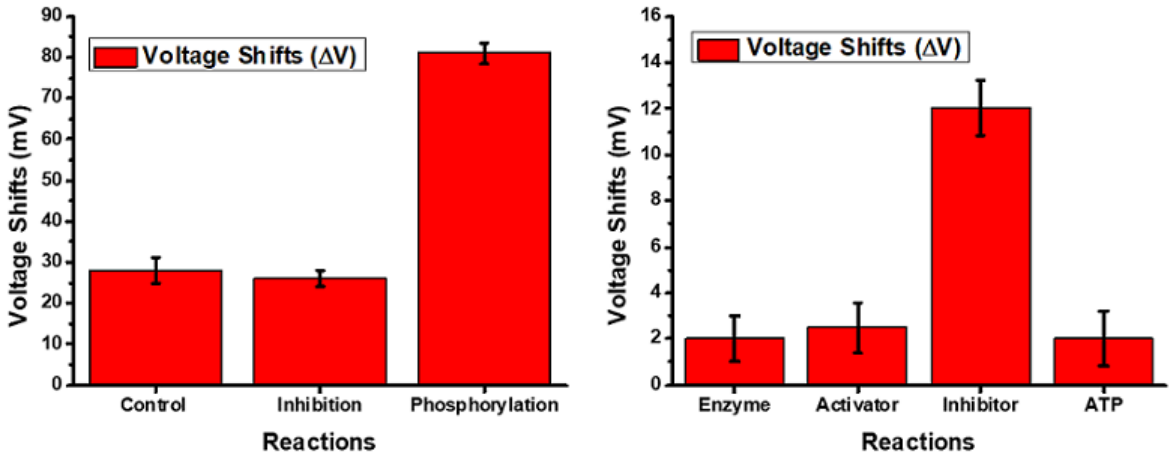

Figure 4.12: Left: Voltage shifts for phosphorylation studies on tin oxide thin film on PCB after incubating the surface with inhibitor. Right: Voltage shifts for interaction of individual solution components with tin oxide thin film on a PCB

Replacing tin oxide with tantalum oxide

In the next attempt, tin oxide was replaced with a different metal oxide, tantalum pentoxide (Ta_2O_5). This is also a pH sensitive material that has been

widely used as a pH sensor and a biosensor [142] [143] [144].

The method of deposition of the thin films was similar to tin oxide. The PCBs milled from double sided copper clad FR4 material were cleaned by sonication in acetone and isopropanol for five minutes each. 10 nm of aluminium was deposited by thermal evaporation as an adhesion layer after which 150 nm of tantalum pentoxide was evaporated from a copper crucible by electron beam evaporation. The thin films were used without any further cleaning.

This approach resulted in films which easily dissolved when exposed to PBS buffer or by washing. To improve the adhesion of the films, a thicker adhesion layer of 100 nm of aluminium was deposited. This only marginally improved the adhesion of the films. Chromium and titanium were also used as adhesion layers by thermal evaporation but did not prove to be successful.

Finally, the PCBs were polished using 5 μm alumina slurry for 8 minutes to remove the thin surface layer of copper oxide and produce a smoother surface for deposition. The PCBs were cleaned once again by sonicating in acetone and isopropanol for 5 minutes each before depositing 10 nm of aluminium and 150 nm of Ta_2O_5. This significantly improved the adhesion of the thin films and further studies on pH sensitivity, stability and phosphorylation were conducted on these PCBs.

pH sensitivity

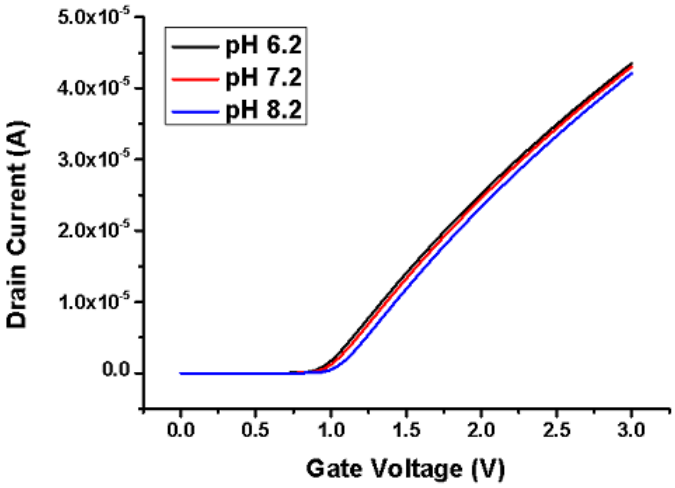

Figure 4.13: Drain current vs gate voltage characteristics for pH sensitivity studies

The Ta_2O_5 films were incubated in PBS 7.2 for 30 minutes before the pH sensitivity studies. A pH sensitivity of 53.2±2.2 mV/pH was achieved in this study (Figure 4.13. The thin films become prone to dissolution at pH less than 5 and higher than 9. pH sensitivities of Ta_2O_5 thin films has been found to range between 55-59 mV/pH in literature. [134]

Stability

The Ta_2O_5 thin films were silanised with 98% GOPTS in vapour phase, similar to the SnO_2 thin films. 2 μl of 156 μM peptide was dispensed on the surface and left to bind for 40 minutes. The stability of Ta_2O_5 thin films with immobilised peptide were measured after incubation in PBS 7.2 for thirty minutes. The results proved that the surface was stable with a maximum shift of 2 mV in 10 minutes (Figure 4.14). It is important to note here that the 20 minute data could not be collected for the devices used in this experiment because the thin films were either wholly or partially removed from the surface by this point. In

order to continue with the same devices towards the phosphorylation experiments, the stability measurements were conducted for only 10 minutes.

Temperature sensitivity of the films could not be tested because the films showed a tendency to be removed easily from the surface on washing when exposed to different temperatures.

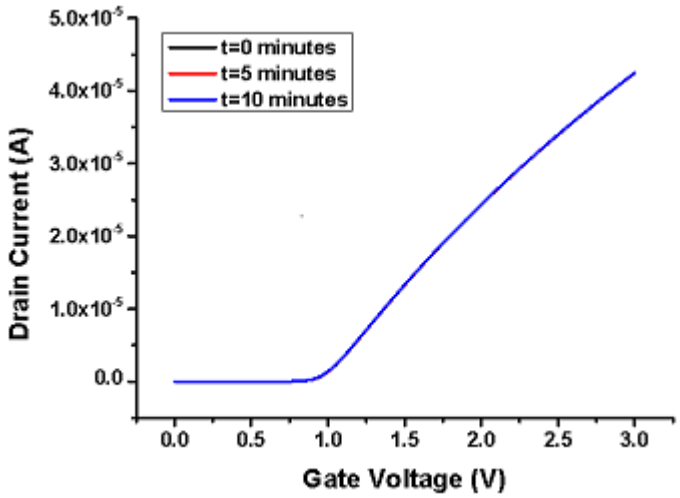

Figure 4.14: Stability of Ta_2O_5 thin films on a PCB with immobilised peptide

Phosphorylation

The results of the phosphorylation reaction are shown in Figure 4.15. The I-V curves were first determined in PBS buffer pH 7.2 to fix the baseline. Each of the measurements were conducted after 13 minutes of incubation in the measuring solution. The control reaction was conducted with 1 μM ATP and 2.5 μl PKC lipid activator. An average shift of 8 mV from the baseline was observed. On addition of the kinase inhibitor along with PKC-α enzyme, the signal shifted by an average of 10 mV from the baseline. The phosphorylation reaction was conducted in the presence of ATP, activator and enzyme. A shift of 47 mV was and an effective phosphorylation signal of 39 mV is observed.

The Ta_2O_5 thin films show some promising results but were not further investigated. The of the deposited films continued to be prone to dissolution on repeated washing which is a necessary step in the studies described. The above results were reported from films that did not dissolve through the duration of the experiment. The number of useful devices per fabrication cycle was an average of 50%. The term 'useful' refers to those devices that retained the thin film on the PCB substrate through the entirety of the phosphorylation experiment.

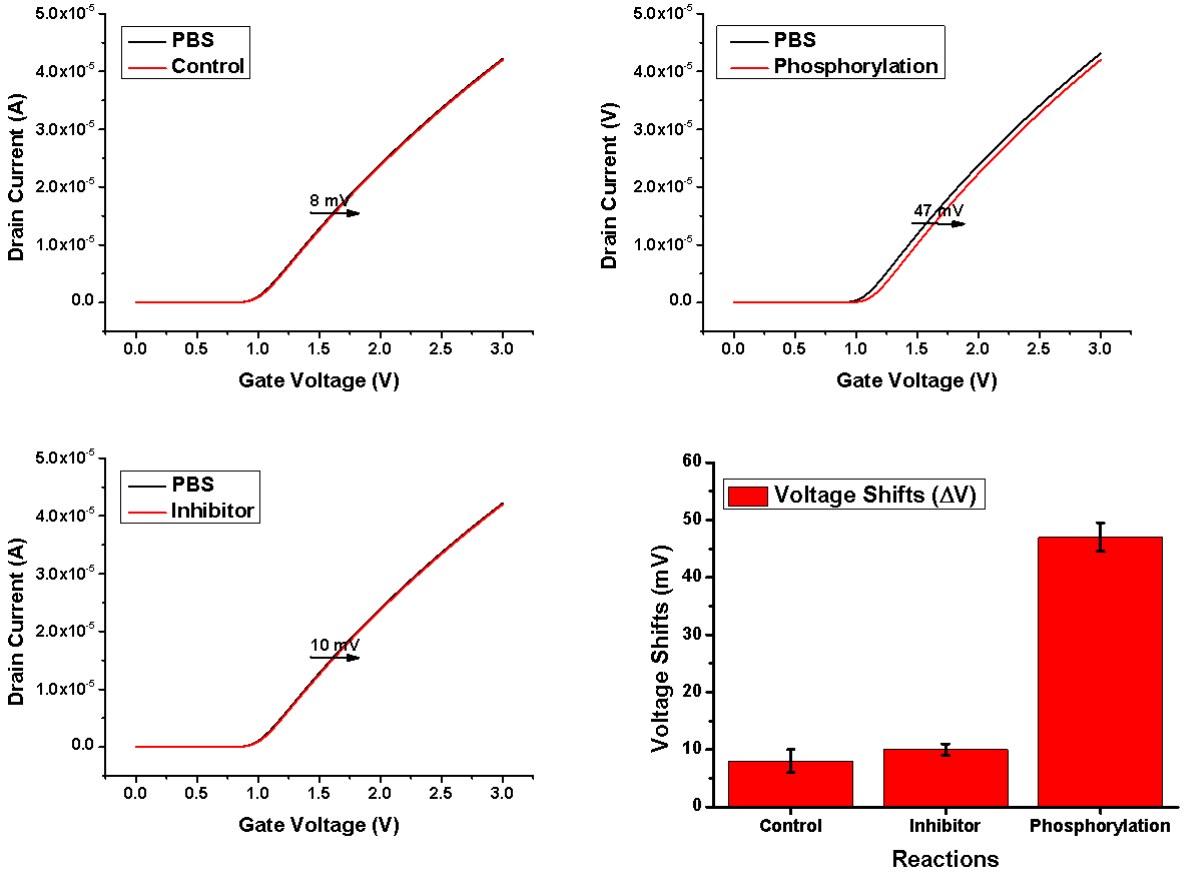

Figure 4.15: Top Left: Drain current versus gate voltage for control reaction for tantalum oxide on a PCB. Top Right: Drain current versus gate voltage for phosphorylation reaction for tantalum oxide on a PCB. Bottom Left: Drain current versus gate voltage for inhibition reaction for tantalum oxide on a PCB. Bottom Right: Voltage shifts for phosphorylation studies for tantalum oxide on a PCB

Tin oxide on polished PCB

The results of the troubleshooting experiments proved that polishing the PCBs prior to thermal deposition improved the adhesion of the thin films. There was roughly a 20% increase in 'useful' devices when the PCBs were polished before the deposition of Ta_2O_5. The same technique was employed to make the tin oxide coated PCBs. As mentioned above, the copper pads of the PCBs were polished with 5 μm alumina slurry for 8 minutes. The remaining steps were kept the same as section 4.1.2. The tests for pH sensitivity, temperature sensitivity, stability and phosphorylation was performed.

The surfaces of the polished and unpolished PCBs were investigated using images from a Scanning Electron Microscope (SEM) as shown in figure 4.16. The SEM (Jeol JSM-6480LV) images revealed that the unpolished PCBs contained a rough, undulating surface containing crests and troughs often as large as a few microns. The polished PCBs revealed a smooth surface with no such irregularities. The images shown in the figure are only upto X6,000 magnification because it was not possible to focus the images at larger values of magnification. The SEM images indicate that the deposition of the thin film on the unpolished PCBs were possibly not uniform and that there a possibility of copper being exposed through them.

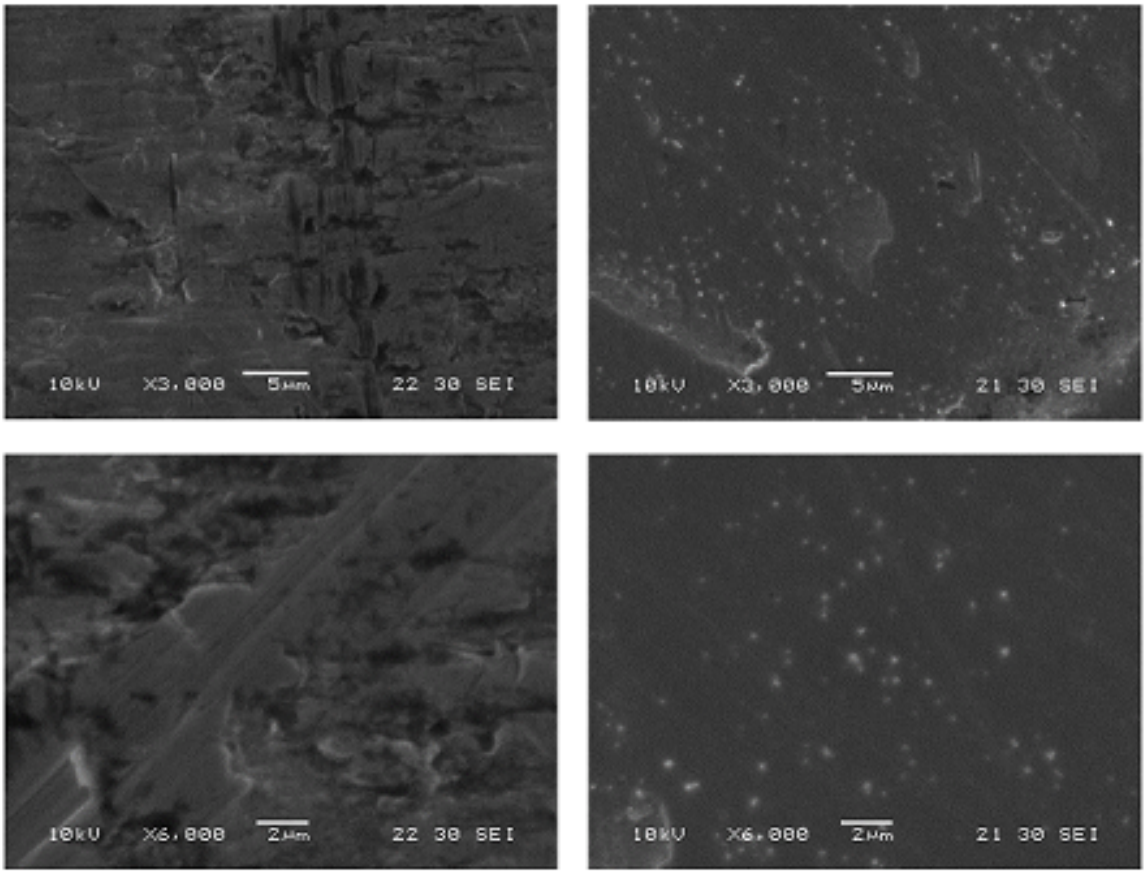

Figure 4.16: SEM Images (Top Left and Bottom Left: Unpolished Copper Surface of the PCB, Top Right and Bottom Right: Polished Copper Surface of the PCB)

To investigate the surface roughness further, Atomic Force Microscopy (AFM) was used. The figures 4.17 and 4.18 show the three dimensional representation of the AFM (Nanoscope IIIA microscope) data for a $1\mu m^2$ area. The mean roughness for the unpolished PCB was 6.62nm. The polished PCB yielded a significantly lower mean roughness of 2.43nm. The improvement in surface roughness by 63.2% could be responsible for better adhesion of the films. The rough surface with a discontinuous and porous film may have allowed for solutions to penetrate under it, resulting in its removal.

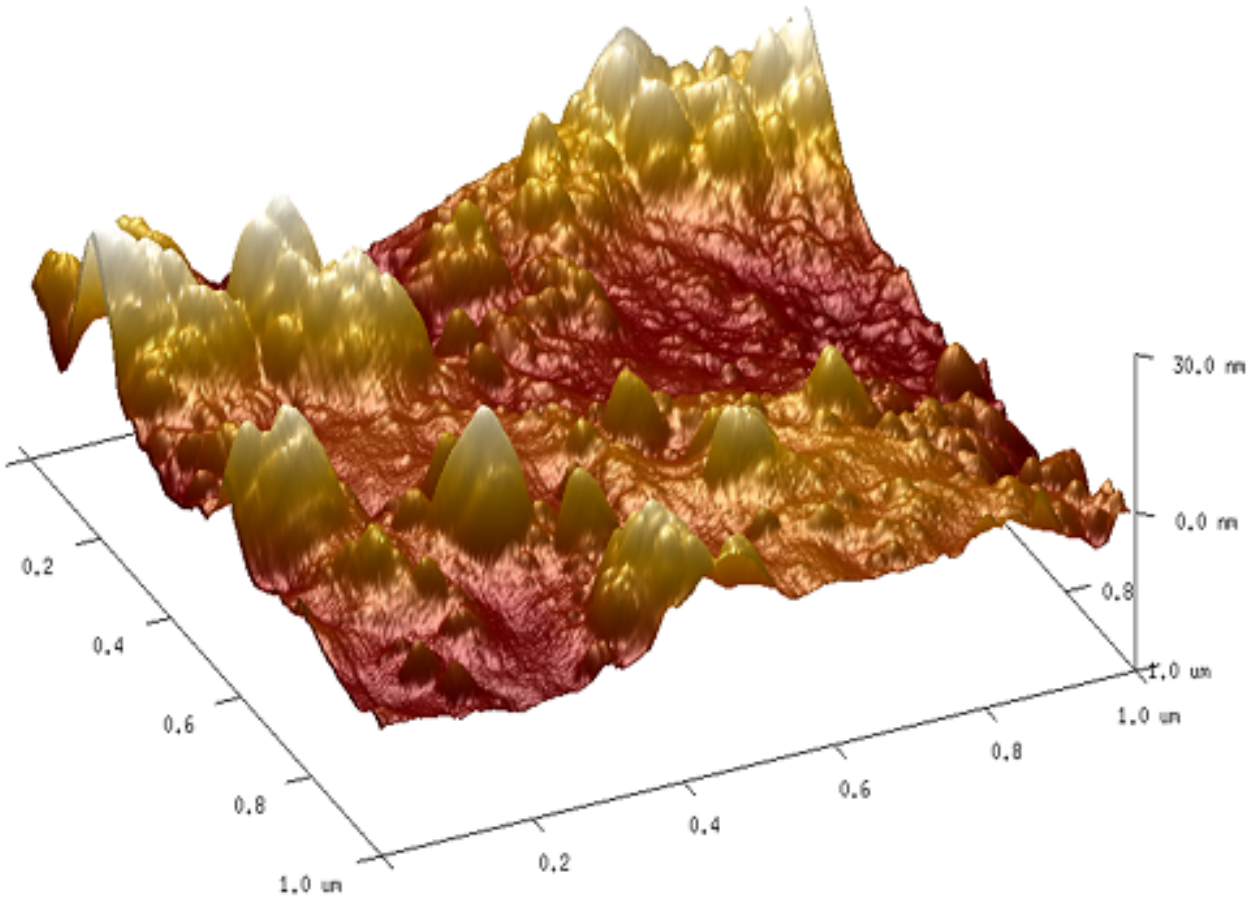

Figure 4.17: 3D AFM Image of Unpolished Copper Surface of PCB

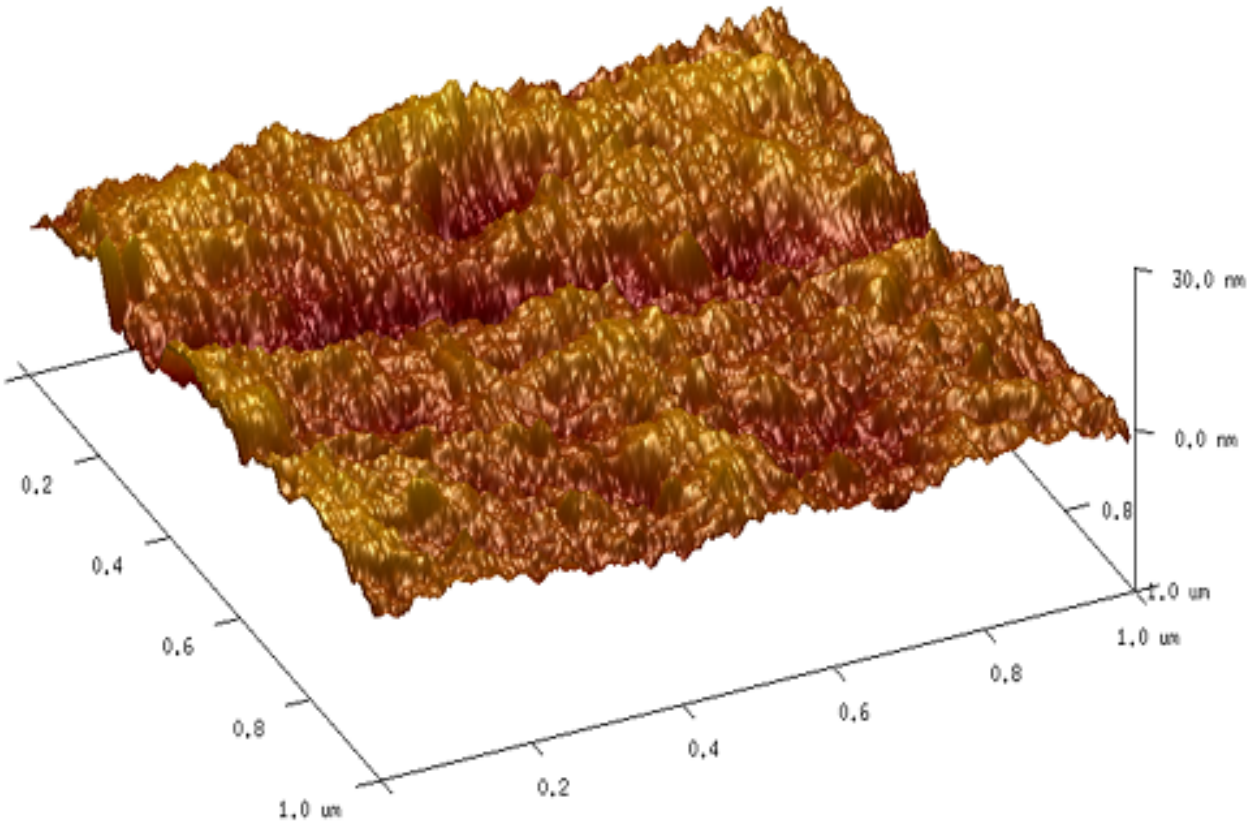

Figure 4.18: 3D AFM Image of Polished Copper Surface of PCB

pH sensitivity and temperature sensitivity

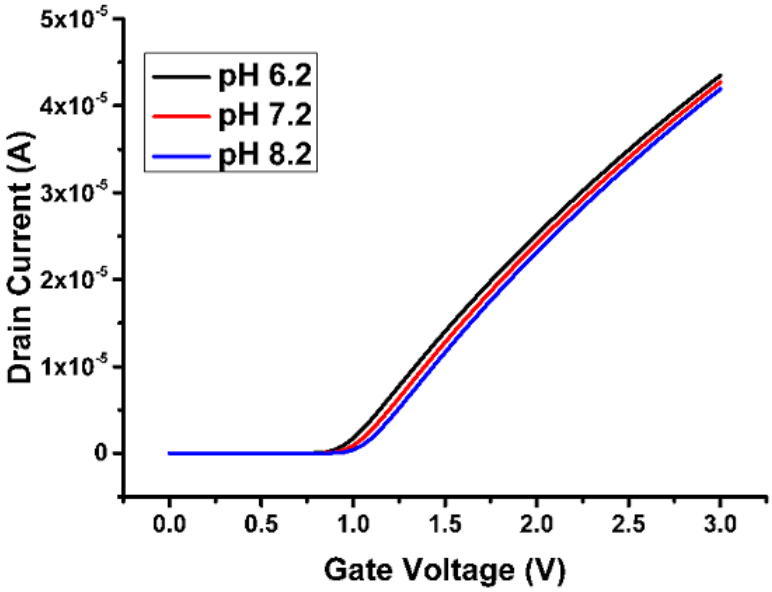

Figure 4.19: pH sensitivity studies for tin oxide thin films on a polished PCB

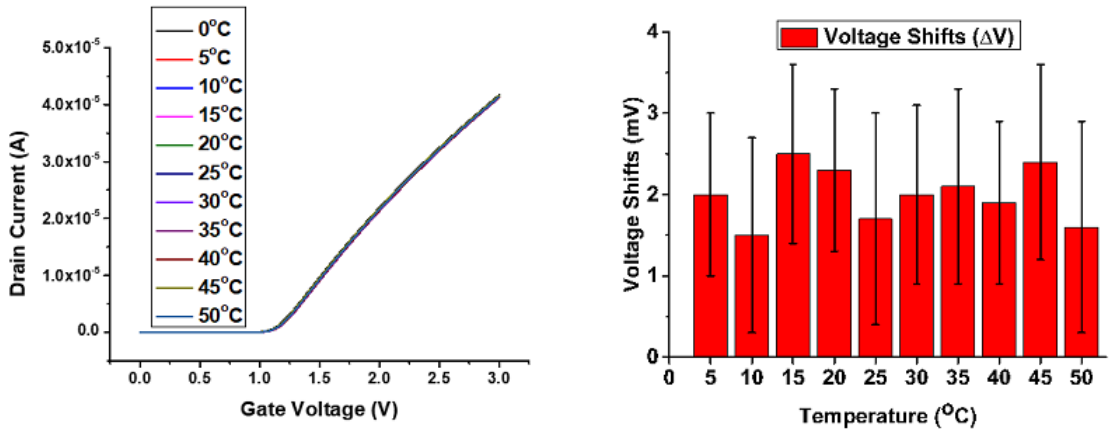

Figure 4.20: Temperature sensitivity studies for tin oxide thin film on a polished PCB in the range of 0-50°C. Left: Drain current vs gate voltage for different temperatures Right: Voltage shifts for different temperatures

The results of the pH sensitivity studies is shown in Figure 4.19. The polished PCBs showed a small increase in pH sensitivity from 51.3±1.2 mV/pH to

53.7±3.3 mV/pH.

The temperature sensitivity studies were significantly improved as shown in Figure 4.20. The voltage shifts with temperature was uniform in the $0 - 50°C$. The results from the unpolished PCB where a . A temperature sensitivity of 0.3 mV/°C was achieved.

Stability

The stability of the tin oxide thin films after peptide immobilisation on the polished PCB substrate remained reasonably good as shown in Figure 4.21. Similar to the previous stability studies, the PCB was left to stabilize in PBS 7.2 for 30 minutes before the experiment. There was a maximum of 4 mV shift in 10 minutes.

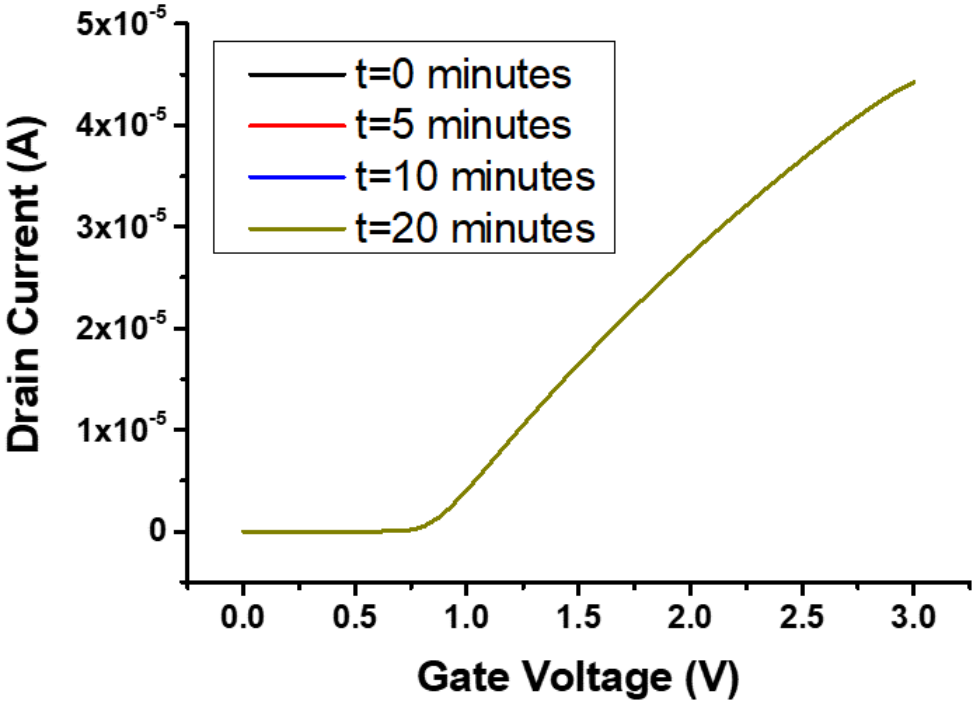

Figure 4.21: Stability of tin oxide thin films with immobilised peptide on a polished PCB substrate

Phosphorylation

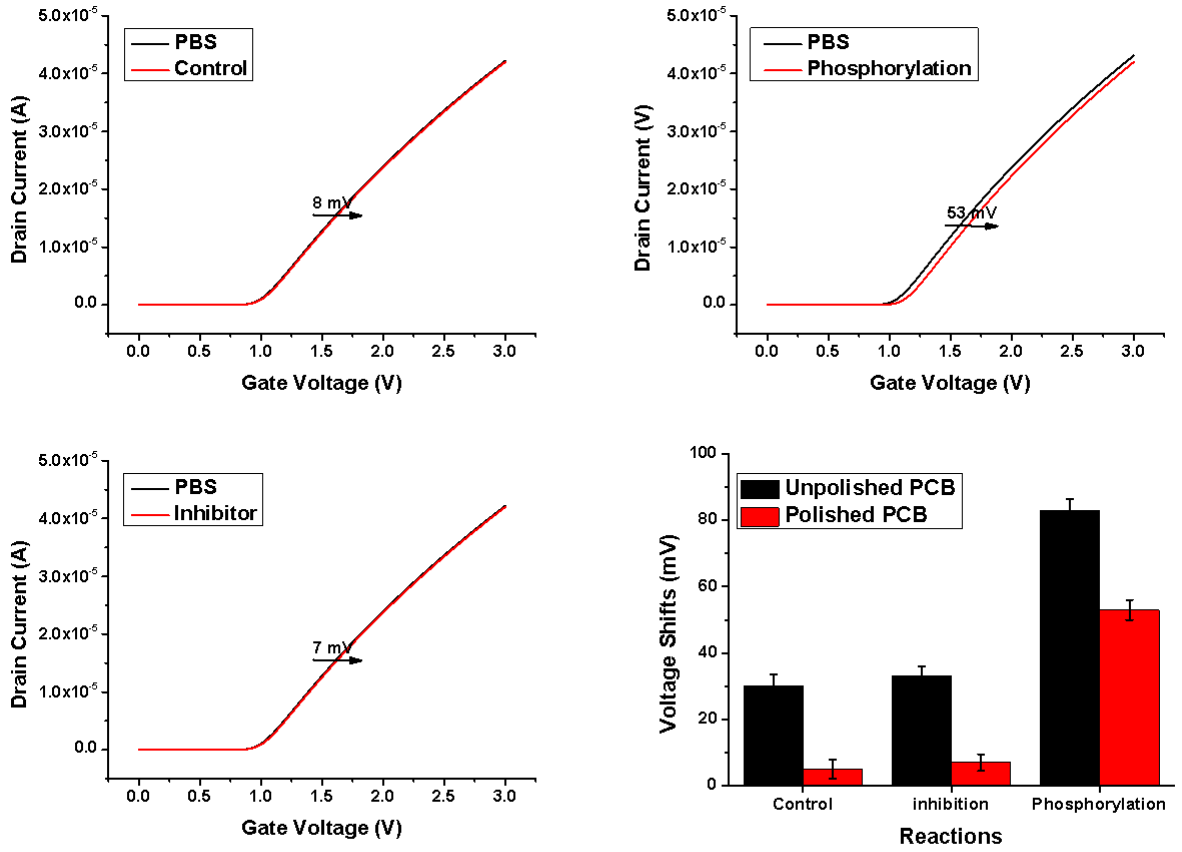

Figure 4.22: Results of phosphorylation studies on tin oxide thin film on a polished PCB. Top Left: Change in I-V characteristics for the control reaction Top Right: Change in I-V characteristics for the phosphorylation reaction Bottom Left: Change in I-V characteristics for the inhibition reaction Bottom Right: Comparison of voltage shifts during the phosphorylation studies for tin oxide thin film on polished and unpolished PCB

The results of the phosphorylation reaction is shown in Figure 4.22. A significant improvement in signal was observed with the polished PCBs. The control signal was reduced to an average of 8 mV from 30 mV in the unpolished PCBs. The

large signal of 83 mV for the phosphorylation reaction was reduced to an average of 53 mV. The inhibitor showed a average 7 mV shift from 33 mV in the unpolished PCBs which is close to that of the control signal. The figure also shows the difference in signal levels for phosphorylation studies for tin oxide thin films on polished and unpolished PCB.

Thin Film	Control(mV)	Inhibition(mV)	Phosphorylation(mV)
SnO_2 on unpolished PCB	30	33	83
SnO_2 on polished PCB	8	7	53
Ta_2O_5 on polished PCB	8	10	47

Table 4.2: Voltage shifts from phosphorylation studies on tin oxide and tantalum oxide

The difference in signals between the polished an unpolished PCBs could be for a variety of reasons. Commercial copper clad FR4 sheets show an uneven, rough surface when checked under an optical microscope. Deposition of materials on such substrates can cause the resulting thin film to be uneven with a larger effective sensor area. The effect of surface roughness of the substrate on the response of tin oxide thin films was studied by Cricenti *et al.*. An increase in response by 30% was observed with the thin films deposited on a rough substrate [145].

Another possible reason for the enhanced signal from the unpolished PCBs is the chance that the tin oxide deposited on the uneven surface was porous. The penetration of solutions into the pores would have resulted in false signals being added to the overall signal [146]. The reason also could be a combination of the above two. Table 4.2 shows the different values from phosphorylation studies for SnO_2 and Ta_2O_5.

From the SEM and AFM images, it can also be hypothesised that the deposited tin oxide thin film on the unpolished PCB might have had copper exposed through them which eventually entered the electrolyte. Copper has been known to

behave as a catalyst in several biological reactions [147] and could be hypothesised that the large shifts were due to some kind of catalytic activity. However, the role of copper as a catalyst in the phosphorylation reaction has not been investigated further in this study and therefore remain inconclusive.

4.1.5 Conclusion

This study forms the first part of developing a REFET based biosensor. The pH sensitive material tin oxide was used to form a thin film on a PCB substrate which was coupled to the gate of a MOSFET as an extended gate. Even though the film showed good pH sensitivity and stability, the signals from the phosphorylation studies was very large. The temperature sensitivity was also variable.

To troubleshoot this problem, tantalum pentoxide was used to replace tin oxide as the sensing layer on the PCB. Poor adhesion of tantalum oxide was improved by polishing the PCBs with alumina slurry before deposition of the thin film. This improved adhesion significantly and the phosphorylation studies showed some promising results. However, some of the films were still prone to dissolution on repeated washing.

The above process was applied to the tin oxide thin films and proved to be very successful in reducing large false signals. The phosphorylation studies showed smaller signals for control, inhibition and phosphorylation reactions. This technique was employed in making the sensor film for the REFET and will be explored in later section.

The limitation of this technique is that the PCBs were polished by hand and can be difficult to produce a uniform surface when a larger sized PCB is used for the 96 well plate. Also the films are single use only and cannot be clean and reused for measurement unlike the silicon nitride coated silicon wafers.

4.2 Development of the Reference Field Effect Transistor

4.2.1 Introduction

This section describes the development of the biosensor that can act as a reference for the final REFET device. Ideally, the sensor should be completely insensitive to pH and phosphorylation. The passive sensor should closely resemble the active sensor surface with the exception of having a peptide immobilised on it which does not contain any phosphorylation sites. The design and synthesis of this peptide was not attempted due to time constraints. Instead, several attempts have been made to cover the gate of an ISFET with a ion insensitive membrane of varying thickness and compositions. Thick layers of materials such as Teflon and PVC (few microns or higher) have failed to show a low pH response [107] [148]. On the other hand, thin polymer layers (tens of nanometers) show a linear response to pH with nearly no change in pH sensitivity. The reason for this is the inability to create pin-hole free surfaces of such low thickness [149].

Chemical modifications of the gate surface has proved more successful in producing pH insensitive layers. In one approach, grafting a dense monolayer of long alkyl-chain silanes was attempted yielding low pH sensitivity of 10 mV/pH [150]. In another attempt the gate was covered with a sodium complex of calixpherand which showed almost no pH sensitivity [148].

In this study, initially the blocking of active GOPTS sites was attempted. This is expected to prevent components of the solution from binding to the surface. Two polymers, namely PDMS and SU-8 were tested for their suitability as the pH insensitive layer. The most successful attempt was using SU-8. SU-8 is an epoxy based negative photoresist which is often used as a passivation layer for microdevices

[151]. SU-8 has been used by to reduce pH sensitivity of surfaces. In a study by Calleja *et al.*, microcantilevers of SU-8 photoresist were fabricated to eliminate pH and temperature sensitivity as compared to gold coated silicon nitride cantilevers [152].

4.2.2 Materials and Methods

Preparing the PCBs

A printed circuit board (PCB) containing four contact pads was made using the LPKF S63 PCB milling machine on double sided copper clad FR4 material. The dimensions and distances between the pads were decided keeping in mind the 96 well microtitre plate (same as Figure 3.23 in the previous section). The PCB was cleaned by sonication in acetone and isopranol for 5 minutes each and dried. The copper pads of the board were polished using 5 μm alumina slurry for 8 minutes. The PCBs were cleaned again by sonication in acetone and isopropanol for 5 minutes each and dried.

Blocking GOPTS on SnO_2 surface

10 nm of aluminium as an adhesion layer was thermally evaporated on to the copper pads from a tungsten boat. 150 nm of tin oxide was deposited by thermally evaporation from an alumina coated tungsten wire basket. The contacts were masked with kapton tape. The thin films were used without any further cleaning.

To silanise the tin oxide, GOPTS was heated to its boiling point (120°C) and the thin films were exposed to the silane vapours for five seconds. They were rinsed with DI water and dried. The silianised surface contains epoxide groups capable of covalently bonding to the amine groups of the peptide [117]. The

epoxide groups convert to ether on reacting with ethanol, preventing the binding of the peptide [119]. The active GOPTS sites were blocked using 20% ethanol. Different incubation times of 5, 10 and 15 minutes were considered. Also, 1% and 2% ethanolamine pH 8.5 was used to block the surface. Different incubation times of 5, 10 and 15 minutes were considered. 50 μl of PBS buffer pH 7.2 was dispensed on to the modified thin films and the sensing surface was allowed to stabilise for 30 minutes before conducting any experiments.

Passivation with SU-8

PDMS and SU-8 photoresist of different thicknesses were spin coated onto the cleaned and dried PCBs to act as a pH insensitive layer. The PDMS was cured at 90°C for 20 minutes. The SU-8 layers baked for 2 minutes at 90°C, exposed to UV radiation and then baked for 2 minutes at the same temperature post exposure. 50 μl of PBS buffer pH 7.2 was dispensed on to films and the sensing surface was allowed to stabilise for 30 minutes.

Current-voltage measurements

The modified PCBs were connected to the gate terminal of an n-type MOSFET for measurement. This MOSFET the same as section 4.1.2. A variable gate to source voltage of 0-3 V was applied through a reference electrode (silver wire coated with silver chloride paste) dipped in PBS buffer pH 7.2. A fixed drain to source voltage of 50 mV was maintained. Agilent B1500A HR CMU Semiconductor Device Analyser was used to record current vs voltage measurements. The experiments were performed in a closed Faraday cage in order to minimise the influence of noise. All measurements were performed on three individual PCBs containing 4 pads each and the average values were considered. Errors were measured from the standard deviation of the data. Voltage shifts were

observed from the shift in threshold voltage. Figure 4.23 shows the schematic of the measurement setup where the PCB coated with the SU-8 layer layer forms the extended gate to a MOSFET. The gate voltage is applied to the reference electrode dipped in the electrolyte (PBS buffer). The connection is similar to the 'active' devices containing the tin oxide thin films which were described in section 4.1.

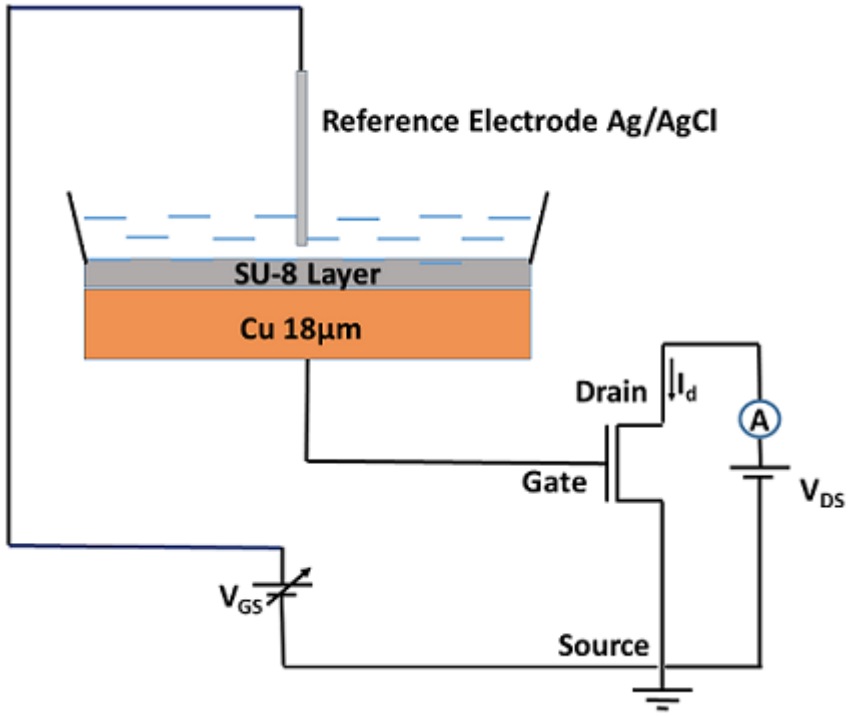

Figure 4.23: Schematic of the measurement setup

4.2.3 Results and Discussion

Blocking silanised SnO_2 surface

The silanised SnO_2 surfaces with the GOPTS sites blocked were used for the phosphorylation reaction. The solution for the control reaction containing ATP and PKC lipid activator was dispensed on the surfaces and allowed to incubate for 13 minutes. The voltage shifts for 1% and 2% ethanolamine as well as 20% ethanol

remained around 10-12 mV irrespective of the blocking time. The solution for the phosphorylation reaction containing ATP, PKC lipid activator and PKC-α kinase was dispensed on to the films and after 13 minutes a shift of 27-30 mV was observed irrespective of the blocking time. Figure 4.24 and 4.25 show the voltage shifts for the control and phosphorylation reaction. The error bars represent the the variability in the data over three different PCBs where the measurements were conducted on each of the four pads.

This process did not prove successful in providing an insensitive surface. This was probably because it was not possible to block all the available GOPTS sites and the chemicals in the solutions were attaching to the GOPTS sites or directly on the surface. The result was the surface being modified and the I-V characteristics showing a shift. The inhibition reaction was not conducted in this case because the control and phosphorylation reaction showed significant shifts and the inhibition reaction would be wasteful.

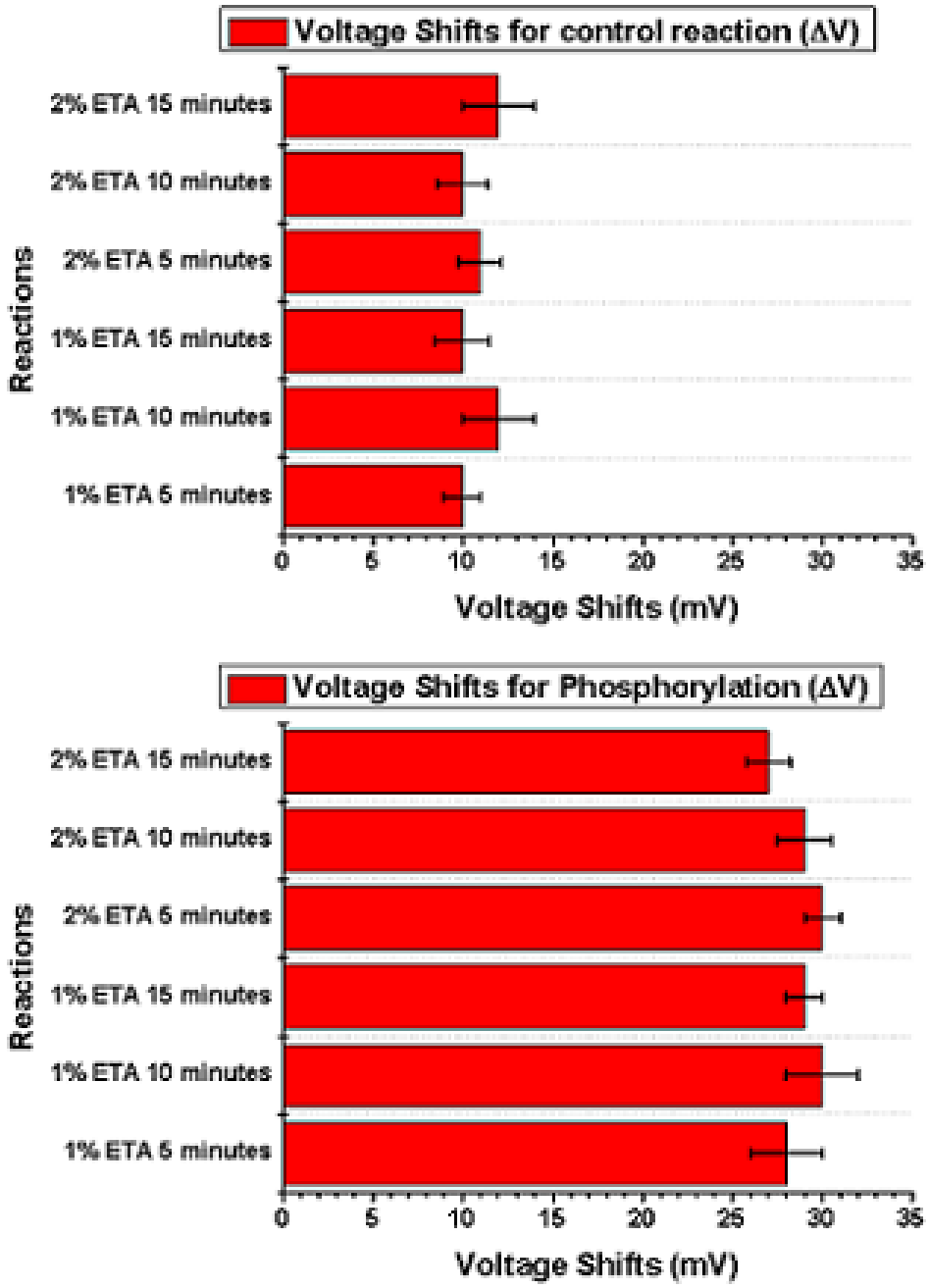

Figure 4.24: Top: Shifts in gate voltage for the control reaction for 1% and 2% ethanolamine (ETA) Bottom: Shifts in gate voltage for the phosphorylation reaction for 1% and 2% ethanolamine (ETA)

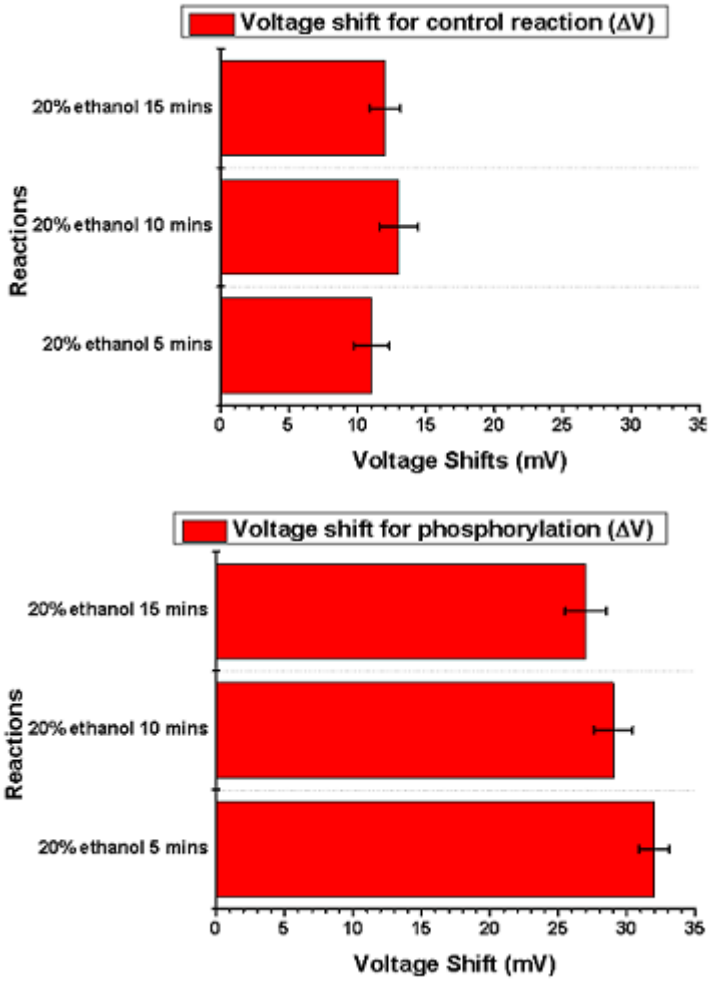

Figure 4.25: Top: Shifts in gate voltage for the control reaction for 20% ethanol Bottom: Shifts in gate voltage for the phosphorylation reaction for 20% ethanol

PDMS and SU-8

In the next attempt, PDMS polymer was spin coated on to the copper pads of the PCB and cured and cured at 90°C for 10 minutes. The thickness of the layer was roughly 100 μm. The extended gate measurements in PBS pH 7.2 showed a noisy signal with low signal strength of a few nanoamps. PDMS was not tested further because it was difficult to tailor its thickness for further experimentation.

SU-8 50 μm was then spin coated on to the tin oxide thin films. I-V measurements showed a signal strength of only a hundred picoamps in PBS pH 7.2 but continued to be very noisy and distorted. This clearly shows that the insulator layer is too thick and is preventing the effect of the electic field from reaching the gate of the MOSFET. The signal strength was too low to be considered as a reference for the final REFET structure. Ideally, the reference FET or the insensitive' FET should produce a signal similar to the 'sensitive' FET when the peptides are not phosphorylated. In the next attempt, SU-8 50 μm was spin coated directly on to the copper pads. The rationale behind this was to reduce the thickness of the insulator at the gate. This would also eliminate any effects at the tin oxide-SU-8 junction. In some previous experiments where the tin oxide surface was heated, the thin film showed visible signs for fragmentation. It is possible that the heating required for curing SU-8 was causing the tin oxide layer to be damaged. The resulting signal strength improved to the range of microamps . Figure 4.26 shows the results of these attempts.

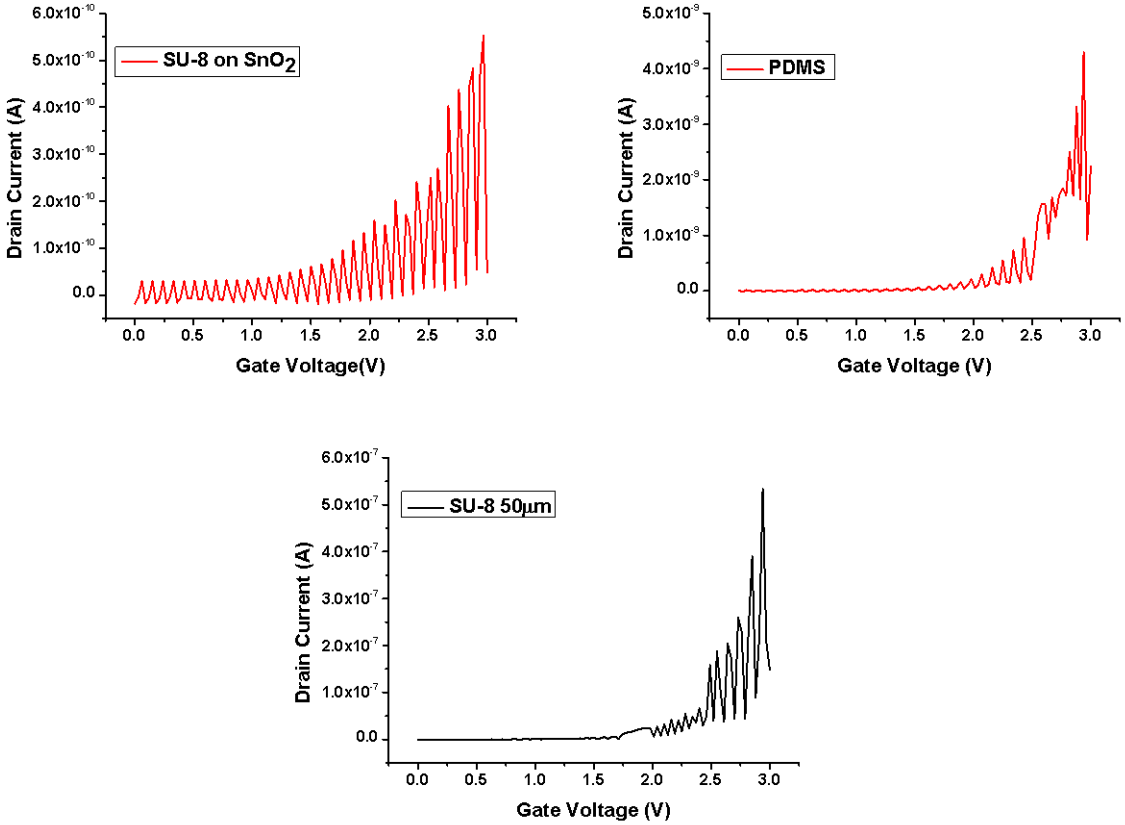

Figure 4.26: Top Left: Drain current vs gate voltage for SU-8 50 μm on SnO_2 Top Left: Drain current vs gate voltage for 100 μm of PDMS Bottom: Drain current vs gate voltage for SU-8 50 μm on copper

To increase signal strength and reduce the noise, the thickness of the SU-8 film was reduced. The results of the extended gate I-V measurements is shown in Figure 4.27. For the SU-8 thin film of 10 μm thickness, the on current increased to microamps. For further noise reduction 2 μm and 115 nm SU-8 was used. The on current increased to double and the noise level reduced significantly when the SU-8 thickness was changed from 2 μm and 115 nm. The best signal was achieved from the 115 nm SU-8 layer and was used for further experiments on stability, temperature sensitivity and phosphorylation.

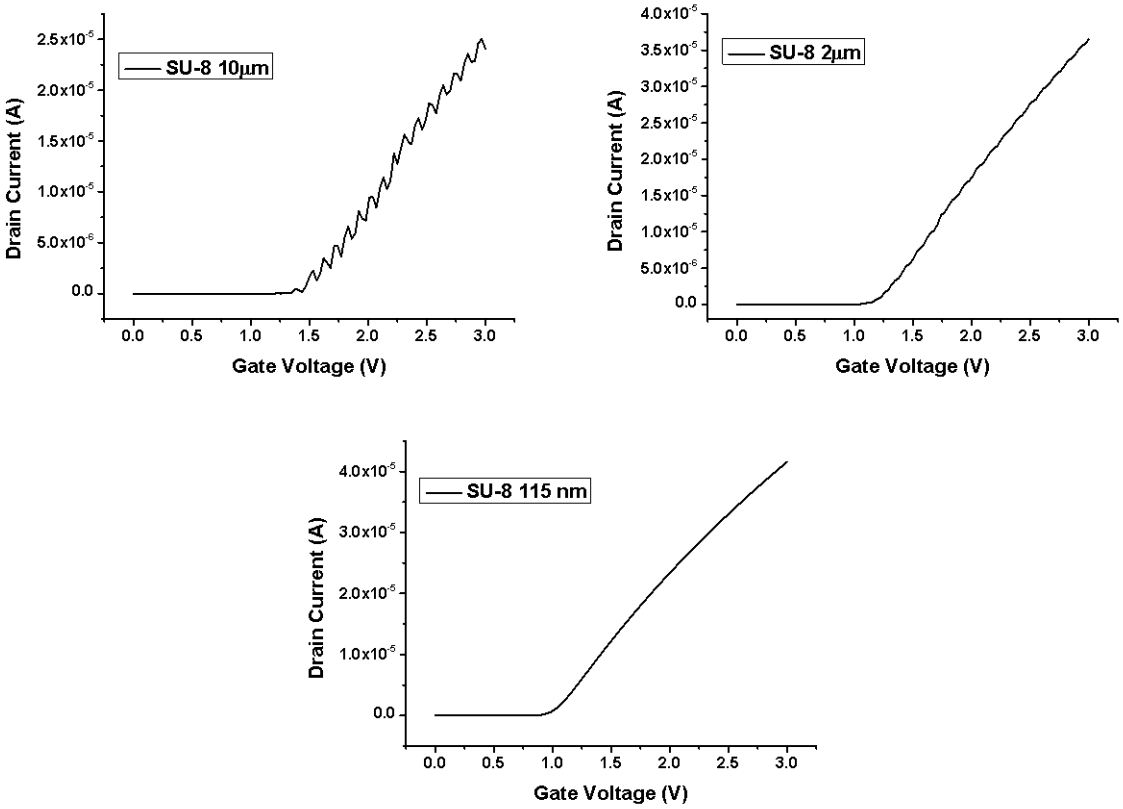

Figure 4.27: Drain current versus gate voltage different thicknesses of SU-8 thin film on a PCB substrate

Stability

The stability of the 115 nm SU-8 film was measured after incubation in PBS pH 7.2 for 30 minutes. The results are shown in Figure 4.28. The shift over 10 minutes was less than 2 mV and can be considered to be stable for further experiments.

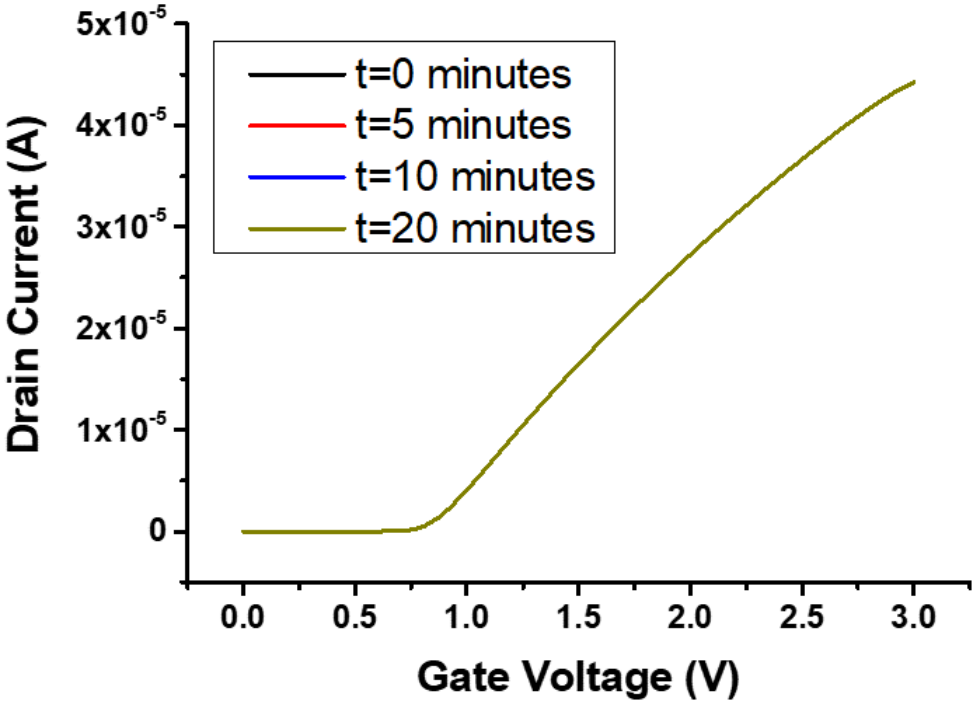

Figure 4.28: Stability of SU-8 115 nm thin film on a PCB in PBS buffer pH 7.2

Temperature sensitivity

Temperature sensitivity was measured after incubating the SU-8 films in PBS pH 7.2 at room temperature for 30 minutes. The temperature of the PBS buffer was varied between 0 and 50°C with 5°C increments. For this experiment the PBS buffer was fist cooled to 0°C and then heated slowly to 50°C in a temperature controlled water bath. The temperature of the PBS was monitored closely during the experiment by using a thermometer immersed in the in the beaker containing the buffer. 50μl of PBS at dispensed on the sensor surface for every 5°C increment and the I-V characteristics were measured immediately. This was done to prevent the temperature of the buffer from reaching room temperature during the measurements. The results are shown in Figure 4.29. A temperature sensitivity of 0.9 mV/°C was observed. The error bars represent the variability in data between 3 different PCBs where all four of the pads were used for measurement.

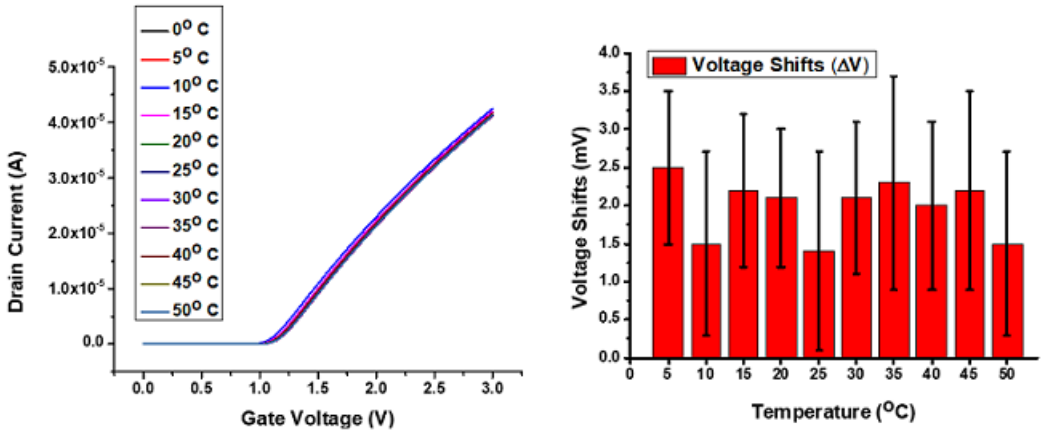

Figure 4.29: Temperature sensitivity studies on SU-8 115 nm on a PCB in the range 0-50° Left: Drain current vs gate voltage for different temperatures on SU-8 surface Right: Voltage shifts for different temperatures

SU-8 pH sensitivity

The SU-8 thin films were incubated in PBS pH 7.2 for 30 minutes before the pH sensitivity studies were conducted. The pH sensitivity archived in this study was 4.3±1.3 mV/pH.

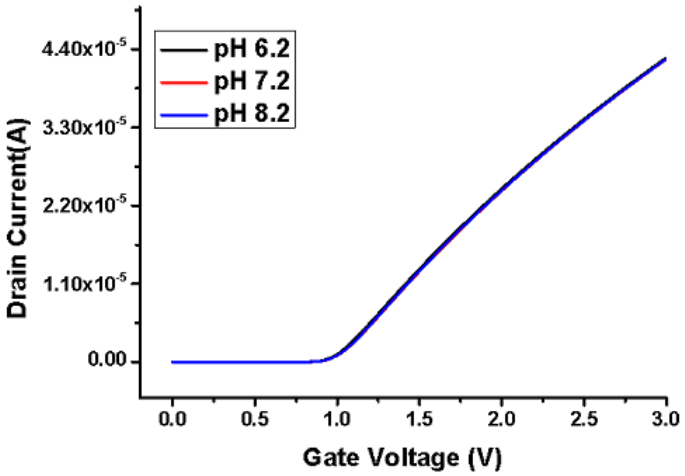

Figure 4.30: Drain current vs gate voltage for pH sensitivity studies

Phosphorylation

The results of the phosphorylation reaction are shown in Figure 4.31. The error bars represent the variability in data between three different PCBs where all four of the pads were used for measurement. The baseline was determined by first conducting measurements in PBS buffer pH 7.2. Each measurement was conducted after 13 minutes of incubation in the measuring solutions. The control reaction was conducted with 1 μM ATP and 2.5 μl PKC lipid activator. An average shift of 3 mV is observed after 13 minutes. On addition of kinase inhibitor along with PKC-α enzyme, a large average shift of 27 mV is observed. The phosphorylation reaction in the presence of ATP, kinase and activator showed a small shift of 4 mV.

The unexpected large shift for the inhibition reaction led to the investigation of how each of the solution components interact with the SU-8 surface. The SU-8 thin films were incubated with individual solution components in the same concentration as in the reactions. ATP, activator and enzyme showed a small voltage shift between 1-2 mV. The activator showed a large shift of 13 mV. These measurements were conducted over three PCBs were each of the four pads was used for measurement. Figure 4.31 shows the results of the experiment.

To reduce the surface interactions of the inhibitor, the SU-8 thin films were incubated in StartingBlock Buffer (PBS) Tween 20 (procured from ThermoFisher) for 30 minutes before the experiment. StartingBlock buffer contains a single purified protein and has been shown to successfully block free spaces on the surface to prevent interactions like non-specific binding [153]. This technique came with the risk that the protein present in the StartingBlock may phosphorylate. However, no significant change was observed. The voltage shift for the inhibition reaction reduced by only 3 mV while the control and phosphorylation reaction reduced by only 1 mV each. The potential for the proteins in the StartingBlock to phosphorylate was not investigated since this method was not taken forward to develop the reference FET.

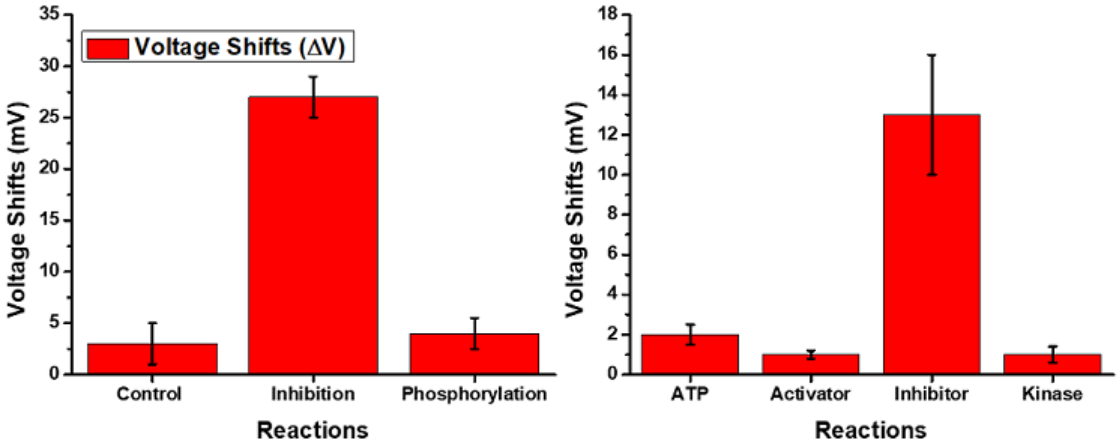

Figure 4.31: Left: Voltage shifts phosphorylation studies on SU-8 thin films on a PCB Right: Voltage shifts due to interaction of individual solution components with the SU-8 surface

In the next attempt, the SU-8 thin films were incubated with the inhibitor in PBS buffer pH 7.2 for 30 minutes before the phosphorylation studies were conducted. This was done to saturte the surface with inhibitor and eliminate the effect that was causing the significant shifts. This method proved to be successful in reducing the large inhibition signal to 2 mV. The control signal was only reduced by 1 mV while the phosphorylation signal remained constant. Figure 4.32 and Table 4.3 shows the comparison between voltage shifts during the phosphorylation studies for the plain SU-8 surface, SU-8 surface treated with StartingBlock buffer and SU-8 treated with inhibitor. Incubating with the inhibitor may not be ideal when a number of inhibitors are being considered but this process was followed to move towards the construction of the REFET in the next chapter.

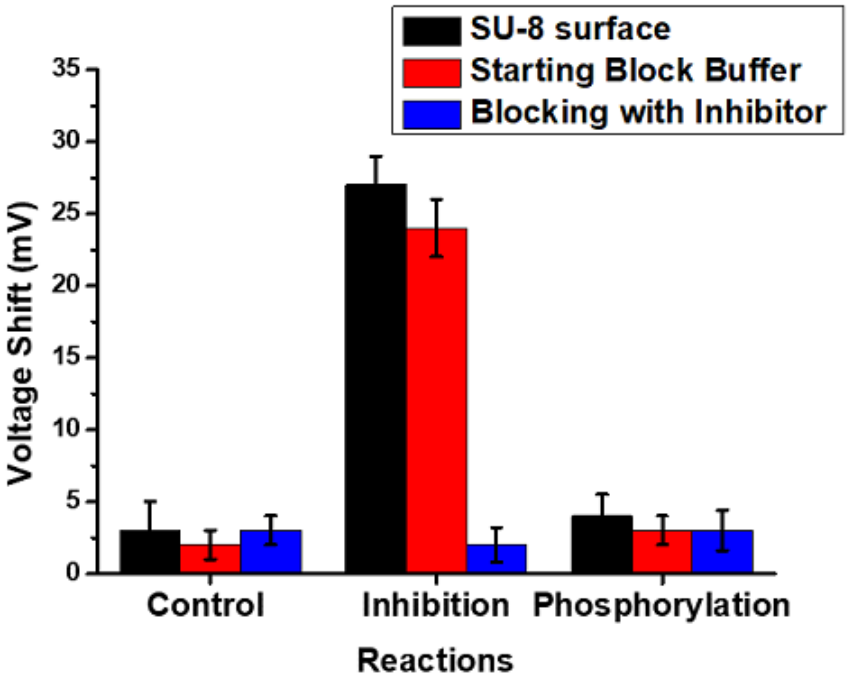

Figure 4.32: Voltage shifts due to phosphorylation studies on SU-8 thin films, SU-8 surface treated with StartingBlock Buffer and SU-8 surface treated with inhibitor

Thin Film	Control(mV)	Inhibition(mV)	Phosphorylation(mV)
SU-8	3	27	4
SU-8+StartingBlock	2	24	3
SU-8+Inhibitor	1	2	3

Table 4.3: Voltage shifts from phosphorylation studies su-8

4.2.4 Conclusion

The development of the pH insensitive surface that does not respond to the phosphorylation reaction forms the second part of the final REFET design. SU-8 as a pH insensitive material was studied. SU-8 115 nm showed the best and most noise free signal and was used for further studies. The pH sensitivity was only 4.3±1.3 mV/pH as compared to 53.7±1.2 mV/pH for the tin oxide thin film in section 4.1.

The SU-8 thin film showed good stability and temperature sensitivity was not insensitive to all the reactions in the phosphorylation studies. The control and inhibition reactions showed small changes in voltage but the inhibition reaction showed a large voltage shift. This was finally minimised by treating the surface with inhibitor before the phosphorylation studies. While this process adds an extra step to the making of the biosensor, a more effective process to suppress the inhibition signal was not discovered during this study. The aim would be to construct two surfaces that closely resemble one another except one is active and the other is passive. One approach would be to deposit tin oxide on both surfaces but modify one with the peptide containing one phosphorylation site and the other with a peptide containing no phosphorylation sites. This technique will be used to make the reference FET for the REFET based biosensor and will be detailed in the next chapter.

Chapter 5

Multiplexed REFET Structures for Screening Protein Kinase Inhibitors

5.1 Introduction

In this chapter the attempts to put the REFET structure together and use it for the purpose of biosensing is described. A commercially available MOSFET IC ALD1106 (Advanced Linear Devices, Inc) containing matched pair FETs is used for extended gate measurements using the tin oxide and SU-8 thin films on a PCB as extended gates. The FETs on this IC have low gate leakage current, typically 0.1 pA and a maximum of 10 pA. Leakage currents can result in addition of false signals and therefore a MOSFET with a low gate leakage desirable [154]. The differential measurement between the 'sensitive' and the 'insensitive' surfaces eliminates the need for a reference electrode.

Next, A PCB was designed such that each well of the 96 well microtitre plate contained 3 copper pads. Two of them act as extended gates to the matched pair transistors for differential measurements and the third acts a ground connection. The four sets of copper pads were multiplexed using an analog multiplexer IC CD74HC4052 (Texas Instruments) after amplification through an

instrumentation amplifier AD620 (Analog Devices). The data was digitised, logged and processed by an Arduino Uno connected to a PC. For the array of 96 REFET structures, a decoder IC will be required for addressing the multiplexers but for the test board this was not used. This setup will help us move towards a portable system of screening protein kinase inhibitors. Similar to the previous chapters, a single protein kinase inhibitor was tested on this device as a proof of concept. Different inhibitors have not been considered on this occasion and forms a part of the future work.

5.2 Materials and Methods

Fabrication of REFET

A printed circuit board was designed using DesignSpark PCB (version 7.2). The copper pads were distributed such that they fit under a 96 well microtitre plate. Three pads were placed under each well to form a REFET structure. For testing purposes a small portion of the PCB containing 4 sets of pads was manufactured on double sided copper clad FR4 material using an LPKF S63 milling machine. Figure 5.1 shows the PCB design for the test board and Figure 5.2 shows the PCB once manufactured.

The boards were cleaned by sonicating in acetone and isopropanol for 5 minutes each. The copper pads were polished for 8 minutes using 5 μm alumina slurry to remove the thin layer of copper oxide and make the surface smoother. The alumina residue was removed by sonicating in acetone and isopropanol again for 5 minutes each.

SU-8 photoresist 115 nm was spin coated on the PCB. The boards were softbaked at 90°C for 2 minutes pre-exposure. The board was exposed to UV through a mask and then developed in Microposit EC solvent 11 (procured from A-Gas

Electronic Materials) to remove the unexposed SU-8 from the board such that only the reference pads were coated in SU-8. Post-exposure, the boards were baked at 90°C for 2 minutes.

The PCBs were loaded immediately into the thermal evaporator and the sensing pad was exposed through a shadow mask. The shadow mask was made from a thin aluminium sheet (hundred micron thick). The deposition of tin oxide first, followed by the spin coating of SU-8 was considered but the removal of the unexposed SU-8 using the EC solvent would contaminate the sensing surface. The masks can be cleaned and reused easily for several evaporations. The major drawbacks of this technique is the pattern spreading near the edges of the holes, in form of a smooth decay. This may be attributed to two effects. Firstly, the source of the vapours is not a point source resulting in a penumbra region and secondly, the atoms scattering the edges of the mask [155]. Since the features on the REFET PCB are large (several milimeters) and there is sufficient distance between pads, the effect of spreading is not significant. 10 nm of aluminium and 150 nm of tin oxide was deposited through thermal evaporation. The boards were used without any further cleaning. The ground pad was coated with silver paste and allowed to air dry.

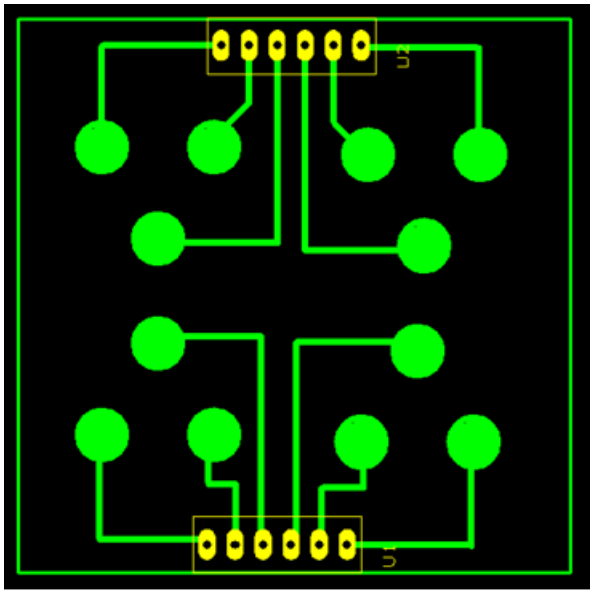

s

Figure 5.1: PCB design for the REFET extended gate structure

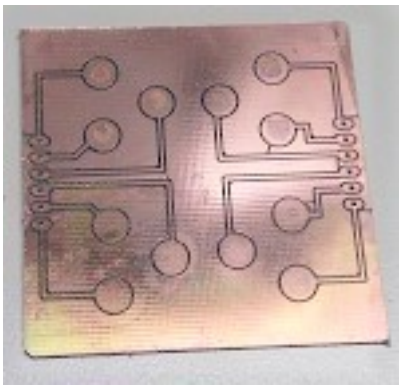

Figure 5.2: Manufactured PCB containing REFET extended gate structures Dimension: 30 mm X 30 mm

Biofunctionalisation

The same process was followed for biofunctionalisation as the previous chapters. GOPTS was heated to 120°C and the PCB was exposed to the vapours for 5 seconds through the shadow mask used for evaporation of aluminium and tin oxide. This was done to prevent silanization of the reference and ground pads. The boards were rinsed in DI water and dried. All pads were covered with teflon tape leaving a circular interrogation area of 7.07 mm^2 exposed. 2 μl of 156 μM peptide solution was dispensed on to tin oxide coated pads and left to bind for 40 minutes. The unreacted GOPTS sites were blocked by washing in 20% ethanol. The pads were left in PBS pH 7.2 for 30 minutes to stabilise before conducting further tests. Figure 5.3 shows the modified copper pads for biosensing.

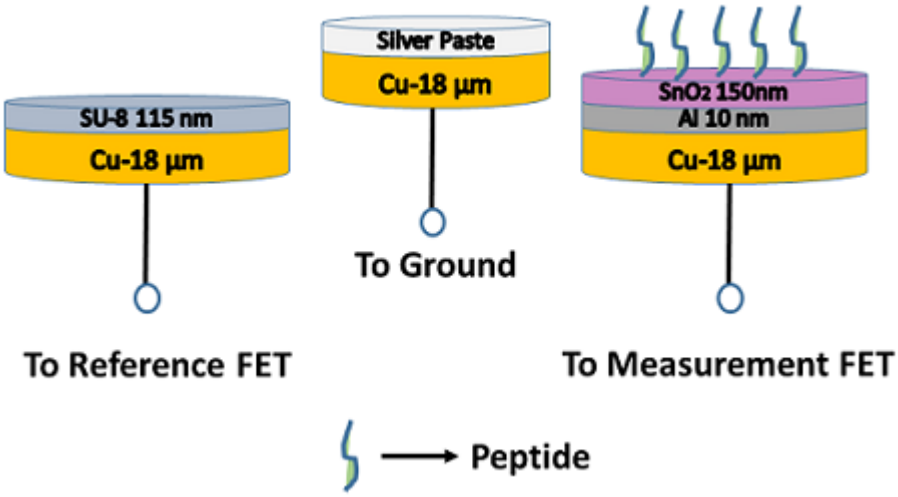

Figure 5.3: Modified copper pads for biosensing

Measurement Setup

The biosensors were interfaced with a commercially available MOSFET array, ALD1106. This IC contains four n-channel enhancement mode matched MOSFET transistors. The sensor pad and the reference pad were connected to the gate terminal of two of the MOSFETs and the ground pad was connected to the common ground of the measurement circuit.

Initially, the response of the MOSFETs to the phosphorylation reaction was recorded for the tin oxide and SU-8 surfaces individually using the Agilent B1500A HR CMU Semiconductor Device Analyser. The MOSFET has a low threshold voltage of 700 mV and low gate leakage current of typically 0.1 pA. The substrate bias was kept at 0 V for the entire measurement. The gate to source voltage (V_{GS}) was varied from 0-3 V while keeping the drain to source voltage (V_{DS}) at 1 V. The gate voltage was applied through a reference electrode and the PCB was enclosed in a Faraday cage to minimise the effect of noise. The reaction volumes were fixed to 50 μl. Figure 5.4 shows the schematic of the sensor setup. The shifts in threshold voltage were observed.

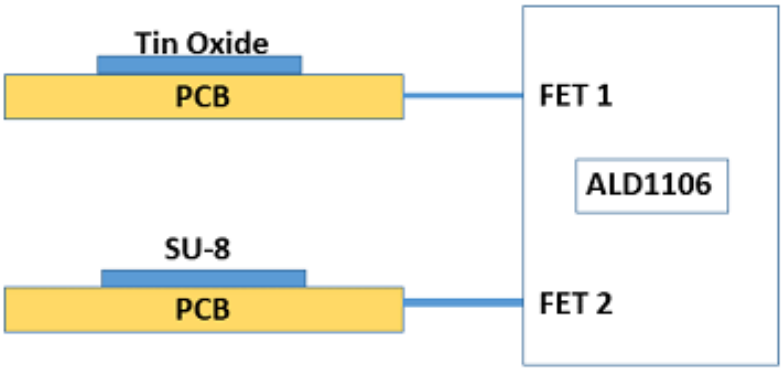

Figure 5.4: Schematic of sensor setup

In the second part of the study, the differential measurement between the sensing and the reference pad was measured by an Arduino Uno. No reference electrode was required in this study. The signal was amplified by an instrumentation amplifier AD620 with a gain of 20. This IC was chosen for its low offset voltage, high accuracy and low cost. The amplification stage was necessary because at the next stage when the sensors were multiplexed, a small amount of the signal was lost (40 mV attenuation).

The signal was then converted to a digital signal by the 10-bit analog-to-digital converter present on the Arduino. The reference voltage for was set to 1.1 V in order to bring the resolution down to 1 mV. The circuit was enclosed in a Farday cage to minimise the effect of noise. The Arduino was powered by connecting it to the USB port of a PC and the other ICs on the board were powered through the Arduino. The V_{GS} and V_{DS} values were fixed at 1 V for the duration of the measurement and the drain current was measured over a fixed interval of time.

The four REFETs were finally multiplexed through an analog multiplexer CD74HC4052. This IC has a low input resistance (7 Ω) and contains four channels that can be selected through the 'address select' lines. Data from each channel was collected for 10 seconds at every 0.5 second interval. Figure 5.5 shows the schematic of the measurement setup. In the final design the multiplexer may be replaced by

one containing more channels on one chip but for the purpose of simplicity, they are retained in the figure. The shift in drain current with time was calculated for stability, pH sensitivity, temperature sensitivity and phosphorylation studies. The reaction volumes were fixed to 200 μl. All measurements were performed on three different PCBs containing four REFET structures each and the average values were considered. The errors were calculated from the standard deviation of the data.

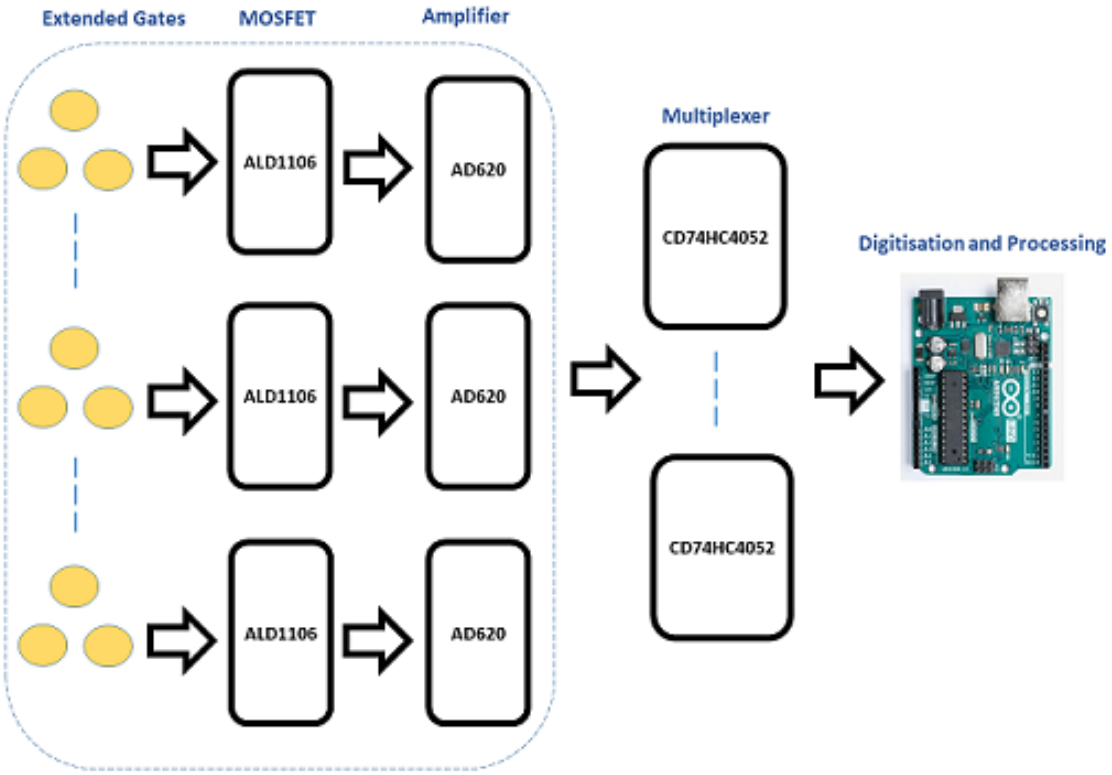

Figure 5.5: Schematic of measurement setup for the multiplexed biosensors. Image source for Arduino: https://www.arduino.cc/

5.3 Results and Discussion

Response of ALD1106

The pH sensitivity of tin oxide and SU-8 thin films were measured individually as extended gates to ALD1106. The drain current vs gate voltage characteristics are shown in Figure 5.6. The surfaces were incubated in PBS buffer pH 7.2 for 30 minutes prior to the experiment. The pH sensitivity of the SU-8 thin films was 5.2±1.1 mV/pH. The pH sensitivity of tin oxide was found to be 50.1±3.5 mV/pH. As expected, the SU-8 surface shows a low pH sensitivity while the tin oxide has a higher sensitivity to pH. We can now move towards phosphorylation studies on the 'sensitive' and 'insensitive' surface.

Figure 5.7 shows the drain current versus gate voltage characteristics for stability studies on the tin oxide thin films were performed after the immobilisation of peptide. The surface was left in PBS buffer pH 7.2 for 30 minutes. The voltage shift over 10 minutes was 2.5 mV. The surface was stable for conducting phosphorylation studies.

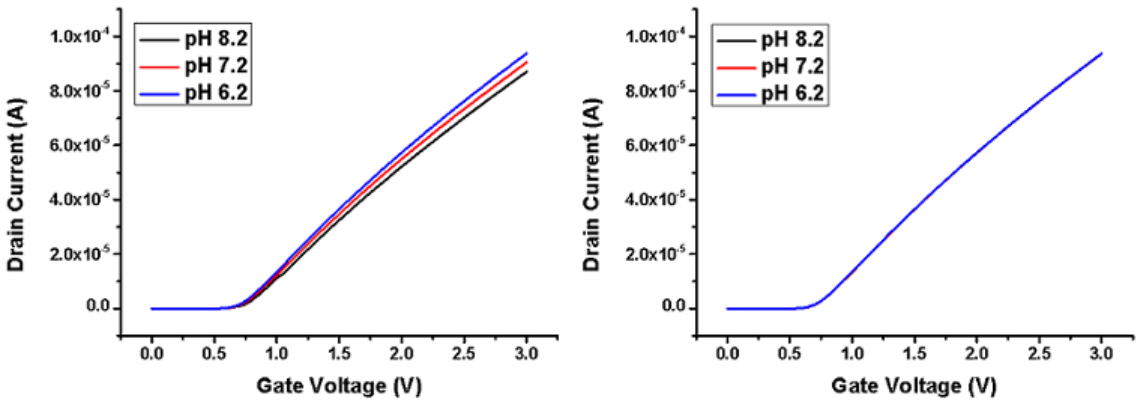

Figure 5.6: Left: pH sensitivity studies on tin oxide measured with ALD1106 Right: pH sensitivity studies on SU-8 measured through ALD1106

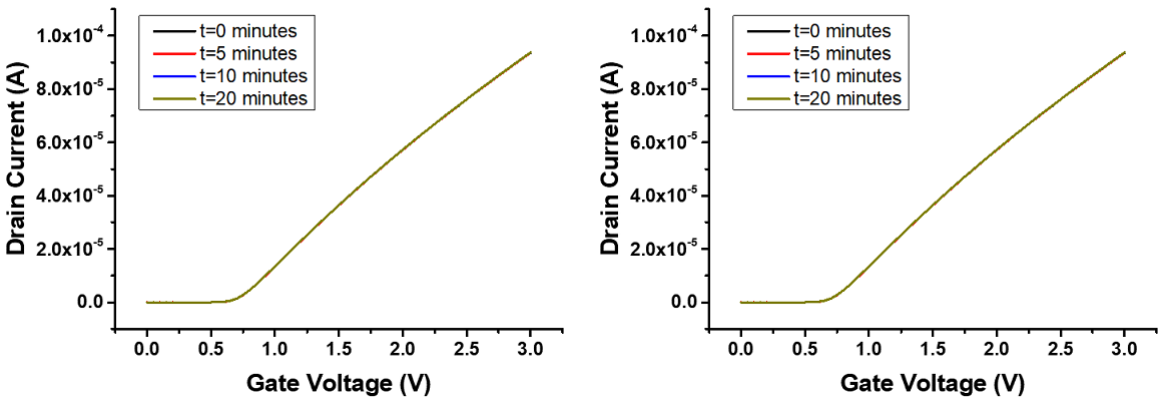

Figure 5.7: Left: Stability studies on tin oxide surface with immobilised peptide measured through ALD1106 Right: Stability studies on SU-8 surface measured through ALD1106

The voltage shifts for the phosphorylation studies on the tin oxide and SU-8 surface are shown in Figure 5.8. The error bars represent the variation over three different PCBs where all four of the pads have been used for measurement. The I-V curves were first measured in PBS buffer pH 7.2 to determine the baseline. Each of the measurements were conducted after 13 minutes of incubation in the measuring solution. The SU-8 surface was incubated with inhibitor in PBS buffer pH 7.2 for 13 minutes prior to the experiment to block the surface and prevent false signals.

The control reaction was conducted with 1 μM ATP and 2.5 μl PKC lipid activator. An average shift of 7 mV from the baseline was observed for the tin oxide surface and a similar shift of 5 mV from the baseline was observed for the SU-8 surface. On addition of the kinase inhibitor along with PKC-α enzyme, the signal shifted by an average of 8 mV for tin oxide and 7 mV for SU-8 from the baseline. The phosphorylation reaction was conducted in the presence of ATP, activator and enzyme. The voltage shift for the tin oxide surface was 48 mV and for the SU-8 surface was only 5 mV. Table 5.1 shows the voltage shifts for the phosphorylation studies.

The results were similar to what was expected. The active surface, tin oxide, produced a large signal for the phosphorylation reaction while the passive surface, SU-8, remained insensitive to all the reactions conducted in this study. The system was compatible with the commercial CMOS IC used for measurement. These form the building blocks of the REFET system described in the next subsection.

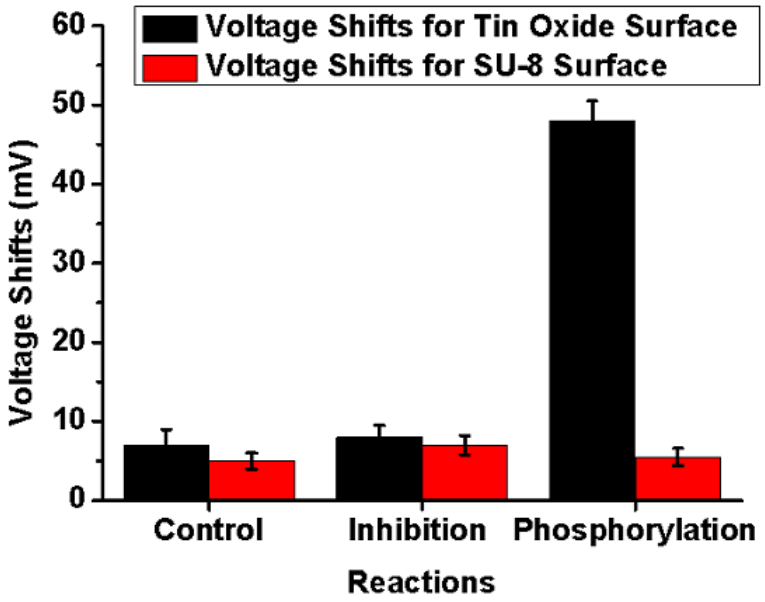

Figure 5.8: Voltage shifts for phosphorylation studies on tin oxide and SU-8 measured by ALD1106

Thin Film	Control(mV)	Inhibition(mV)	Phosphorylation(mV)
Tin Oxide	7	8	48
SU-8	5	7	5

Table 5.1: Voltage shifts for phosphorylation studies on tin oxide and SU-8 measured through ALD1106

Response of REFET

The stability of the REFET was measured individually for the tin oxide thin film and SU-8 thin film with ground connection as a reference. The results of ten minutes of the study is shown in Figure 5.9 (Left). The surfaces were incubated in PBS buffer pH 7.2 for 30 minutes prior to the study. The stability was measured over 10 minutes with 30 second intervals. The average difference in drain current values between the two surfaces is 0.6 μA over 10 minutes. 1 μA shift in drain current on the transfer characteristics of ALD1106 corresponds to 10 mV shift in drain current. Usually, a stable surface is expected to have a voltage shift below 10 mV in 10 minutes. Therefore, 0.6 μA shift in drain current is considered stable.

Figure 5.9 (Right) shows the drain current variations over 10 seconds for pH sensitivity studies. The extended gates were incubated in PBS buffer pH 7.2 for thirty minutes prior to the study. The difference in drain current between the tin oxide and SU-8 surface is measured. A pH sensitivity of 22.9±4.3 μA/pH was achieved in this study.

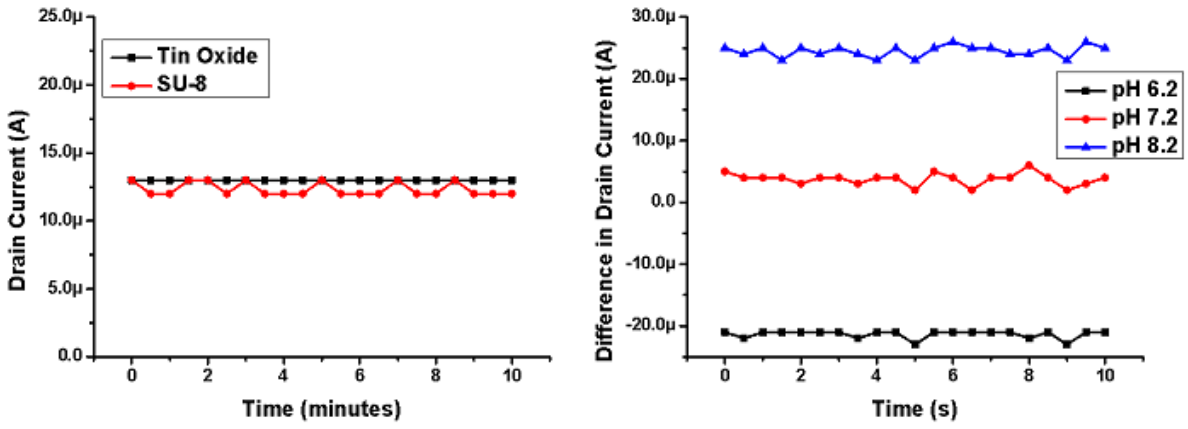

Figure 5.9: Left: Stability studies on the REFET. Right: pH sensitivity studies on the REFET

Figure 5.10 shows the drain current shifts of temperature sensitivity

studies on the REFET. The extended gates were incubated at PBS buffer pH 7.2 at room temperature for 30 minutes prior to the experiments. The temperature of the buffer was varied from 0-50°C in 5°C intervals. PBS buffer at 0°C was heated slowly in a temperature controlled water bath. THe temperature of the buffer was monitored closely using a thermometer immersed in the solution. For each 5°C increment, the buffer was dispensed on the sensor surface and the measurements were taken immediately. The measurements were taken over ten seconds for each interval and measured over three boards where the four sets of pads were multiplexed. The temperature sensitivity of 1.1 μA/°C. The REFET structures do not exhibit a significant temperature sensitivity. The variations due to temperature possibly appear as a common mode signal between the two transistors and does not appear in the differential measurements.

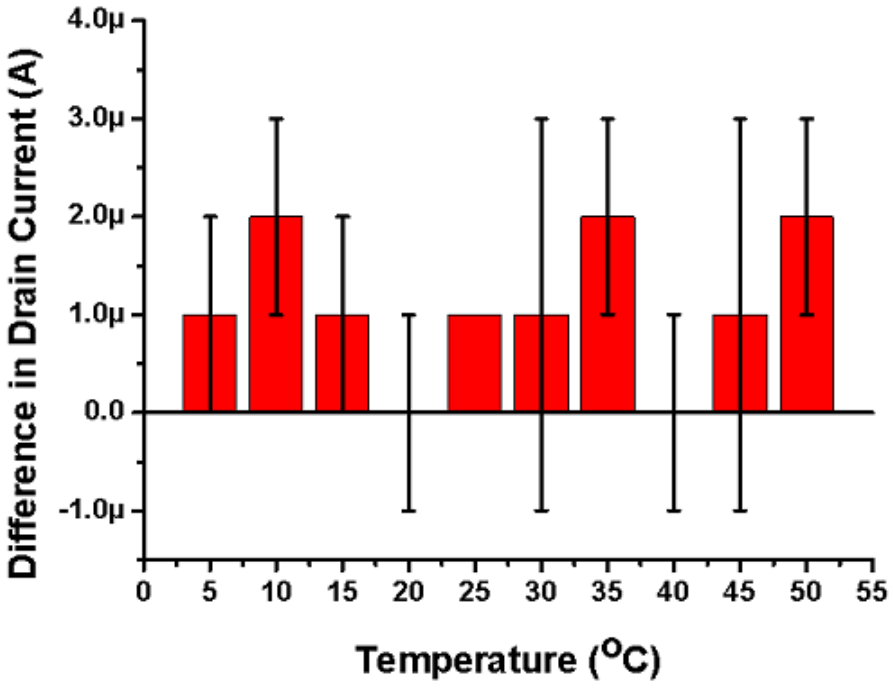

Figure 5.10: Drain current shifts with temperature on the REFET

The results for the phosphorylation studies on the tin oxide and SU-8 surface are shown in Figure 5.8. The error bars represent the variation in values

over three different PCBs where sets of four of pads have been used for measurement through the multiplexer. The difference in drain current was first measured in PBS pH 7.2 for 10 seconds to determine the baseline. Each of the measurements were conducted after 13 minutes of incubation in the measuring solution, similar to the protocols in the previous chapters. The SU-8 surface was incubated with inhibitor in PBS buffer pH 7.2 for 13 minutes prior to the experiment to block the surface and prevent false signals due to interaction of inhibitor with the thin film.

The control reaction was conducted with 1 μM ATP and 2.5 μl PKC lipid activator. An average difference in drain current of 3.9 μA was observed between the SU-8 and the tin oxide surfaces. On addition of the kinase inhibitor along with PKC-α enzyme, the average difference in drain current remained close to the control signal at 6.0 μA. The phosphorylation reaction was conducted in the presence of ATP, activator and enzyme. The average difference in drain current was measured to be 23.4 μA. The effective phosphorylation signal measured was 19.5 μA.

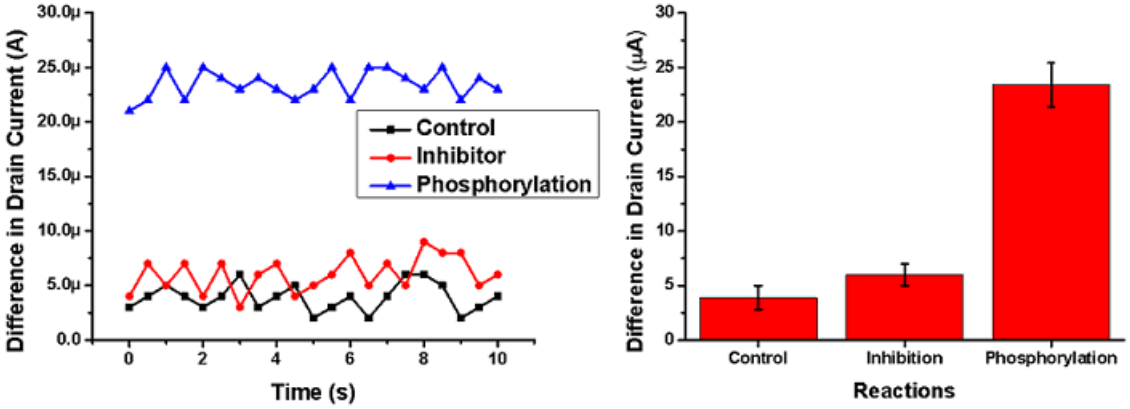

Figure 5.11: Left: Shift in drain current versus time for phosphorylation studies on the REFET. Right: Drain current shifts due to phosphorylation

While the phosphorylation signal is significantly higher than the control and inhibition signal, a more stable result would be desirable. The instability in the readings may be due to a number of reasons. Firstly, the ground connection might not be at a stable voltage. Secondly, there might be other sources of noise

in the circuit arising from the connections. Thirdly, the instabilities may be due to the fact that the extended gates are at a floating potential. Further investigation is required to determine the true cause of the instability and steps can be taken to reduce it. Different inhibitors have not been tested on the REFET as a part of this study. This system can be considered to be proof of concept for screening protein kinase inhibitors.

5.4 Conclusion

In this chapter the initial stages of developing a REFET structure for multiplexed screening of protein kinase inhibitors is described. A PCB with three copper pads that were able to fit under the well of a 96 well plate was designed. Building from the previous chapter, the sensing and reference layers were deposited on to the PCB. The REFET structure was interfaced with a commercial CMOS IC for measurement.

The initial measurements were conducting by connected the thin films individually to the CMOS IC. The results were comparable to that in the previous chapters. The REFET structure was assembled in the next part of the study and the sensors were multiplexed for the measurement. The results are promising but the fluctuations need more investigation in the future for further development of the device. Presently, the device works as a proof of concept and can form a base platform for screening other kinase inhibitors.

There are a few limitations of this study. Firstly, the manual polishing of the board is not very practical when the 96 sets of sensors are fabricated. Secondly, the blocking of the surface with the inhibitor needs to be replaced by a more efficient method of producing an 'insensitive' surface. When different inhibitors are considered, they might interact differently with the surface depending on their chemical composition and this method may not be successful.

Also, this adds an extra step to the processing of the board and requires one to know exactly which wells are going to be used for the inhibition reaction. The measuring circuitry is very easy to construct from commercially available integrated circuits but in the future, designing monolithic integration may be considered to bring the cost down for mass production.

Chapter 6

Conclusion and Outlook

6.1 Conclusion

There is a pressing need in today's world for faster and more cost effective drug discovery systems. This has led to the widespread popularity of HTS methods for screening new compounds. Protein kinase inhibitors have emerged as a major class of drugs which target several diseases caused by abnormal protein phosphorylation. This research aims at developing a HTS method to screen kinases both time and cost effectively. Unlike the assays currently used by the pharmaceutical industries, which rely heavily on the presence of antibodies and radio tags, this biosensor platform depends on the simple concept of detecting pH changes due to phosphorylation.

This thesis was aimed towards developing a biosensor compatible with a 96 well microtitre plate for screening of protein kinase inhibitors. The REFET device structure appeared very promising as it would allow the elimination of the reference electrode. In the initial part of this study, pH sensitive silicon nitride was interfaced with a PCB to act as a biosensor. While this method showed some promising results, it had some practical limitations in constructing the sensor array. Firstly, the process to mounting the wafers on the PCB was by attaching them manually with silver conductive paste. This process may prove to be too cumbersome when there are 96 sensors instead of the four on the test board. Also, when silver paste is

completely dry, it is a poor adhesive so the shelf life of these sensors would only be a few hours long.

OTFTs were considered for this application in the next part of this study. The devices themselves were very promising by virtue of their small size and the ability to include both extended gates and FETs on the same chip for a reasonable price. However, the stability of the batch of devices under test was poor and could not provide reliable results for the phosphorylation studies. These devices may be explored in the future for this application if a batch of devices with improved stability can be acquired.

Tin oxide as sensing layer, deposited directly on to a PCB formed the next part if the study. Though a stable surface with a good pH response was achieved, the phosphorylation signals were greatly amplified. In an attempt to troubleshoot the device, the PCB was polished prior to the deposition of tin oxide. The signals from the phosphorylation, inhibition and control reaction signals improved by this process. The PCBs were polished manually for this thesis but when the full array needs to be polished, a mechanised process with consistent results will need to be implemented. This study formed the first part of developing the REFET biosensor.

For developing the reference FET, 115 nm of SU-8 proved to be the most successful in producing a noise free signal with sufficient signal strength among the different processes that were tried. The signal due to the reaction of the inhibitor with the SU-8 surface is suppressed by blocking the SU-8 thin films with inhibitor prior to the phosphorylation studies being performed. This might not be the best approach to producing an insensitive surface but due to time restrictions we did not wasn't further investigate other methods. The pH sensitivity and signals due to phosphorylation studies were low enough to consider the SU-8 thin film as a reference sensor for the final REFET design.

Finally, the SU-8 and tin oxide thin films were interfaced with commercial

MOSFET ICs. The signal levels were similar to previous studies. The extended gates for the REFET structure was fabricated on a PCB. The devices were multiplexed for measurement. This allowed the elimination of the reference electrode from the device setup. While some reasonable differences in drain current were measured, there were fluctuations in the measured signal with time.

The integration of the sensing layer on the FR4 substrate with commercially available integrated circuits facilitated the designing of a low cost, simple system for screening protein kinase inhibitors. The present system was only tested for its capability to provide 'yes' and 'no' answers to the drug activity of the kinase inhibitor under test. The data collection can be made faster by measuring over a smaller duration. The fast switching times of the multiplexer will further aid the speed of this screening test.

Research questions in our aim were addressed. The material for the pH sensitive sensor was selected to be tin oxide. The insensitive surface was constructed with SU-8 with its surface blocked with inhibitor. The field effect device structure chosen was the REFET for differential measurement without a reference electrode. Finally, the sensors were interfaced with integrated circuits.

6.2 Outlook

This system for drug discovery is still in early phases of development. One of the major avenues that can be explored is to test the device using different kinase inhibitors and potentially try to quantify the extent of inhibition that each drug provides. In order to do this study, it will be necessary to develop a more accurate method of collecting data from the REFET structure. An analog-to-digital converter of a higher resolution is required and the ground connection should provide a more stable voltage.

A better method for the fabrication of the pH insensitive surface needs to be developed. The blocking of the surface with inhibitor is not a very effective method because different inhibitors may interact differently with the surface. Other polymers or post processing of SU-8 might be more effective.

One can decide to move away from the 96 well plate and design a more compact sensor array of a smaller size. In this thesis, commercial ICs have been used to keep the cost low but integration of matched pair MOSFETs, microcontrollers and multiplexers can be considered. Addition of a digital readout system can make the system independent of computers for displaying data.

Finally, the device features can be expanded by integration of a microfluidics module to make up a new sample delivery system for the device to replace the existing liquid handling systems used for 96 well plates. The measurement circuit can be made smaller and more compact by designing an integrated circuit consisting of multiplexers, analog-to-digital converter and processor. A display system can also be added to ensure better portability of the device.

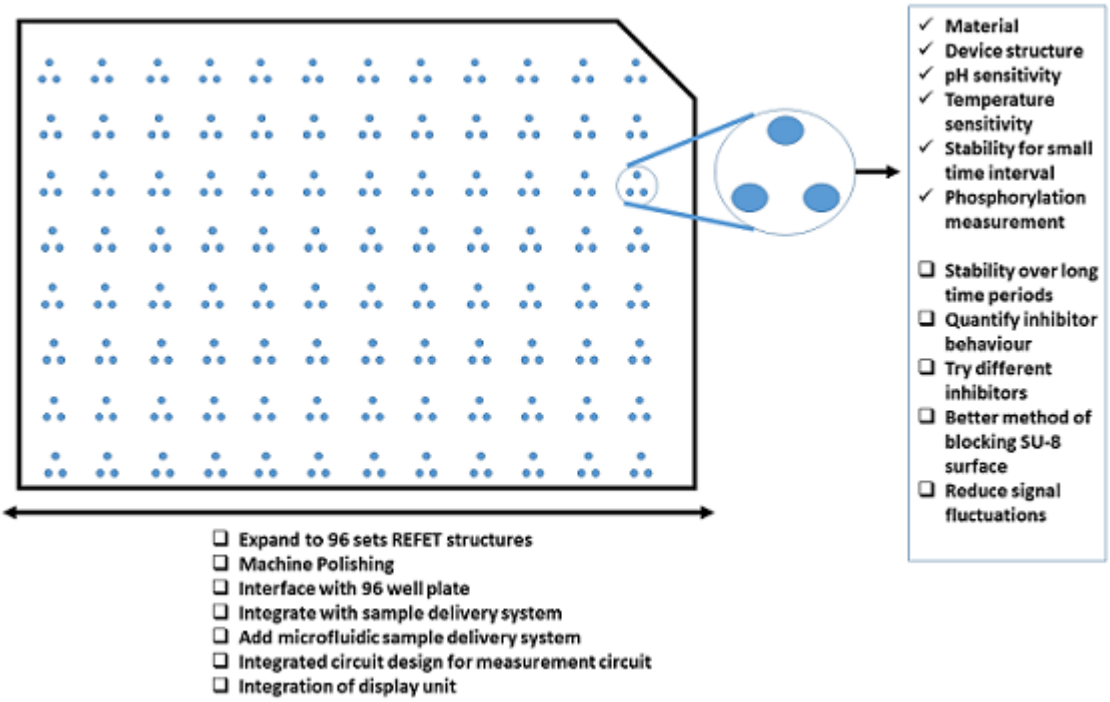

Figure 6.1: Ideas on future implementation

References

[1] Szymanski P, Markowicz M, and Mikiciuk-Olasik E. "Adaptation of High-Throughput Screening in Drug Discovery-Toxicological Screening Tests". *International Journal of Molecular Sciences* 13 (2012), pp. 427–452.

[2] Taylor D. "The Pharmaceutical Industry and the Future of Drug Development". In: *Pharmaceuticals in the Environment*. The Royal Society of Chemistry, 2016, pp. 1–33.

[3] Cohen P. "The Role of Protein Phosphorylation in Human Health and Disease." *European Journal of Biochemistry* 268 (2001), pp. 5001–5010.

[4] Cohen P and Alessi DR. "Kinase Drug Discovery - What's Next in the Field?" *ACS Chemical Biology* 8 (2013), pp. 96–104.

[5] Lahiry P et al. "Kinase Mutations in Human Disease: Interpreting Genotype-Phenotype Relationships". *Nature Reviews Genetics* 11 (2010), pp. 60–74.

[6] Johnson LN. "The Regulation of Protein Phosphorylation". *Biochemical Society Transactions* 37 (2009), pp. 627–641.

[7] Mehrotra P. "Biosensors and their applications – A review". *Journal of Oral Biology and Craniofacial Research* 6.2 (2016), pp. 153–159.

[8] Clark Jr. LC. and Lyons C. "Electrode Systems For Continuous Monitoring in Cardiovascular Surgery". *Annals of the New York Academy of Sciences* 102.1 (1962), pp. 29–45.

[9] Anthony P. F. Turner. "Biosensors: sense and sensibility". *Chemical Society Reviews* 42 (2013), pp. 3184–3196.

[10] Newman JD and Turner APF. "Home blood glucose biosensors: a commercial perspective". *Biosensors and Bioelectronics* 20.12 (2005), pp. 2435–2453.

[11] Syu YC, Hsu WE, and Lin CT. "Review—Field-Effect Transistor Biosensing: Devices and Clinical Applications". 7.7 (2018), Q3196–Q3207.

[12] Bergveld P. "Development of an Ion-Sensitive Solid-State Device for Neurophysiological Measurements". *IEEE Transactions on Biomedical Engineering* BME-17.1 (1970), pp. 70–71.

[13] Milgrew MJ, Riehle MO, and Cumming DRS. "A large transistor-based sensor array chip for direct extracellular imaging". *Sensors and Actuators B: Chemical* 111-112 (2005). Eurosensors XVIII 2004, pp. 347–353.

[14] Bausells J et al. "Ion-sensitive field-effect transistors fabricated in a commercial CMOS technology". *Sensors and Actuators B: Chemical* 57.1 (1999), pp. 56–62.

[15] Liu Y et al. "An Extended CMOS ISFET Model Incorporating the Physical Design Geometry and the Effects on Performance and Offset Variation". *IEEE Transactions on Electron Devices* 58.12 (2011), pp. 4414–4422.

[16] Kaisti M et al. "Hand-Held Transistor Based Electrical and Multiplexed Chemical Sensing System". *ACS Sensors* 1.12 (2016), pp. 1423–1431.

[17] Prodromakis T, Liu Y, and Toumazou C. "A Low-Cost Disposable Chemical Sensing Platform Based on Discrete Components". *IEEE Electron Device Letters* 32.3 (2011), pp. 417–419.

[18] Kamahori M, Ishige Y, and Shimoda M. "Detection of DNA hybridization and extension reactions by an extended-gate field-effect transistor: Characterizations of immobilized DNA–probes and role of applying a superimposed high-frequency voltage onto a reference electrode". *Biosensors and Bioelectronics* 23.7 (2008), pp. 1046–1054.

[19] Ishige Y, Shimoda M, and Kamahori M. "Extended-gate FET-based enzyme sensor with ferrocenyl-alkanethiol modified gold sensing electrode". *Biosensors and Bioelectronics* 24.5 (2009). Selected Papers from the Tenth

World Congress on Biosensors Shangai, China, May 14-16, 2008, pp. 1096–1102.

[20] Lee TN et al. "Electrolyte-Insulator-Semiconductor pH Sensors with Arrayed Patterns Manufactured by Nano Imprint Technology". *Journal of The Electrochemical Society* 165.14 (2018), B767–B772.

[21] Oh JY et al. "Highly sensitive electrolyte-insulator-semiconductor pH sensors enabled by silicon nanowires with Al_2O_3/SiO_2 sensing membrane". *Sensors and Actuators B: Chemical* 171-172 (2012), pp. 238–243.

[22] Pan TM et al. "Impact of postdeposition annealing on the sensing and impedance characteristics of TbYxOy electrolyte–insulator–semiconductor pH sensors". *RSC Advances* 6 (80 2016), pp. 76673–76678.

[23] Weng WH et al. "Enzymatic Glucose Biosensor Based on TbYxOy Electrolyte-Insulator-Semiconductor". *Journal of The Electrochemical Society* 163.8 (2016), B445–B452.

[24] Kaisti M. "Detection principles of biological and chemical FET sensors". *Biosensors and Bioelectronics* (2017), pp. 437–448.

[25] Barbaro M et al. "Label-free, direct DNA detection by means of a standard CMOS electronic chip". *Sensors and Actuators B: Chemical* 171-172 (2012), pp. 148–154.

[26] Guan W et al. "Quantitative probing of surface charges at dielectric–electrolyte interfaces". *Lab Chip* 13 (7 2013), pp. 1431–1436.

[27] Spijkman M. et al. "Beyond the Nernst-limit with dual-gate ZnO ion-sensitive field-effect transistors". *Applied Physics Letters* 98.4 (2011), p. 043502.

[28] Huang Y et al. "High performance dual-gate ISFET with non-ideal effect reduction schemes in a SOI-CMOS bioelectrical SoC". In: *2015 IEEE International Electron Devices Meeting (IEDM)*. 2015, pp. 29.2.1–29.2.4.

[29] Jia M, Lin WK, and Souchelnytskyi S. “Phosphoproteomics: Detection, Identification and Importance of Protein Phosphorylation, Integrative Proteomics”. *InTech* (2012), pp. 5772–31305.

[30] Blume-Jensen P and Hunter T. “Oncogenic kinase Signalling”. *Nature* 411 (2001), pp. 355–365.

[31] Prével C et al. “Fluorescent Biosensors for High Throughput Screening of Protein Kinase Inhibitors”. *Biotechnology Journal* 9 (2014), pp. 253–265.

[32] Burnett G and Kennedy EP. “The Enzymatic Phosphorylation of Protiens”. *Journal of Biological Chemistry* 211 (1954), pp. 969–980.

[33] Krebs EG and Fischer EH. “The Phosphorylase b to a Converting Enzyme of Rabbit Skeletal Muscle”. *Biochimica et Biophysica Acta* 20 (1956), pp. 150–157.

[34] Fischer EH. and Krebs EG. “Conversion of Phosphorylase b to Phosphorylase a in Muscle Extracts”. *Journal of Biological Chemistry* 216 (1955), pp. 121–132.

[35] Sutherland EW. and Wosilait WD. “Inactivation and Activation of Liver Phosphorylase”. *Nature* 4447 (1955), pp. 169–170.

[36] Norman RA., Toader D., and Ferguson AD. “Structural Approaches to Obtain Kinase Selectivity”. *Trends in Pharmacological Sciences* 33 (2012), pp. 273–278.

[37] Noble MEM., Endicott JA., and Johnson LN. “Protein Kinase Inhibitors: Insights into Drug Design from Structure”. *Science* 5665 (2004), pp. 1800–1805.

[38] Peck SC. “Analysis of protein phosphorylation: methods and strategies for studying kinases and substrates”. *The Plant Journal* 45 (2006), pp. 512–522.

[39] Sawasdikosol S. “Detecting Tyrosine-Phosphorylated Proteins by Western Blot Analysis”. In: *Current Protocols in Immunology.* John Wiley & Sons, Inc., 2001, pp. 1–11.

[40] Delom F and Chevet E. "Phosphoprotein Analysis: From Proteins to Proteomes". *Proteome Science* 4 (2006), pp. 4–15.

[41] Matthias M et al. "Analysis of Protein Phosphorylation Using Mass Spectrometry: Deciphering the Phosphoproteome". *Trends in Biotechnology* 20 (2002), pp. 261–268.

[42] Brill LM. et al. "Robust Phosphoproteomic Profiling of Tyrosine Phosphorylation Sites from Human T Cells Using Immobilized Metal Affinity Chromatography and Tandem Mass Spectrometry". *Analytical Chemistry* 76 (2004), pp. 2763–2772.

[43] Ma H, Deacon S, and Horiuchi K. "The Challenge of Selecting Protein Kinase Assays for Lead Discovery optimization". *Expert Opinion on Drug Discovery* 3 (2008), pp. 607–621.

[44] Pan L et al. "Sensitive Measurement of Total Protein Phosphorylation Level in Complex Protein Samples". *Analyst* 140 (2015), pp. 3390–3396.

[45] Kurumi YH et al. "Microarrays for the Functional Analysis of the Chemical-Kinase Interactome". *Journal of Biomolecular Screening* 11 (2006), pp. 48–56.

[46] Haiching M and Kurumi YH. "Chemical Microarray: a New Tool for Drug Screening and Discovery". *Drug Discovery Today* 11 (2006), pp. 661–668.

[47] Weinmann H and Metternich R. "Editorial: Drug Discovery Process for Kinease Inhibitors". *ChemBioChem* 6 (2005), pp. 455–459.

[48] Walters WP and Namchuk M. "Designing Screens: How to Make Your Hits a Hit". *Nature Reviews Drug Discovery* 2 (2003), pp. 259–266.

[49] von Ahsen O and Bömer U. "High-Throughput Screening for Kinase Inhibitors". *ChemBioChem* 6 (2005), pp. 481–490.

[50] Gopalakrishna R et al. "Rapid Filtration Assays for Protein Kinase C Activity Andphorbol Ester Binding Using Multiwell Plates with Fitted Filtration Discs". *Analytical Biochemistry* 206 (1992), pp. 24–35.

[51] Wu JJ. "Comparison of SPA, FRET, and FP for Kinase Assays". In: *High Throughput Screening: Methods and Protocols*. Totowa, NJ: Humana Press, 2002, pp. 65–85.

[52] Fraser GJ, Schmid A, and Ferrand S. "Scintillation Proximity Assays in High-Throughput Screening". *Assay and Drug Development Technologies* 6 (2008), pp. 433–455.

[53] Zhang J and Allen MD. "FRET-Based Biosensors for Protein Kinases: Illuminating the Kinome". *Molecular BioSystems*. 3 (2007), pp. 759–765.

[54] Van TNN and Morris MC. "Fluorescent Sensors of Protein Kinases: From Basics to Biomedical Applications". In: *Fluorescence-Based Biosensors From Concepts to Applications*. Academic Press, 2013, pp. 217–274.

[55] Engelman JA., Luo J, and Cantley LC. "The Evolution of Phosphatidylinositol 3-kinases as Regulators of Growth and Metabolism". *Nature Reviews Genetics* 7 (2006), pp. 606–619.

[56] Newman M and Josiah S. "Utilization of Fluorescence Polarization and Time Resolved Fluorescence Resonance Energy Transfer Assay Formats for SAR Studies: Src Kinase as a Model System". *Journal of Biomolecular Screening* 9 (2004), pp. 525–532.

[57] Kashem MA et al. "Three Mechanistically Distinct Kinase Assays Compared: Measurement of Intrinsic ATPase Activity Identified the Most Comprehensive Set of ITK Inhibitors". *Journal of Biomolecular Screening* 12 (2007), pp. 70–83.

[58] Turek-Etienne TC et al. "Evaluation of Fluorescent Compound Interference in 4 Fluorescence Polarization Assays: 2 Kinases, 1 Protease, and 1 Phosphatase". *Journal of Biomolecular Screening* 8 (2003), pp. 176–184.

[59] Li Y. "Homogeneous Assays for Adenosine 5-Monophosphate-Activated Protein Kinase". *Analytical Biochemistry* 321 (2003), pp. 151–156.

[60] Ullman EF et al. "Luminescent Oxygen Channeling Immunoassay: Measurement of Particle Binding Kinetics by Chemiluminescence". *Proceedings of the National Academy of Sciences of the United States of America* 91 (1994), pp. 5426–5430.

[61] Schöning MJ. ""Playing Around" with Field-Effect Sensors on the Basis of EIS Structures, LAPS and ISFETs". *Sensors* 3 (2005), pp. 126–138.

[62] Taing MH. "Characterization and Fabrication of a Multiarray Electrolyte Insulator Semiconductor Biosensor". PhD thesis. Griffith University, Brisbane, Australia, 2007.

[63] Yuqing M, Jianguo G, and Jianrong C. "Ion Sensitive Field Effect Transducer-Based Biosensors". *Biotechnology Advances* 21 (2003), pp. 527–534.

[64] Harame DL et al. "Ion-Sensing Devices with Silicon Nitride and Borosilicate Glass Insulators". *IEEE Transactions on Electron Devices* 34 (1987), pp. 1700–1707.

[65] Fung CD, Cheung PW, and Ko WH. "A Generalized Theory of an Electrolyte-Insulator-Semiconductor Field-Effect Transistor". *IEEE Transactions on Electron Devices* 33 (1986), pp. 8–18.

[66] Corrado DN Lvova LK and Audrey L. "Capacitive EIS sensor". In: *Multisensor Systems for Chemical Analysis: Materials and Sensors*. Pan Stanford, 2014, pp. 339–344.

[67] Chen P. et al. "High-frequency capacitance–voltage measurement of plasma-enhanced chemical-vapor-deposition-grown SiO2/n-GaN metal-insulator-semiconductor structures". *Applied Physics Letters* 79.21 (2001), pp. 3530–3532.

[68] Fritz J et al. "Electronic Detection of DNA by Its Intrinsic Molecular Charge". *Proceedings of the National Academy of Sciences* 99 (2002), pp. 14142–14146.

[69] Wei F et al. “Monitoring DNA Hybridization on Alkyl Modified Silicon Surface Through Capacitance Measurement”. *Biosensors and Bioelectronics* 18 (2003), pp. 1157–1163.

[70] Siqueira Jr JR. et al. “Penicillin Biosensor Based on a Capacitive Field-Effect Structure Functionalized with a Dendrimer/Carbon Nanotube Multilayer”. *Biosensors and Bioelectronics* 25 (2009), pp. 497–501.

[71] Beyer M et al. “Development and Application of a New Enzyme Sensor Type Based on the EIS-Capacitance Structure for Bioprocess Control”. *Biosensors and Bioelectronics* 9 (1994), pp. 17–21.

[72] Poghossian A et al. “Field-effect Sensors for Monitoring the Layer-by-Layer Adsorption of Charged Macromolecules”. *Sensors and Actuators B: Chemical* 118 (2006), pp. 163–170.

[73] Schöning MJ et al. “Miniaturised Flow-Through Cell with Integrated Capacitive EIS Sensor Fabricated at Wafer Level Using Si and SU-8 Technologies”. *Sensors and Actuators B: Chemical* 108 (2005), pp. 986–992.

[74] Bhalla N et al. “Protein Phosphorylation Analysis Based on Proton Release Detection: Potential Tools for Drug Discovery”. *Biosensors and Bioelectronics* 54 (2014), pp. 109–114.

[75] Bergveld P. “Thirty Years of ISFETOLOGY: What Happened in the Past 30 Years and What May Happen in the Next 30 Years”. *Sensors and Actuators B: Chemical* 88.1 (2003), pp. 1–20.

[76] Pachauri V. and Ingebrandt S. “Biologically Sensitive Field-Effect Transistors: From ISFETs to NanoFETs”. *Essays in Biochemistry* 60 (2016), pp. 81–90.

[77] Lee C, Kim SK, and Kim M. “Ion-Sensitive Field-Effect Transistor for Biological Sensing”. *Sensors* 9 (2009), pp. 7111–7131.

[78] Dzyadevych SV et al. “Enzyme Biosensors Based on Ion-Selective Field-Effect Transistors”. *Analytica Chimica Acta* 568 (2006), pp. 248–258.

[79] Veigas B, Fortunato E, and Baptista PV. "Field Effect Sensors for Nucleic Acid Detection: Recent Advances and Future Perspectives". *Sensors* 15 (2015), pp. 10380–10398.

[80] Freeman R, Gill R, and Willner I. "Following a Protein Kinase Activity Using a Field-Effect Transistor Device". *Chemical Communications* (33 2007), pp. 3450–3452.

[81] Li J, Sun Z, and Feng Y. "Solution Processable Low-Voltage Organic Thin Film Transistors with High-k Relaxor Ferroelectric Polymer as Gate Insulator". *Advanced Materials* 24.1 (2012), pp. 88–93.

[82] Arias AC et al. "Materials and Applications for Large Area Electronics: Solution-Based Approaches". *Chemical Reviews* 1 (2010), pp. 3–24.

[83] Reese C et al. "Organic thin film transistors". *Materials Today* 7 (2004), pp. 20–27.

[84] Sokolov AN, Mark E. Roberts, and Zhenan Bao. "Fabrication of low-cost electronic biosensors". *Materials Today* 12 (2009), pp. 12–20.

[85] Han CY et al. "A Study on Pentacene Organic Thin-Film Transistor With Different Gate Materials on Various Substrates". *IEEE Electron Device Letters* 6 (2017), pp. 744–747.

[86] Tang ML. et al. "Ambipolar, High Performance, Acene-Based Organic Thin Film Transistors". *Journal of the American Chemical Society* 19 (2008), pp. 6064–6065.

[87] Murphy AR. and Fréchet JMJ. "Organic Semiconducting Oligomers for Use in Thin Film Transistors". *Chemical Reviews* 107.4 (2007), pp. 1066–1096.

[88] Zhenan B, Ananth D, and Lovinger AJ. "Soluble and processable regioregular poly(3-hexylthiophene) for thin film field-effect transistor applications with high mobility". *Applied Physics Letters* 26 (1996), pp. 4108–4110.

[89] Ong BS. et al. “High-Performance Semiconducting Polythiophenes for Organic Thin-Film Transistors”. *Journal of the American Chemical Society* 11 (2004), pp. 3378–3379.

[90] LeMieux MC. et al. “Self-Sorted, Aligned Nanotube Networks for Thin-Film Transistors”. *Science* 5885 (2008), pp. 101–104.

[91] Newman CR. et al. “Introduction to Organic Thin Film Transistors and Design of n-Channel Organic Semiconductors”. *Chemistry of Materials* 23 (2004), pp. 4436–4451.

[92] Horowitz G. “Organic Field-Effect Transistors”. *Advanced Materials* 5 (1998), pp. 365–377.

[93] Sokolov AN, Roberts ME, and Bao Z. “Fabrication of low-cost electronic biosensors”. *Materials Today* 9 (2009), pp. 12–20.

[94] Bartic C., Campitelli A., and Borghs S. “Field-effect detection of chemical species with hybrid organic/inorganic transistors”. *Applied Physics Letters* 3 (2003), pp. 475–477.

[95] Casalini S et al. “Organic field-effect transistor for label-free dopamine sensing”. *Organic Electronics* 1 (2013), pp. 156–163.

[96] Zhang Q and Subramanian V. “DNA hybridization detection with organic thin film transistors: Toward fast and disposable DNA microarray chips”. *Biosensors and Bioelectronics* 12 (2007), pp. 3182–3187.

[97] Scarpa G et al. “Biocompatibility studies of solution-processable organic thin-film transistors for sensing applications”. In: *2009 IEEE 3rd International Conference on Nano/Molecular Medicine and Engineering*. 2009, pp. 265–268.

[98] Khanna VK. “Remedial and adaptive solutions of ISFET non-ideal behaviour”. *Sensor Review* 3 (2013), pp. 228–237.

[99] Bergveld P et al. “How electrical and chemical requirements for refets may coincide”. *Sensors and Actuators* 3 (1989), pp. 309–327.

[100] Matsuo T and Nakajima H. “Characteristics of reference electrodes using a polymer gate ISFET”. *Sensors and Actuators* 4 (1984), pp. 293–305.

[101] Matsuo T et al. “Parylene-gate isfet and chemical modification of its surface with crown ether compounds”. *Sensors and Actuators* 2 (1986), pp. 115–123.

[102] Bousse L, Shott J, and Meindl JD. “A process for the combined fabrication of ion sensors and CMOS circuits”. *IEEE Electron Device Letters* 1 (1988), pp. 44–46.

[103] Hammond PA, Cumming DRS, and Ali D. “A single-chip pH sensor fabricated by a conventional CMOS process”. In: *SENSORS, 2002 IEEE*. vol. 1. 2002, pp. 350–355.

[104] Antoni BC et al. “Ion Sensor Based On Differential Measurement And Manufacturing Mthod”. 2016.

[105] Wong H and White MH. “A CMOS-integrated ’ISFET-operational amplifier’ chemical sensor employing differential sensing”. *IEEE Transactions on Electron Devices* 3 (1989), pp. 479–487.

[106] Pan CW et al. “Using polypyrrole as the contrast pH detector to fabricate a whole solid-state pH sensing device”. *IEEE Sensors Journal* 2 (2003), pp. 164–170.

[107] Nakajima H., Esashi M., and Matsuo T. “The Cation Concentration Response of Polymer Gate ISFET”. *Journal of The Electrochemical Society* 1 (1982), pp. 141–143.

[108] Errachid A, J Bausells, and N Jaffrezic-Renault. “A simple REFET for pH detection in differential mode”. *Sensors and Actuators B: Chemical* 1 (1999), pp. 43–48.

[109] Chang KM, Chang CT, and Chan KM. “Development of an ion sensitive field effect transistor based urea biosensor with solid state reference systems”. *Sensors (Basel)* (2010), pp. 6115–6127.

[110] Pundir CS and Chawla S. "Determination of glycated hemoglobin with special emphasis on biosensing methods". *Analytical Biochemistry* (2014), pp. 47–56.

[111] Salm E et al. "Electrical Detection of Nucleic Acid Amplification Using an On-Chip Quasi-Reference Electrode and a PVC REFET". *Analytical Chemistry* 14 (2014), pp. 6968–6975.

[112] Bhalla N. "Biosensors for Drug Disovery Applications". PhD thesis. University of Bath, 2015.

[113] Lindsay S and Labaer J. *Method and apparatus for measuring phosphorylation kinetics on large arrays*. US patent, US20140357527A1. 2014.

[114] Lindsay S. "Biochemistry and Semiconductor Electronics—The Next Big Hit for Silicon?" *Journal of Physics: Condensed Matter* 24 (2012), p. 164201.

[115] Aguilar M. "HPLC of Peptides and Proteins". In: *HPLC of Peptides and Proteins: Methods and Protocols*. Totowa, NJ, 2004, pp. 3–8.

[116] To TD et al. "Modification of silicon nitride surfaces with GOPES and APTES for antibody immobilization: computational and experimental studies". *Advances in Natural Sciences: Nanoscience and Nanotechnology* 6.4 (2015), p. 045006.

[117] Psarouli A et al. "Covalent Binding vs. Adsorption of Biomolecules on Silicon Nitride Planar Waveguides". *Procedia Engineering* 25 (2011), pp. 350–353.

[118] Zhan-Hui W and Gang J. "Covalent immobilization of proteins for the biosensor based on imaging ellipsometry". *Journal of Immunological Methods* 285.2 (2004), pp. 237–243.

[119] Piehler J. et al. "A High-Density Poly(ethylene glycol) Polymer Brush for Immobilization on Glass-Type Surfaces". *Biosensors and Bioelectronics* 9-10 (2000), pp. 473–481.

[120] de Boer B and Facchetti A. "Semiconducting Polymeric Materials". *Polymer Reviews* 3 (2008), pp. 423–431.

[121] Yan F et al. “Label-free DNA sensor based on organic thin film transistors”. *Biosensors and Bioelectronics* 5 (2009), pp. 1241–1245.

[122] Aifeng LV, Yong Pan, and Lifeng Chi. “Gas Sensors Based on Polymer Field-Effect Transistors”. *Sensors* 17.1: 213 (2017).

[123] Ogier SD et al. “Uniform, high performance, solution processed organic thin-film transistors integrated in 1 MHz frequency ring oscillators”. *Organic Electronics* 54 (2018), pp. 40–47.

[124] Bhalla N et al. “Plasmonic Ruler on Field-Effect Devices for Kinase Drug Discovery Applications”. *Biosensors and Bioelectronics* 71 (2015), pp. 121–128.

[125] Formisano N. “A study on the optimisation of electrochemical impedance spectroscopy biosensors”. PhD thesis. University of Bath, 2015.

[126] Jia X et al. “Stable organic thin-film transistors”. *Science Advances* 4.1 (2018).

[127] van der Spiegel J et al. “The extended gate chemically sensitive field effect transistor as multi-species microprobe”. *Sensors and Actuators* (1983), pp. 291–298.

[128] Kim DS. “An extended gate FET-based biosensor integrated with a Si microfluidic channel for detection of protein complexes”. *Sensors and Actuators B: Chemical* 2 (2006), pp. 488–494.

[129] Li-Lun C et al. “Study on extended gate field effect transistor with tin oxide sensing membrane”. *Materials Chemistry and Physics* 63.1 (2000), pp. 19–23.

[130] Becker H and Laurie E. Locascio. “Polymer microfluidic devices”. *Talanta* 56 (2002), pp. 267–287.

[131] Yates DE., Samuel Levine, and Thomas W. Healy. “Site-binding model of the electrical double layer at the oxide/water interface”. *Journal of the Chemical Society Faraday Trans. 1* 70 (1974), pp. 1807–1818.

[132] Tsai CN et al. “Study on the sensing characteristics and hysteresis effect of the tin oxide pH electrode”. *Sensors and Actuators B: Chemical* 108 (2005), pp. 877–882.

[133] Bousse L, De Rooij NF, and Bergveld P. “Operation of chemically sensitive field-effect sensors as a function of the insulator-electrolyte interface”. *IEEE Transactions on Electron Devices* 30.10 (1983), pp. 1263–1270.

[134] Kurzweil P. “Metal Oxides and Ion-Exchanging Surfaces as pH Sensors in Liquids: State-of-the-Art and Outlook”. *Sensors* 6 (2009), pp. 4955–4985.

[135] Bergveld P. “The impact of MOSFET-based sensors”. *Sensors and Actuators* 8.2 (1985), pp. 109–127.

[136] Razavi B. *Fundamentals of Microelectronics*. Vol. 2nd Edition. 2012.

[137] Armstrong NR and Shepard VR. “Voltammetric studies of silane-modified SnO2 surfaces in selected aqueous and non-aqueous media”. *Journal of Electroanalytical Chemistry and Interfacial Electrochemistry* 115.2 (1980), pp. 253–265.

[138] Hijazi M et al. “Synthesis and characterization of tin dioxide thick film modified by APTES in vapor and liquid phases”. *Journal of Materials Science* 53 (2018), pp. 727–738.

[139] Liao HK et al. “Study of amorphous tin oxide thin films for ISFET applications”. *Sensors and Actuators B: Chemical* 50 (1998), pp. 104–109.

[140] Hijazi M et al. “Selective Ammonia Gas Sensor based on SnO2-APTES Modification”. *Procedia Engineering* 168 (2016), pp. 280–283.

[141] Gunda NSK et al. “Optimization and characterization of biomolecule immobilization on silicon substrates using (3-aminopropyl)triethoxysilane (APTES) and glutaraldehyde linker”. *Applied Surface Science* 305 (2014), pp. 522–530.

[142] Kulisch W et al. “Tantalum Pentoxide As A Material For Biosensors: Deposition, Properties And Applications”. In: 2009, pp. 509–524.

[143] Lue CE et al. “Optimization of Urea-EnFET Based on Ta2O5 Layer with Post Annealing”. *Sensors* 11 (2011), pp. 4562–4571.

[144] Mikolajick T, Kühnhold R, and Ryssel H. “The pH-sensing properties of tantalum pentoxide films fabricated by metal organic low pressure chemical vapor deposition”. *Sensors and Actuators B: Chemical* 44 (1997), pp. 262–267.

[145] Cricenti A et al. “Morphological, chemical and electrical characterization of thin film grown on rough and mechanically polished substrates”. *Journal of Physics D: Applied Physics* 29 (1996), pp. 2235–2239.

[146] Le MH et al. “A Label-Free Impedimetric DNA Sensor Based on a Nanoporous SnO2 Film: Fabrication and Detection Performance”. *Sensors* 5 (2015), pp. 10686–10704.

[147] Festa RA and Thiele DJ. “Copper: An essential metal in biology”. *Current Biology* 21.21 (2011), R877–R883.

[148] Chudy M, Wróblewski W, and Brzózka Z. “Towards REFET”. *Sensors and Actuators B: Chemical* 57.1 (1999), pp. 47–50.

[149] van den Berg A et al. “Sensitivity control of ISFETs by chemical surface modification”. *Sensors and Actuators* 8.2 (1985), pp. 129–148.

[150] Chovelon JM et al. “Sensitization of dielectric surfaces by chemical grafting: application to pH ISFETs and REFETs”. *Sensors and Actuators B: Chemical* 8.3 (1992), pp. 221–225.

[151] Olziersky A et al. “Insight on the SU-8 resist as passivation layer for transparent Ga2O3–In2O3–ZnO thin-film transistors”. *Journal of Applied Physics* 108.6 (2010), p. 064505.

[152] Calleja M et al. “Low-Noise Polymeric Nanomechanical Biosensors”. *Applied Physics Letters* 88.11 (2006), p. 113901.

[153] Arya SK et al. “Capacitive aptasensor based on interdigitated electrode for breast cancer detection in undiluted human serum”. *Biosensors and Bioelectronics* 102 (2018), pp. 106–112.

[154] Kaisti M. “Detection principles of biological and chemical FET sensors”. *Biosensors and Bioelectronics* 98 (2017), pp. 437–448.

[155] Tiggelaar RM et al. “Spreading of thin-film metal patterns deposited on nonplanar surfaces using a shadow mask micromachined in Si (110)”. *Journal of Vacuum Science & Technology B: Microelectronics and Nanometer Structures Processing, Measurement, and Phenomena* 25.4 (2007), pp. 1207–1216.

Appendix A

Protocols

A.0.1 Thermal Evaporation of Tin Oxide and Aluminium

1. Clean PCBs by sonication in acetone and isopropanol for 5 minutes each, dry using N_2 or compressed air.
2. Polish PCBs with electrode polishing pads coated in 5 μm alumina slurry
3. Sonicate in acetone and isopropanol for 5 minutes each to remove any residues, dry using N_2 or compressed air
4. Mask contacts with kapton tape or shadow mask
5. Load onto vacuum evaporator
6. Load aluminium piece on a titanium boat
7. Load tin oxide in an alumina coated wire basket
8. Pump system until the vacuum reaches $2X10^{-6}$ Torr
9. Set the substrate rotation motor to a supply of 2 V
10. Evaporate at a rate of 0.3 nm/s
11. Proceed without any further cleaning of the PCBs once unloaded

A.0.2 Protocol for Immobilisation of Peptide on Si_3N_4 surfaces

1. Immerse the clean sensor surface in 98% GOPTS for 45 minutes or heat GOPTS in a beaker to 120°C and hold the thin film surfaces close to the vapours for five seconds
2. Wash with de-ionised water thoroughly to remove excess silane, dry with N_2 gun
3. Drop 2 μl of the peptide solution on to the dry surface and leave to bind for 40 minutes
4. Wash with 20% ethanol to block the unreacted GOPTS sites
5. Store in PBS for further studies

A.0.3 PDMS Membrane Preparation Protocol

1. Mix PDMS base and curing agent in the ratio 10:1 by weight
2. Degas the mixture for 20 minutes in a desiccator
3. Pour the PDMS on the mould
4. Place the PDMS coated mould in an oven at 90°C for 30 minutes
5. Release the membrane from the mould

A.0.4 Protocol for SU-8 spin coating

1. Clean PCBs by sonication in acetone and isopropanol for 5 minutes each, dry using N_2 or compressed air.

2. Polish PCBs with electrode polishing pads coated in 5 μm alumina slurry
3. Sonicate in acetone and isopropanol for 5 minutes each to remove any residues, dry using N_2 or compressed air
4. Cover contacts with teflon tape
5. Load in spin coater
6. Start the vacuum pump to secure the PCB
7. Dispense SU-8 on the substrate
8. Spin at 500 rpm for 30 seconds to spread the SU-8
9. Spin at 1000 rpm for 60 seconds
10. Remove PCB from spin coater, soft-bake at 90°C for 2 minutes
11. Expose SU-8 to UV through a mask aligner
12. Post exposure bake at 90°C for 2 minutes
13. Develop by immersing in Microposit EC Solvent 11
14. Wash with isopropanol thoroughly to remove residues of undeveloped SU-8
15. Use without further cleaning

Appendix B

Trials on Microfluidics

B.0.1 Microfluidics

B.0.2 Design of the microfluidics module

A number of different designs and approaches were adopted to explore the methods to construct a mould for a microfluidic cell. This cell will eventually aid in the delivery of samples to the final sensor array. PDMS will be poured on the mould to replicate the design after which it will be irreversibly bonded to a glass slide or silicon wafer containing the sensors. To acknowledge the importance of repeat measurements to validate results and ensure the reproducibility of the sensor system, the microfluidic mould is envisioned to contain different wells where the same liquid will flow. Here, we explore a 3-well based system through simulation. The construction of a two well based system is attempted using 3D printing and laser cutting technologies.

B.0.3 Materials and Methods

A number of possible designs for the microfluidics cell was explored. The fluid flow through different cell designs were first simulated using COMSOL Multiphysics 5.1. The cell designs were constructed using AutoCAD 2015 and then exported to COMSOL for further studies. With the view of simplicity and to save

time, the simulations were performed in two dimensions instead of three. A laminar flow was assumed for all the tests. For the purpose of 3D printing, the designs were further simplified.

B.0.4 Results and Discussion

Initially, a design with three wells and three channels of equal width was designed. Assuming a flow rate of 2 μl/min at the inlet, with channels of dimension 350 μm each, feeding circular wells of 5 mm diameter, the simulation was performed to display the steady state for 1 second. Figure B.1 shows the surface velocity profile of the cell and it is quite clear that the velocity in the middle channel is higher than the other two channels.

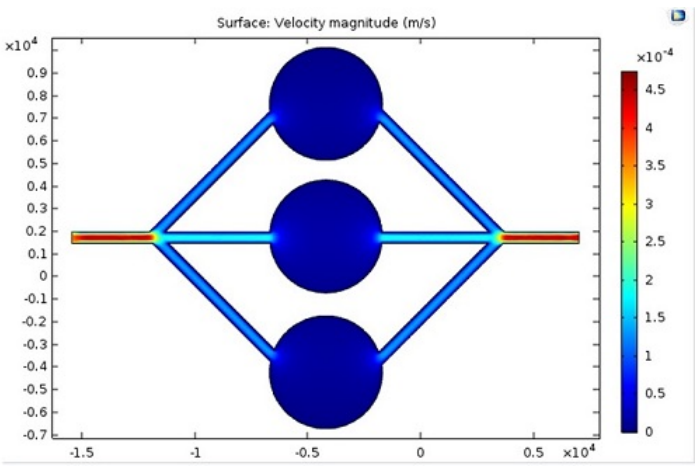

Figure B.1: Surface velocity profile of circular wells with channels of equal thickness

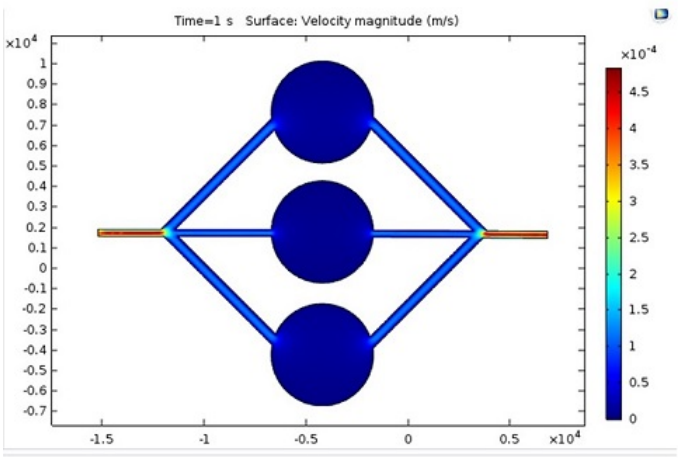

Figure B.2: Surface velocity profile for circular wells with adjusted channel thickness

Next, it was investigated through simulation to find out how wide the middle channel needs to be in order to ensure the same flow rate in each of the channels. The results revealed that the middle channel needs to be constricted to 213 μm for this condition, as illustrated in Figure B.2. Finally, the wells were changed from circular to elliptical (major axis=5 mm, minor axis=3 mm). The simulation results are shown in Figure B.3.

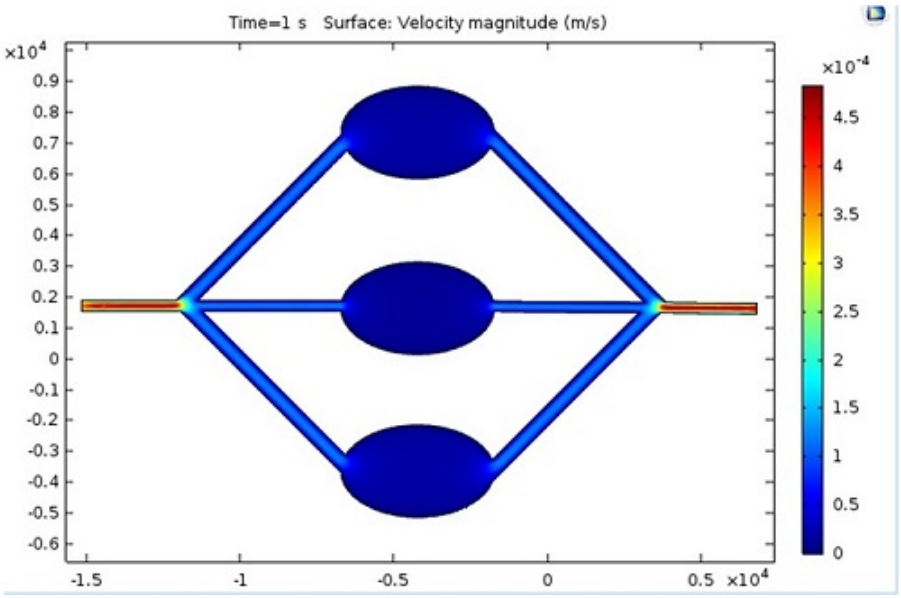

Figure B.3: Surface velocity profile for elliptical wells with adjusted channel thickness

The design was further simplified to evaluate its ability to be 3D printed and laser cut. The two well design is shown in Figure B.4. The channel width was 1 mm and length of 500 microns. The elliptical wells had a major axis of 3 mm and a minor axis of 5mm. This design was laser cut on a perspex sheet and is shown in Figure B.5. 3D printing was also attempted using ABS plastic and is shown in Figure B.6.

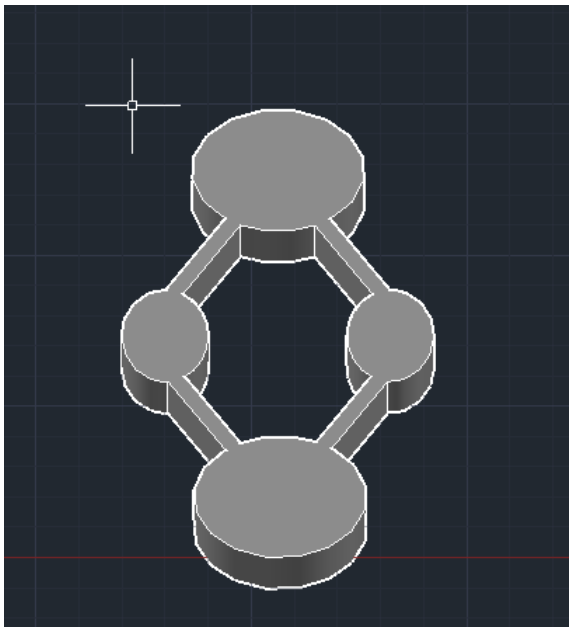

Figure B.4: AutoCAD design for microfluidic mould

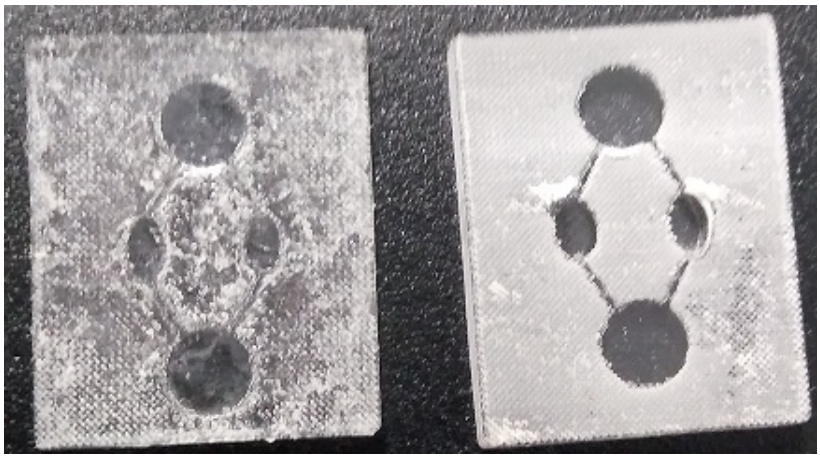

Figure B.5: Laser cut microfluidic mould

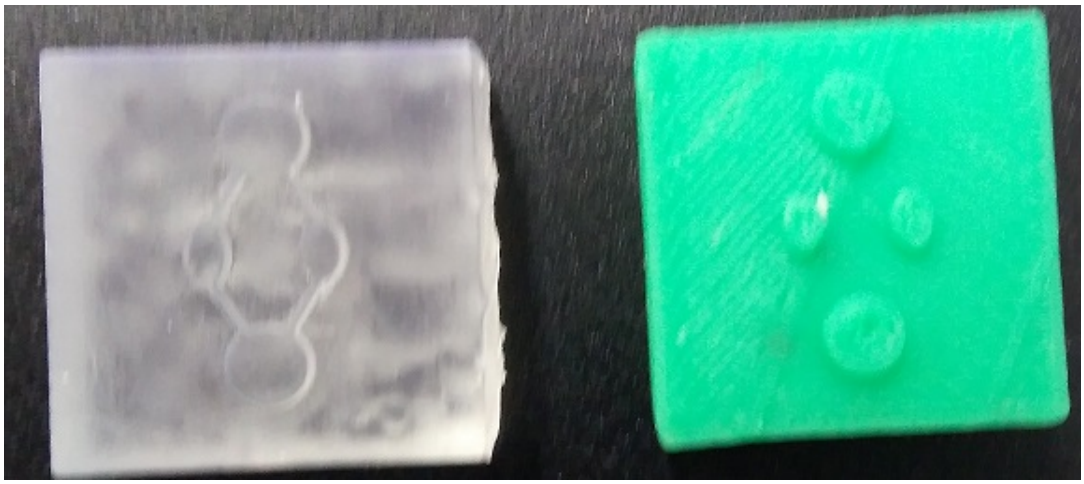

Figure B.6: 3D printed microfluidic module

The attempts were unsuccessful for a number of reasons. The MakerBot 3D printer did not have the required resolution to reproduce the dimensions of the design. The laser cutting of perspex sheets was comparatively better but the surface of the finished product was too rough to be used as a PDMS mould. To make the surface smooth, chloroform was rubbed on the finished product but proper smoothness was not achieved as shown in Figure B.5. The best result was obtained from the stereolithography (SLA), printer shown in Figure B.5 When this was used as a mould, the PDMS replicated the undulations on the surface and hence did not form a proper bond to the glass surface.

Appendix C

Notes on ICs

C.0.1 IC pin diagrams

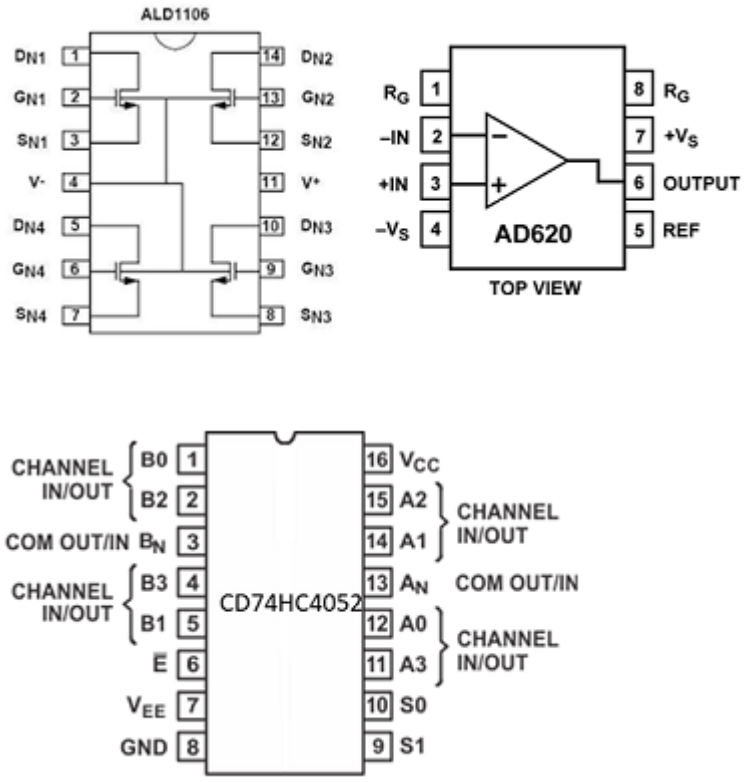

Figure C.1: Pin diagrams of ICs used in the study [Image source: component data sheet]

C.0.2 Essential Features of ICs

ALD1106

- Low gate leakage 0.1 pA typically, 10 pA maximum
- Low threshold voltage 700 mV
- High input impedance of 10^{14} Ω
- Off drain current 10 pA typically, 400 pA maximum
- Mismatch 0.5%

AD620

- Gain set with single external resistor
- Low noise 0.28 μV noise p-p between 0.1 Hz and 10 Hz
- Low power, 1.3 mA maximum current supply
- Common mode rejection ration 110 dB at gain 10

CD74HC4052

- Low on resistance of 7 Ω
- Low crosstalk between channels
- Break-before-make switching
- Maximum switch turn-on delay 65 ns